Mapping and Modulating the Stomach-Brain Neuroaxis

by

Jiayue Cao

A dissertation submitted in partial fulfillment
of the requirements for the degree of
Doctor of Philosophy
(Biomedical Engineering)
in the University of Michigan
2021

Doctoral Committee:

Associate Professor Zhongming Liu, Chair
Associate Professor Tim M. Bruns
Professor Jiande Chen
Professor Douglas C. Noll

Jiayue Cao

jccao@umich.edu

ORCID iD: 0000-0002-9040-1929

Acknowledgements

I am sincerely grateful to those who have helped me during my PhD journey. Firstly, I would like to share my deep gratitude to my PhD advisor, Prof. Zhongming Liu. It is my pleasure to meet him and join the Laboratory of Integrated Brain Imaging (LIBI). With the help from Prof. Liu, I am able to learn advanced techniques and knowledge, build up critical thinking, and in the meantime, enjoy life. This experience will be precious treasures and worth being memorized forever. Secondly, I would like to thank all my advisors and thesis committee members, Prof. Tim Bruns, Prof. Jiande Chen, Prof. Douglas Noll, Prof. Terry Powley, Prof. John Furness, Prof. Edward Bartlett, Prof. Riyi Shi, for their constructive comments and feedbacks.

I would also like to thank all my colleagues in LIBI lab for their contributions to this study and also for their company over the past few years. Thank you, Dr. Haiguang Wen, Dr. Kun-Han Lu, Dr. Lauren Lynch, Mr. Junxing Shi, Mr. Jun-Young Jeong, Ms. Yizhen Zhang, Dr. Ranajay mandal, Dr. Jung-Hoon Kim, Mr. Nishant Babaria, Mr. Steven Oleson, Ms. Xiaokai Wang, Mr. Kuan Han, Mr. Minkyu Choi, and Ms. Yuanhanqing Huang for the insightful feedback and helps in experiments. I would also like to express my gratitude toward Dr. Ulrich Scheven, Dr. Shiying Li, Dr. Robert Phillips, Dr. Elizabeth Baronowsky, Dr. Matthew Ward, and Dr. Mark Sayles for their technical trainings in various aspects. Without their help, I cannot become who I am today. I also appreciate the help from Dr. Deborah Jaffey, Dr. Zhenjun Tan, and Dr. Nicholas Race for their generous and kind help in experiments and scientific investigations.

Last but not Least, I would like to thank my parents, my daughter, and my husband Dr. Zhenhua Hu. It's such a blessing to have their love and support every day. I cannot finish this long journey without their companion.

Table of Contents

List of Tables

List of Figures

List of Abbreviations

ANOVA	One-way analysis of variance
BOLD	Blood-oxygen-level-dependent
BS	Brainstem
CNS	Central nervous system
CPM	Cycles per minute
Cpu	Dorsal caudate putamen
DMV	Dorsal motor nucleus of the vagus
EGG	Electrogastrogram
ENS	Enteric nervous system
EPI	Echo planar imaging
FA	Flip angle
FGID	Functional gastrointestinal disorder
fMRI	Functional magnetic resonance imaging
FWHM	Full width at half maximum
GE	Gradient echo
GES	Gastric electrical stimulation
GI	Gastrointestinal
GLM	General linear model
GMA	Gastric myoelectrical activity
HADS	Hospital anxiety and depression scale
HRF	Hemodynamic response function
IC	Independent component
ICA	Independent component analysis
ICC	Interstitial cells of Cajal
IGLE	intra-ganglionic laminar ending
IMA	Intramuscular array

LFP	Local field potential
MRI	Magnetic resonance imaging
MUA	Multi-unit activity
NTS	Nucleus tractus solitarius
OSI	Orientation selectivity index
PAG	Periaqueductal gray
PBC	Parabrachial complex
PSD	Power spectrum density
PSTH	Post-stimulus time histogram
RARE	Rapid acquisition with relaxation enhancement
ROI	Region of interest
RSC	Retrosplenial cortex
S1FL	Primary somatosensory cortex, forelimb region
SpO_2	Oxygen saturation level
SUA	Single-unit activity
TE	Effective echo time
TR	Repetition time
VNS	Vagus nerve stimulation

Abstract

The stomach and the brain interact closely with each other. Their interactions are central to digestive functions and the "gut feeling". The neural pathways that mediate the stomach-brain interactions include the vagus nerve and the thoracic nerve. Through these nerves, the stomach can relay neural signals to a number of brain regions that span a central gastric network. This gastric network allows the brain to monitor and regulate gastric physiology and allows the stomach to influence emotion and cognition. Impairment of this gastric network may lead to both gastric and neurological disorders, e.g., anxiety, gastroparesis, functional dyspepsia, and obesity. However, the structural constituents and functional roles of the central gastric network remain unclear.

In my dissertation research, I leveraged complementary techniques to characterize the central gastric network in rats across a wide range of scales and different gastric states. I used functional magnetic resonance imaging (fMRI) to map blood-oxygen-level-dependent (BOLD) activity synchronized with gastric electrical activity and to map brain activations induced by electrical stimulation applied to the vagus nerve or its afferent terminals on the stomach. I also used neurophysiology to characterize gastric neurons in the brainstem in response to gastric electrical stimulation.

My results suggest that gastric neurons in the brainstem are selective to the orientation of gastric electrical stimulation. This electrical stimulation can also evoke neural activity beyond the brainstem and drive fast blood oxygenation level dependent (BOLD) activity in the central gastric network, primarily covering the cingulate cortex, somatosensory cortex, motor cortex, and insular cortex. Stimulating the vagus nerve – the primary neural pathway between the stomach and the

brain, can evoke BOLD responses across widespread brain regions partially overlapped with the brain network evoked by gastric electrical stimulation. BOLD activity within the gastric network is also coupled to intrinsic gastric activity. Specifically, gastric slow waves are synchronized with the BOLD activity in the central gastric network. The synchronization manifests itself as the phase-coupling between BOLD activity and gastric slow waves as well as the correlation between BOLD activity and power fluctuations of gastric slow waves. This synchronization is primarily supported by the vagus nerve and varies across the postprandial and fasting states.

My dissertation research contributes to the foundation of mapping and characterizing the central and peripheral mechanisms of gastric interoception and sheds new light on where and how to stimulate the peripheral nerves to modulate stomach-brain interactions.

Chapter 1 Introduction

Summary

The stomach and the brain are two major organs in mammals and have tonic interactions with each other (Furness and Stebbing, 2018). Their bi-directional interactions (Carabotti et al., 2015) are important for maintaining gastric function (Holtmann & Talley, 2014). Impaired stomach-brain interactions can lead to both gastric and brain disorders, such as gastroparesis (Ali et.al, 2017; Camilleri et al., 2018), functional dyspepsia (Tack et al., 2004; Talley & Ford, 2015), and anxiety (Haug et al., 2002; Klarer et al., 2014). So far, gastric electrical stimulation (GES) (Abell et al., 2003; Cigaina, 2002) and vagus nerve stimulation (VNS) (Paulon et al., 2017; Pardo et al., 2007) are two promising techniques that have the potential to modulate the stomach-brain interaction for treatment of drug-refractory gastric or neurological disorders. The therapeutic effects of GES and VNS, however, are variable across individuals and conditions, due to the lack of functional characterization of the stomach-brain interaction.

Current knowledge about the structural pathways between the stomach and the brain has been increasingly complete (Browning & Travagl, 2011; Levinthal & Strick, 2020). There are two major neural pathways connecting the brain and the gut: the vagus nerve and the great thoracic splanchnic nerve (Furness et al., 2020). Both pathways send afferent signals to the brain and convey efferent commands to the stomach. In the brain, the dorsal vagal complex consists of the nucleus of the solitary tract (NTS) and the dorsal motor nucleus of the vagus (DMV). NTS and DMV are the major nuclei that monitor and control gastric functions. The NTS neurons integrate signals from the stomach. The DMV neurons send commands back to the stomach (Travagli &

Anselmi, 2016). The dorsal vagal complex projects to and receives inputs from many other brain regions within and beyond the brainstem (Browning & Travagli, 2011). These connections may be responsible for interacting with cognitive processes and other visceral functions (Craig, 2009; Mayer, 2011; Van Oudenhove et al., 2004). However, anatomical mapping does not readily reveal the functional interactions along the peripheral and central pathways.

Given the current understanding about the stomach-brain neuroaxis, my dissertation aimed to assess the effects of VNS and GES on the stomach-brain interaction and to decode the information flow between the stomach and the brain within and beyond the brainstem. Specifically, we aimed to apply GES and VNS, assess the neural response in the brainstem and beyond, and evaluate their effects on gastric motility. We also aimed to map neural activity in the brain coupled to intrinsic gastric activity. In particular, we focused on gastric motility, or the peristaltic contraction of the stomach, in terms of the frequency and amplitude, and to assess how such mechanical features were coded and relayed by vagal nerve signaling and how they were processed and represented by the brain. For these aims, we used anesthetized rats in preclinical studies.

Anatomy and function of the stomach-brain neuroaxis

Anatomy and function of the stomach

The stomach is an essential organ in the digestive system (Furness et al., 2014; Furness and Stebbing, 2018; Lacy & Weise, 2005). It has three compartments, including the fundus (sometimes referred to the forestomach for rats), corpus, and antrum (Figure 1-1). The fundus can change its luminal volume for food storage. The corpus and the antrum can generate gastric contractions for food grinding and mixture (Boeckxstaens et al., 2016). These functions are carried out by two muscular sheets, running in the longitudinal and circular directions. In the fundus, gastric smooth muscles maintain the luminal volume through the regulation of contraction and relaxation. In the

corpus and the antrum, smooth muscles are electrically coupled to propagate contractions like a wave with a temporal frequency around three cycles per minute (CPM) in humans and 4-6 CPM in rats. The stomach contains thousands of interstitial cells of Cajal (ICC) and an intrinsic nervous system to support the coordinated contractions, named the enteric nervous system (ENS) (Hansen, 2003). ICCs can generate spontaneous oscillations, serving as a clock to orchestrate gastric smooth muscles (Sanders et al., 2006). In the meantime, gastric motor neurons in the ENS modulate gastric smooth muscles to achieve specific patterns of contractions.

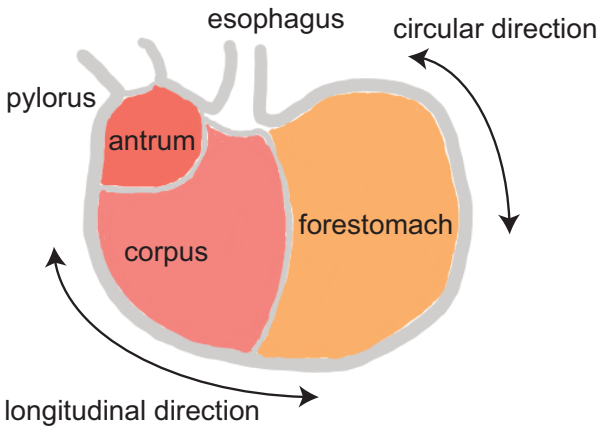

Figure 1-1 Anatomical compartments of the rat stomach

Stomach-brain interaction

The stomach is not an isolated organ but extends neural connections to the brain. The stomach sends gastric information to the brain and receives commands from the brain (Furness et al., 2014, Rogers et. al., 1995), to form bi-directional interactions. The interaction is supported by the vagus nerve (i.e., parasympathetic pathway) and the great thoracic splanchnic nerve (i.e., sympathetic pathway) (Furness et al., 2020) and is critical in maintaining the normal gastric function (Van Oudenhove et al., 2004). 65% of gastric motor neurons receive inputs from the vagal efferents and can be directly modulated by the dorsal vagal complex in the brainstem (Berthoud et al., 1990). The stomach-brain interaction also helps the brain monitor gastric activity. In contrast

to the vagal efferent fibers, 70-80% of the vagus nerve are afferents (the percentage varies across species) (Patterson et al., 2002). In healthy physiological conditions, the stomach-brain interaction plays a critical role in supporting basic gastric reflexes, such as the esophago-gastric reflex that relaxes the forestomach with triggers of esophageal distension (Rogers et al., 1999), enterogastric reflex that weakens gastric motility given stretches in the duodenum (Schapiro & Woodward, 1959), and gastrocolic/gastroileal reflex that promotes colic and ileal contractions after the presence of food in the stomach (Malone & Thavamani, 2020). Impairment in the stomach-brain interaction can lead to changes in gastric sensation, visceral hypersensitivity, unregulated gastric motility, and delayed gastric emptying (Ali et.al, 2017; Camilleri et al., 2018; Tack et al., 2004; Talley & Ford, 2015).

Vago-vagal reflex

There are two major pathways connecting the stomach and the brain: the vagus nerve and the great thoracic splanchnic nerve (Furness et al., 2014, Rogers et. al., 1995). Results from histological studies suggest that the vagus nerve is more important in sensing and modulating the gastric motility, whereas the great thoracic splanchnic nerve dominates the sensation and control of vasoconstriction (Brookes et al., 2013; Furness et al., 2014). Because gastric motility is more important for the function of food grinding and emptying (Camilleri et al., 1985; Ehrlein & Schemann, 2005; Horowitz et al., 1994), most studies target the vagus nerve when studying the role of stomach-brain interactions in digestive functions (Payne et al., 2019).

Sensory receptors of vagal afferents include the intra-ganglionic laminar endings (IGLEs), intramuscular arrays (IMAs), and mucosal arbors (Brookes et al., 2013; Powley et al., 2019). Among these receptors, IGLEs co-occur with the ganglia of the myenteric plexus and likely serve as tension receptors. IMAs lay in parallel to gastric smooth muscles and likely serve as stretch

receptors. Gastric mucosal arbors sit in the mucosal or submucosal layer and respond to different contents in gastric chyme. All receptors connect to the nucleus tractus solitarius (NTS) through the vagus nerve, with cell bodies sitting in the nodose ganglia. Neurons in NTS receive gastric inputs through the vagus nerve and directly project to the dorsal motor nucleus of the vagus (DMV) (Rogers et al., 1995; Travagli & Anselmi, 2016). DMV neurons send vagal efferents to innervate the ganglia in the myenteric plexus between gastric smooth muscle layers. Efferent vagal terminals selectively target nitrergic and cholinergic ganglionic cells to regulate the contraction and relaxation of gastric smooth muscles, respectively (Powley et al., 2019; Travagli et al., 2006). The vagal afferents and efferents, together with interconnections between NTS and DMV, underlies the vago-vagal reflex.

One classic vago-vagal reflex is gastric accommodation (Harper et al., 1959; Tack et al., 2002; Takahashi & Owyang, 1997). The reflex starts once food gets into the stomach. Gastric sensory receptors in the antrum detect gastric chyme and send signals to NTS. The information is further relayed to DMV. DMV sends motor commands back to the stomach and dilate the fundus to accommodate the incoming food. This process continues during meal consumption and allows the stomach to expand appropriately to match the food volume. Failure in this reflex can restrict gastric distension, cause high gastric pressure, delay gastric emptying, and lead to gastroesophageal reflux (Tack et al., 1998).

Neural connections in the central gastric network

NTS and DMV are the central nuclei in the brainstem and form the dorsal vagal complex as the relay station between the stomach and the forebrain (Rogers et al., 1995; Travagli et al., 2003). As illustrated in Figure 1-2, NTS neurons project to many other nuclei (Browning & Travagli, 2011). The parabrachial complex (PBC) and periaqueductal gray (PAG) are primary

targets along the pathway from NTS to the forebrain. PBC is essential to integrating gustatory and gastrointestinal sensory information. It projects to the thalamus, striatum, insular cortex, amygdala, and hypothalamus, and receives projections from the insular cortex, medial prefrontal cortex, striatum, amygdala, and hypothalamus. PBC also directly projects back to NTS and DMV to regulate the vagal activity. In contrast, PAG is more critical to autonomic processing and integrating autonomic and emotional information. PAG projects to the anterior cingulate cortex, medial prefrontal cortex, amygdala, and hypothalamus, and receives projections from the amygdala and hypothalamus. PAG is more directly involved in sympathetic regulation. Moreover, the cerebellum is also involved in the central gastric network. It receives inputs from other gut-related nuclei and projects to NTS and DMV directly. Most recent histological studies also uncovers that the somatosensory and motor cortex and the insular cortex interact with the stomach through the sympathetic and parasympathetic pathways, respectively (Levinthal & Strick, 2020), and the hippocampus is partially engaged in the gastric network through the striatum (Suarez et al., 2018).

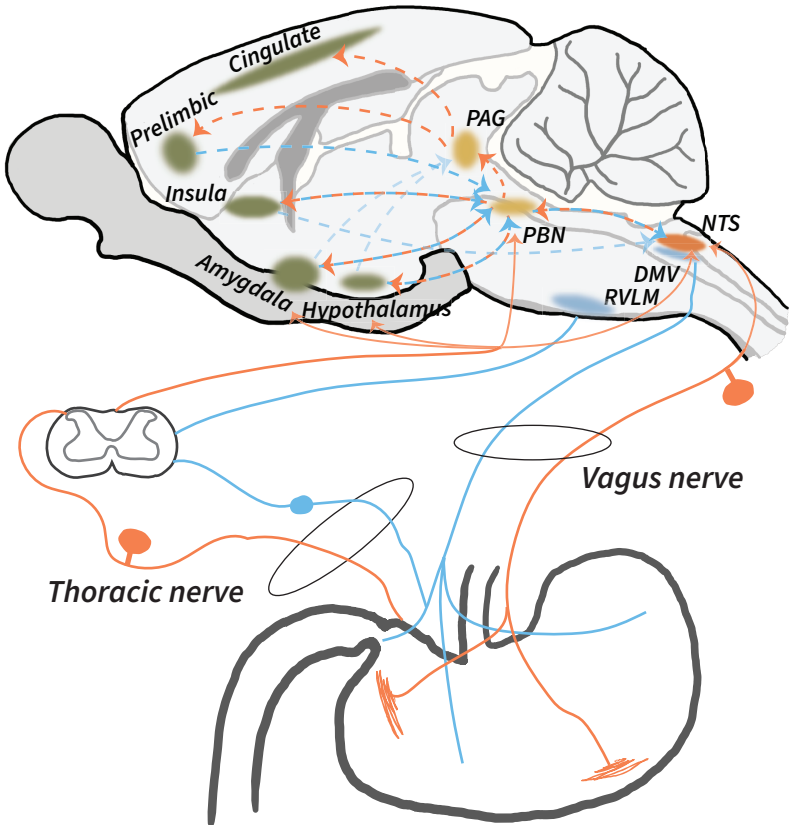

Figure 1-2 Stomach-brain neuroaxis*. For peripheral and central circuits, red lines illustrate afferent and ascending pathways; blue lines illustrate efferent and descending pathways.*

Current understanding of the stomach-brain interaction

Functional characterization of the stomach-brain interaction remains largely unclear. Most studies focus on structural connections between the stomach and the brain rather than functional representation and information processing. Many histological studies have identified different sensory receptors on the stomach wall as well as their ultrastructural phenotypes (Brookes et al., 2013; Furness et al., 2014; Powley et al., 2019). The functional roles of those receptors remain largely speculative. Limited knowledge is available as to how the brain processes gastric information. One may generate hypotheses about how the brainstem processes gastric information given existing knowledge about the neural connections between the dorsal vagal complex and other nuclei (Browning & Travagl, 2011). However, the connections beyond the brainstem and

toward the forebrain are complex and involve many regions central for a wide range of cognitive and emotional functions (e.g., the insula, striatum, cingulate cortex, medial prefrontal cortex, amygdala (Browning & Travagli, 2011; Farmer et al., 2018; Levinthal & Strick, 2020).

Besides the histological studies, some functional studies use external stimulation to study the stomach-brain interaction (Ladabaum et al., 2001; Min et al., 2011; Wang et al., 2008). In those studies, a balloon is inserted into the stomach; the volume of the balloon can be modulated using fluid infusion to stretch the stomach wall. The mechanical distention can mimic different volumes of the food content to study how the brain responds to a varying stomach volume. However, the balloon-based stimulation has limitations. First, the extended balloon stretches the stomach in a way different from naturalistic gastric distension given food intake. It does not involve nutrient handling alongside gastric accommodation. Second, the balloon stimulation only provides static stretching but does not involve peristaltic contractions (Camilleri et al., 1985; Ehrlein & Schemann, 2005). Thus, most understanding is through non-physiological probing of the system.

Diseases related to the impaired stomach-brain neuroaxis

Gastric disorders

Functional gastrointestinal disorders (FGIDs) are in part related to the impaired gut-brain interaction. FGIDs refer to dysregulations in different segments of the gastrointestinal (GI) tract. Depending on the specific locations, FGIDs can be specified as functional dyspepsia, nausea and vomiting disorders, irritable bowel disease, functional diarrhea, and functional constipation. Each of these diseases has at least one of the following chronic symptoms: heartburn, delayed gastric emptying, early fullness, nausea, vomiting, bloating, abdominal pain, diarrhea, or constipation (Drossman, 2016). FGIDs are commonly. According to a recent study, more than 40% of people suffer from FGID worldwide (Sperber et al., 2021). A major cause of FGIDs is the impairment in

the interaction between the gut and the brain. This impairment can originate from the GI tract, the central autonomic nervous system, or the nervous or endocrine connections between the GI tract and the brain (Drossman, 2016). None of these impairments is associated with tumors or local inflammation. FGID is often hard to diagnose with existing clinical exams, such as CT, X-ray, and endoscopy. The diagnosis of FGID relies on repeated doctor visits to rule out other potential GI diseases.

Functional dyspepsia is one of the FGIDs related to the stomach. One of the major causes of functional dyspepsia is that the stomach fails to accommodate the food, likely reflecting a failure in the vago-vagal reflex that controls the distension of the stomach (Enck et al., 2017; Tack et al., 2004; Talley & Ford 2015). The impairment of gastric accommodation causes a high luminal pressure (Tack et al., 1998). The high pressure leads to many gastric symptoms, such as early fullness (satiety), nausea, belching, bloating, and slow emptying. Functional dyspepsia is a common disorder that affects nearly 20% of the general population worldwide and causes a big financial burden to individuals and the society (Ford et al., 2020; Lacy et al., 2009; Stanghellini, 2016; Talley & Ford, 2015).

Gastroparesis is another gastric disorder related to the impaired stomach-brain interaction. Gastroparesis refers to the paralyzed stomach that cannot empty normally, thus causing various gastric symptoms, including delayed gastric emptying, early fullness, bloating, nausea, and vomiting (Ali et al., ,2007; Camilleri et al., 2018; Lacy & Weiser, 2005). There are three types of gastropareses, including diabetic gastroparesis, post-surgical gastroparesis, and idiopathic gastroparesis. Both the diabetic and post-surgical gastropareses are caused by damage to the stomach-brain neuroaxis due to either high blood glucose or structural damage during a surgery. Idiopathic gastroparesis has unknown causes but is possibly related to epilepsy or migraine

induced dysregulation of the central and/or autonomic nervous system. The population affected by gastroparesis shares the similar symptoms with other gastric disorders (functional dyspepsia). According to an early study, gastroparesis affect one out of two thousand people in the US (Jung et al., 2009). However, this number is likely under-estimated, because of the high relevance between diabetes and gastroparesis. Based on the population of diabetic patients, an estimation suggests that there are more than 1.5 million people suffering from severe gastroparesis in the US alone (Gastroparesisclinic.org, 2014).

Brain disorders

Anxiety and depression are also associated with the impaired stomach-brain interaction. Previous studies have identified a significant association between FGIDs and anxiety/depression symptoms (Drossman et al., 1999; Haug, et al., 2002; Haug et al., 2002; Levy et al., 2006; Mayer, 2000). Patients with FGIDs have greater hospital anxiety and depression scale (HADS) scores than healthy ones (Aro et al., 2009; Hartono et al., 2012). The percentage of anxiety and depression in FGID patients is much higher than the general population (Kani et al., 2019; Woodhouse et al., 2017). The association between anxiety or depression and gastric disorders is not surprising since the central gastric network includes many regions associated with emotion regulation, including the amygdala, medial prefrontal cortex, cingulate cortex, and periaqueductal gray (Browning & Travagli, 2011). An animal study also reports that rats without vagal innervation to the gut can develop anxiety-like behavior (Klarer et al., 2014).

Treatments for repairing the stomach-brain neuroaxis

Gastric electrical stimulation (GES)

GES is an FDA-approved therapy for drug-resistant gastroparesis of diabetic and idiopathic etiology (Abell et al., 2003; U.S. Food and Drug Administration, 2000). It is initially designed to

pace gastric contractions, with high-amplitude long-duration currents (pulse width, 10-600ms, current, ~5mA) to entrain contractions. Gastric pacing has not become widely accepted because of its high-power consumption and inconsistent effects on gastric emptying (Yin & Chen, 2008). As an alternative, high-frequency and short-duration pulses (pulse width, ~0.3-3ms; inter-pulse duration, ~0.07s; stimulation pattern, 0.1s-ON-5s-OFF) are used in the commercial stimulator known as Enterra (Gonzalez and Velanovich, 2010; McCallum et al., 2010, 2013). Enterra therapy (Medtronic, Minneapolis, MN, USA) may be effective in relieving nausea and vomiting. Its efficacy is still variable across patients (Lal et al., 2015; Levinthal & Bielefeldt, 2017). This inconsistency is likely due to the unclear working mechanism of GES. One hypothesis about the mechanism is related to the stomach-brain neuroaxis. That is, GES can relieve discomforts and promote gastric emptying through its ascending signaling to the central nervous system (CNS) (Mayer et al., 2006; Payne et al., 2019). GES may activate multiple central nuclei, including the NTS (Qin et al., 2005) and the paraventricular nucleus of the hypothalamus (Tang et al., 2006). However, it remains largely unclear how to parameterize GES to activate CNS and whether and how the CNS activations with GES depend on the location, orientation, amplitude, and frequency of GES. Addressing these questions may help improve the efficacy and reliability of GES.

Vagus nerve stimulation (VNS)

VNS is a promising technique for modulating visceral organs, including the gut (Paulon et al., 2017; Payne et al., 2019). The vagus nerve is the primary neuronal pathway that connects the brain with the stomach (Carabotti et al., 2015, Furness et al., 2020). Stimulating the vagus nerve can directly affect the stomach through the efferent pathway (Schemann & Grundy, 1992) and alter the neural activity in the brain through the efferent pathway (Hachem et al., 2018). Whereas VNS often requires surgical implantation of a device, transcutaneous stimulation applied to the

neck or the ear may activate the vagus nerve non-invasively (Farmer, 2020; Gottfried-Blackmore et al., 2020; Weinkauf et al., 2005). This noninvasive technique makes VNS an inexpensive and accessible alternative therapy for a larger patient population. It may bring more treatment options for patients with gastric disorders. However, VNS is still explored mostly in preclinical studies. The working hypothesis is that VNS can activate gastric centers in the brain and trigger descending motor commands to modulate gastric physiology (Payne et al., 2019). It is thus of interest to map the VNS response in the brain in comparison with the central gastric network.

Assessing the intrinsic stomach-brain interaction

Assessing neural activity in the brain

Functional magnetic resonance imaging (fMRI) is the primary technique used here to measure brain activity and map functional brain networks. FMRI measures T_2*-weighted signals, reflecting the blood-oxygen-level-dependent (BOLD) fluctuations (Ogawa et al., 1990a, 1990b, 1992). The active vasodilation feeds more oxygenated blood to over-compensate for the metabolic consumption of oxygen by neural activity (Hillman, 2014; Logothetis & Wandell, 2004). This makes the BOLD signal as a hemodynamic surrogate of neural activity. Neural activity can increase regional cerebral blood flow and volume, leading to a net increase in the BOLD signal. The relationship between neural activity and the BOLD signal is often modeled as the hemodynamic response function (HRF). It describes the neurovascular coupling as the transfer function of a linear system, of which the output is the BOLD response given an impulse input (neural activity). HRF is similar to a double-gamma function, with a peak delay of 5~6s in humans (Buxton et al., 2004; Ogawa et al., 1998) and ~3s in rodents (Martindale et al., 2003; Weber et al., 2004). In summary, fMRI measures BOLD activity, which is a slow signal accompanying neural activity.

In this study, multi-unit activity (MUA) recordings were also used to directly measure neural activity. When a neuron fires, ions (e.g., sodium, potassium, and calcium) flow across the cell membrane, triggering an action potential. Occurrences of action potentials induce extracellular changes of the field potential, named spikes, which can be captured by the penetrating electrodes, such as the Michigan and Utah arrays (Bean, 2007; Gold et al., 2006). Depending on the distance between neurons and electrodes, one recording electrode can capture spikes from multiple neurons, named MUA recordings. MUA recordings allow the assessment of neural activity with high throughput but yield low specificity to individual neurons. This drawback can be solved with a post-processing technique, named spike sorting, which utilizes shape differences of spikes from different neurons. The shape of each spike depends on the distance and orientation of the recording electrode with respect to the activated neuron (Buzsáki, 2004). As such, the shape features of individual spikes can be sorted to identify neurons that generate the spikes, and the spike timing of individual neuron can be generated to represent the single-unit activity (SUA) (Lewicki, 1998).

Assessing gastric activity

Gastric myoelectrical activity (GMA) reflects the electrical activity of smooth muscles as well as that of interstitial cells of Cajal (ICCs) that innervate the smooth muscles. GMA measures the electrical potential on the serosal layer of the stomach (Abell & Malagelada, 1988; Code & Marlett, 1975). It is a mixture of gastric slow waves and myoelectrical activity from gastric smooth muscles. Gastric slow waves are rhythmic activity initiated by ICC and propagating from the corpus to the antrum. The normal frequency of gastric slow waves is around three cycles per minute (CPM) in humans and 4-6 CPM in rats. The frequency of gastric slow waves can be slower (bradygastria) or faster (tachygastria) (Chen et al., 1995). It serves as a clock and sets the frequency of muscle contractions. Importantly, gastric smooth muscles are modulated by motor neurons in

the enteric nervous system (Furness et al., 2020). The changes in the contractile amplitude is presumably correlated with the power fluctuation of GMA with a higher power corresponding to a stronger contraction. Therefore, GMA is closely related to gastric contractions. Its phase is coupled to muscle contraction. Its power co-fluctuates with the strength of muscle contraction.

Electrogastrogram (EGG) is a noninvasive measurement of gastric electrical activity (Parkman et al., 2003). The electrical current running on the stomach causes far-field changes in electrical potential observable on the body surface (Du et al., 2010; Wolpert et al., 2020; Smout et al., 1980). Similar to GMA, EGG also reflects gastric slow waves and gastric contractions. EGG can be decomposed into phase, amplitude, and frequency fluctuations, reflecting contraction cycle, contraction strength, and slow-wave frequency, respectively (Chen J, McCallum RW, 1991). EGG recording is noninvasive, thus allowing easier translational studies on humans.

Combining techniques to study the stomach-brain interaction

My study combined brain fMRI with EGG/GMA to study the stomach-brain interaction. EGG reflects gastric electrical activity coupled to gastric motility (Smout et al., 1980; Yin & Chen, 2013), and fMRI measures the BOLD fluctuations related to neural activity throughout the brain (Fox & Raichle, 2007). EGG-fMRI allows us to investigate the intrinsic coupling between the stomach and the brain, without applying external stimulation to the stomach, such as the balloon extension as commonly used in previous studies (Ladabaum et al., 2001; Wang et al., 2008).

Contents of this dissertation

This dissertation summarizes findings from my studies aimed to delineate the functional activity in the stomach-brain interaction with external stimulation and during intrinsic gastric conditions.

Chapter 2 focuses on GES and introduces a new stimulating strategy targeting one type of gastric sensory receptors of the vagus. The effects of stimulation was assessed with multi-unit and single-unit activity in the nucleus tractus solitaries (NTS) in rats. The stimulation paradigm was optimized to maximize neural activity in NTS.

In Chapter 3, the effects of GES were further evaluated in the forebrain regions using fMRI in rats. The feasibility of using fMRI to map the GES evoked response was first confirmed. Then fMRI was used to map the central network activated with gastric stimulation.

The study in Chapter 4 also combined peripheral stimulation with fMRI mapping. The stimulation was applied to the vagus nerve, the primary neural pathway between the stomach and the brain. The effects of the vagus nerve stimulation were assessed by applying model-free analysis to the fMRI signals for mapping brain activations with VNS.

Studies in Chapters 5 & 6 mapped neural activity in the brain in response to intrinsic gastric activity. Gastric activity measured as either EGG or GMA was recorded simultaneously with brain fMRI in rats. The gastric representation in the brain was evaluated in terms of the phase-coupling and power correlation between the EGG/GMA and fMRI signals. The intrinsic relationship between the brain and the stomach was assessed in both postprandial and fasting states and with or without vagotomy to test whether and how the stomach-brain interactions were dependent on the gastric state or the vagal signaling.

Chapter 2 Neurons in the Nucleus Tractus Solitarius are Selective to the Orientation of Gastric Electrical Stimulation [1]

Summary

Gastric electrical stimulation (GES) is a bioelectric intervention for gastroparesis, obesity and other functional gastrointestinal disorders. In a potential mechanism of action, GES activates the nerve endings of vagal afferent neurons and induces the vago-vagal reflex through the nucleus tractus solitarius (NTS) in the brainstem. However, it is unclear where and how to stimulate in order to optimize the vagal afferent responses. To address this question with electrophysiology in rats, we applied short electrical currents to two serosal hotspots on the distal forestomach with dense distributions of vagal intramuscular arrays that innervated the circular and longitudinal smooth muscle layers. During stimulation, we recorded neurophysiological responses in NTS and evaluated the dependence of the recorded responses on the stimulus orientation and amplitude. We found that NTS neuronal responses were highly selective to the stimulus orientation for a range of stimulus amplitudes. The strongest responses were observed when the applied current flowed in the same direction as the intramuscular arrays in parallel with the underlying smooth muscle fibers. Our results suggest that gastric neurons in NTS may encode the orientation-specific activity of gastric smooth muscles relayed by vagal afferent neurons. This finding suggests that the orientation of gastric electrical stimulation is critical to effective engagement of vagal afferents and should be considered in light of the structural phenotypes of vagal terminals in the stomach.

[1] The contents of this chapter will be submitted for review with Journal of Neuroscience (Cao et al., in submission)

Introduction

The vagus is the primary neural pathway connecting the brain and the stomach. Vagal afferents ascend sensory signals from the stomach to the nucleus tractus solitarius (NTS). Vagal efferents convey motor commands from the dorsal motor nucleus of the vagus (DMV) to regulate gastric functions. The vagus connects the central nervous system and the enteric nervous system (Powley et al., 2019), mediates rapid stomach-brain interactions (Carabotti et al., 2015; Furness and Stebbing, 2018; Mayer, 2011), and enables reflexive control of the gastrointestinal tract (Davis et al., 1986; De Ponti et al., 1987; Rogers et al., 1995; Browning & Travagli, 2011; Travagli & Anselmi, 2016).

Both vagal afferents and efferents innervate the stomach with extensive and specialized terminals in the stomach wall (Powley et al., 2019). Although there has been increasing progress made in describing the structural phenotypes of vagal projections to the stomach, very little is known about the specific gastric information transmitted to and encoded by the brain. In particular, it is unclear how NTS, as the first brainstem nucleus responsible for visceral sensation, represents and integrates gastric information relayed through vagal afferents.

Gastric electrical stimulation (GES) is an FDA-approved therapy for drug-resistant gastroparesis of diabetic or idiopathic etiology (Abell et al., 2003; U.S. Food and Drug Administration, 2000). GES works well in relieving nausea and vomiting but yields inconsistent responses across patients (Lal et al., 2015; Levinthal & Bielefeldt, 2017). This inconsistency is likely due to the unexplained working mechanism of GES. One hypothesis of the GES mechanism relates to the stomach-brain neuroaxis, stating that GES can relieve discomforts and promote gastric emptying through its modulatory effects in the central nervous system (CNS) (Mayer et al., 2006; Payne et al., 2019). Multiple central nuclei have been reported to respond to GES, including

NTS (Qin et al., 2005) and the paraventricular nucleus of the hypothalamus (Tang et al., 2006). However, it is unclear about effective stimulating paradigms in activating CNS neurons and whether the varying stimulating targets, orientations, and current evoke neural activity differently. It is necessary to address these questions since the well-delineated GES protocol can help achieve efficient and consistent therapeutic effects across patients.

Although there is insufficient knowledge on the working mechanism of GES and the explicit information flow in the stomach-brain interaction, the gastric innervation has been increasingly mapped (Browning & Travagli, 2011; Furness et al., 2020; Powley & Phillips, 2002). The stomach-brain interaction is supported by the vagus nerve and thoracic spinal nerve containing efferent and afferent fibers. The efferents innervate neurons in NTS and the spine to modulate gastric secretion, blood volume in the gastric wall, and smooth muscle contractions; the afferents receive neural inputs from various sensory receptors and convey chemical and mechanical information to the brain (Brookes et al., 2013). There are five types of gastric receptors, in which the intramuscular array (IMA) is proposed to detect stretches of gastric smooth muscles due to its unique array-like structure (Powley et al., 2016). IMAs have two subtypes distinguished by their orientations. One lies in the longitudinal direction (i.e., longitudinal IMA); the other is in the circular direction (i.e., circular IMA). It is of great interest to study IMAs due to the importance of their hypothesized function in monitoring stretches of gastric smooth muscles.

Here, we focused on the GES-evoked activation of IMAs. Given the unique structure of these receptors, we hypothesized that IMAs are selective to the stimulating orientation. To test this hypothesis, we chose two targets in the rat's distal forestomach with high IMA densities and applied stimulation over these regions with electrical currents flowing in different orientations. We monitored the post-stimulus spiking activity in NTS neurons to test whether NTS neurons would

respond to the stimulus and whether the response was orientation-selective. The orientation-selectivity was examined using multi-unit activity (MUA) and single-unit activity (SUA) and confirmed at two stimulation sites with varying current amplitudes. The successful confirmation could yield an efficient stimulating strategy of activating IMAs and engaging the stomach-brain neuroaxis.

Materials and Methods

Subjects

This study used seven Sprague–Dawley rats (male, weight: 250–400 g; Envigo RMS, Indianapolis, IN) according to a protocol approved by the Institutional Animal Care and Use Committee and the Laboratory Animal Program at Purdue University. All animals were housed in a strictly controlled environment (temperature: 21 ± 1 °C; 12 h light-dark cycle with light on at 6:00 a.m. and off at 6:00 p.m.). Every animal received acute surgical implantation of patch electrodes for gastric electrical stimulation and depth electrodes for neuronal recordings in the brainstem.

Electrode implantation for gastric electrical stimulation

Every animal received an abdominal surgery to be implanted with patch electrodes on the serosal surface of the distal forestomach. The animal was initially anesthetized with 5% isoflurane mixed with oxygen (flow rate: 1 L/min). The dose of isoflurane was then reduced to 2% to keep a surgical plane. Then, the animal was placed in a supine position on the surgical table. Following a toe-pinch test, an incision was made starting from the xiphoid and moving 4 cm caudally. Skin and muscle layers were retracted and separated to expose the ventral forestomach.

Patch electrodes (Microprobes, Gaithersburg, MD, USA) were sutured at two target locations, namely Target 1 and 2, on the serosal surface of the distal forestomach (Figure 2-1A).

Target 1 was on the greater curvature and about 4 mm away from the limiting ridge. Target 2 was on the ventral stomach, 2 mm away from the limiting ridge, and halfway in between the lesser curvature and the greater curvature. According to our previously mapped distributions of longitudinal and circular IMAs (Powley et al., 2016; Tan et al., 2021), Target 1 had a high density of longitudinal IMAs but a low density of circular IMAs (Figure 2-2A), whereas Target 2 had a high density of circular IMAs but a low density of longitudinal IMAs (Figure 2-2D). Target 1 and Target 2 were chosen as complementary targets selective to the "hotspots" of longitudinal and circular IMA, respectively.

Each patch electrode consisted of either 1 or 2 bipolar pairs of contacts. Each contact was made of a Pt/Ir foil (12 mm^2) on a thin perylene substrate (77 mm^2) and was positioned 2 mm away from the center of the substrate. Each bipolar pair was oriented for current delivery along either the longitudinal or circular direction. We attached 2 bipolar pairs of electrodes on Target 1 for four animals, 2 bipolar pairs of electrodes on Target 2 for four animals, and 1 bipolar pair of electrodes on Target 1 for three animals (Table 2-1). We fixed the electrodes by securing the four corners of the substrate on the serosal layer. After electrode implantation, the muscle layer and the skin were closed with sutures, while the electrode wires were kept outside of the abdomen and were connected to a current stimulator (model 2200, A-M systems, Sequim, USA).

For each target location, electrical current was delivered in 4 plausible orientations: longitudinal pointing towards the proximal (0^o) or distal stomach (180^o) with one pair of electrodes, or circular pointing toward the lesser (90^o) or greater (270^o) curvature with the other pair of electrodes (Figure 2-2B). Current stimuli were delivered as a train of rectangular pulses (pulse width: 0.3 ms, pulse amplitude: 0.6, 0.8, or 1 mA with alternating polarity, and inter-stimulus-interval: 100 ms for two animals and 250 ms for the other five animals). A pulse train lasted 10 s

followed by a stimulus-free rest period of >20 s. Different pulse trains were configured to stimulate in either the longitudinal or circular direction in an order randomized and counter-balanced across animals.

Table 2-1 The number and orientation of the implanted electrodes in each animal. *The number of electrodes is specified with respect to the location (Target 1 vs. 2) and the direction (longitudinal vs. circular).*

Animal ID	Target 1		Target 2	
	Longitudinal	Circular	Longitudinal	Circular
1	2	2	0	0
2	2	2	0	0
3	2	2	0	0
4	2	2	2	2
5	2	0	2	2
6	2	0	2	2
7	2	0	2	2

Neurophysiological recording

To record neuronal spiking activity, we implanted a 32-channel silicon probe (Neuronexus, Ann Arbor, USA) in NTS for each animal. The surgery was performed by placing the animal in the prone position on a stereotaxic frame (Stoelting Co., Wool Dale, IL, USA). To expose the skull, a midline skin incision was made from the middle between the eyes to the neck. Two stainless steel screws were drilled into the skull above the olfactory bulb and were used as the ground and reference for neural recordings. A 5x5 mm^2 cranial window was created at the bottom of the occipital bone to expose the brainstem until the obex was identifiable.

The silicon probe was inserted at about 0-0.8mm left and 0-0.2mm rostral to the obex (Figure 2-1B & C). The depth of insertion was determined by using a searching process to identify gastric neurons in NTS. Specifically, gastric stimulation was delivered (pulse width = 0.3 ms, current = 1.0 mA, pulse frequency = 1 Hz), while the probe was being inserted into NTS. The insertion was stopped once the stimulus-evoked spiking activity was observable in one or multiple channels. See Figure 2-1D & E for the responses from the identified gastric neurons given a train of current stimuli. The searching process was repeated about 4 times to identify different groups of neurons, while each time the probe was pulled out and re-inserted to different depths (from 0.5 to 1.3 mm). At each depth of insertion, neural data was recorded from all 32 channels by using a broadband recording system (Tucker Davis Technologies, Alachua, USA) with a sampling rate of 24 kHz.

Single and multi-unit firing rate

We applied a high-pass filter (>300 Hz) to the raw signals to extract the neuronal spiking activity. First, unsorted spikes were identified if they surpassed a threshold (between 50 and 100 **μ**V) defined for each animal. The unsorted spikes were stored by channel as the multi-unit activity (MUA). Second, spike sorting was applied separately to each channel to extract the single-unit activity (SUA). The spike sorting extracted from each spike two features based on the peak-trough differences: the difference between the first peak and the trough (Feature 1) and the difference between the second peak and the trough (Feature 2). As illustrated in Figure 1F, the spike features were used to group every spike into distinct clusters where each cluster corresponded to a neuron. The clustering was based on the k-means clustering (kmeans in Matlab), where the distance between spikes was their Euclidean distance in the feature space. The number of clusters was

determined manually by visual inspection of the spike representations in the feature space. The sorted spikes across all channels were stored as SUA.

Based on the SUA or MUA, we evaluated the neuronal responses to gastric electrical stimulation in the level of either single neurons or neuronal ensembles, respectively. For each neuron, the SUA response was quantified as the number of spikes within the (100 ms) post-stimulus period in each trial of GES parameterized by its location (Target 1 & 2), direction (0^o, 90^o, 180^o, 270^o), and amplitude (0.6, 0.8, 1 mA). The single-trial SUA response was averaged across repeated stimuli with the same parameters and then across animals. Similarly, the time-averaged MUA response was quantified for each channel.

For a given location and amplitude of GES, the time-averaged MUA response was compared across four stimulus orientations (0^o, 90^o, 180^o, 270^o). The orientation that resulted in the highest MUA response was considered as the preferred orientation for each channel under evaluation. Then, the MUA response was averaged across channels and then across animals, to obtain the group averaged NTS responses as a function of the current amplitude (0.6, 0.8, 1 mA).

In addition to the time-averaged SUA or MUA response, we further evaluated the response as a function of the post-stimulus latency. The time-resolved response was based on the post-stimulus time histogram (PSTH). Specifically, the number of spikes was calculated within a 5 ms sliding window stepping by one time point (1/24 kHz) until reaching 100 ms after the stimulus. The fire rate (i.e., the number of spikes per 5ms) was averaged across repeated trials of the same stimulus setting. Neurons (for SUA) or channels (for MUA) that showed their maximal PSTH less than 0.05 spikes per 5 ms were discarded and excluded from subsequent analyses. Further, the PSTH was averaged within four coarsely defined post-stimulus periods of interest: 0-13 ms, 13-29 ms, 29-73 ms, and 73-100 ms.

Statistical analysis and orientation selectivity

We used paired t-test to evaluate the statistical significance of any response difference given GES applied in any two different orientations. The t-test was separately performed for the time-averaged SUA or MUA response averaged over the (100 ms) post-stimulus period. Bonferroni correction was used to correct for multiple comparisons (i.e., 6 pairs of different orientations for comparison). The significance level α was set as 0.05. Similarly, we also used paired t-test to evaluate the difference between GES applied to two different locations (i.e., Target 1 and 2).

We used an orientation selectivity index (OSI) to measure how a neuron (SUA) or neuronal ensemble (MUA) was selective to GES applied in the preferred orientation vs. other orientations. Specifically, let N_{PO} be the firing rate in response to GES in the preferred orientation (e.g., 0^o), and let N_i (i=1 to 3) be the firing rate in response to GES in the non-preferred orientations (e.g., 90^o, 180^o, 270^o). The OSI was the average difference in the firing rate between the preferred orientation and every non-preferred orientation, as expressed by Equation 2-1. The OSI was between 0 and 1. A higher value of OSI indicated that the neuron or channel under evaluation was more selective to the GES in one specific orientation.

$$OSI = \frac{\sum_{i=1}^{n=3}(N_{PO}-N_i)}{3} \qquad \textit{Equation 2-1}$$

We used a permutation test to evaluate the statistical significance of the OSI. Specifically, the SUA or MUA responses were randomly shuffled into different groups defined by the stimulus orientation. The shuffled dataset disrupted any real response-stimulus association. After repeating the process for 100,000 times and at each time evaluating the OSI with the shuffled dataset, a null distribution of OSI was generated. The real OSI was compared against this null distribution to calculate the *p* value.

Results

In 7 rats, we recorded single and multi-unit activity from gastric neurons in NTS while applying GES to two complementary regions of interest in the distal forestomach (Figure 2-1A): Target 1 with a high density of longitudinal IMA (Figure 2-1B left) and Target 2 with a high density of circular IMA (Figure 2-1B right). We evaluated the neuronal responses as a function of the orientation, location and amplitude of GES, with our special emphasis on the orientation selectivity of NTS.

Orientation dependence of NTS population responses to GES

When GES was delivered as a current pulse with a short width (0.3 ms) and a low amplitude (<1 mA), the stimuli were too brief and too weak to directly pace the stomach or induce muscle contractions (Du et al., 2009; Li & Chen, 2010; Tomita, 1966; Cheng et al., 2021). However, such GES could evoke population spikes (Figure 2-1D & E) observable with a 32-channel silicon probe inserted into NTS (Figure 2-1C). Figure 2-1D shows a typical MUA recording in NTS during a train of alternating currents delivered to Target 1 in two opposing directions (i.e., positive and negative pulses). In this example, many more spikes were observed following the negative pulses than following the positive pulses (Figure 2-1D). The spikes occurred shortly after each negative pulse (Figure 2-1E). By spike sorting (Figure 2-1F), two neurons were identified (Figure 2-1G) and their responses were observed mostly in the first 20 ms following the pulse (Figure 2-1H). This observation led us to hypothesize that gastric neurons in NTS were selective to the orientation of GES.

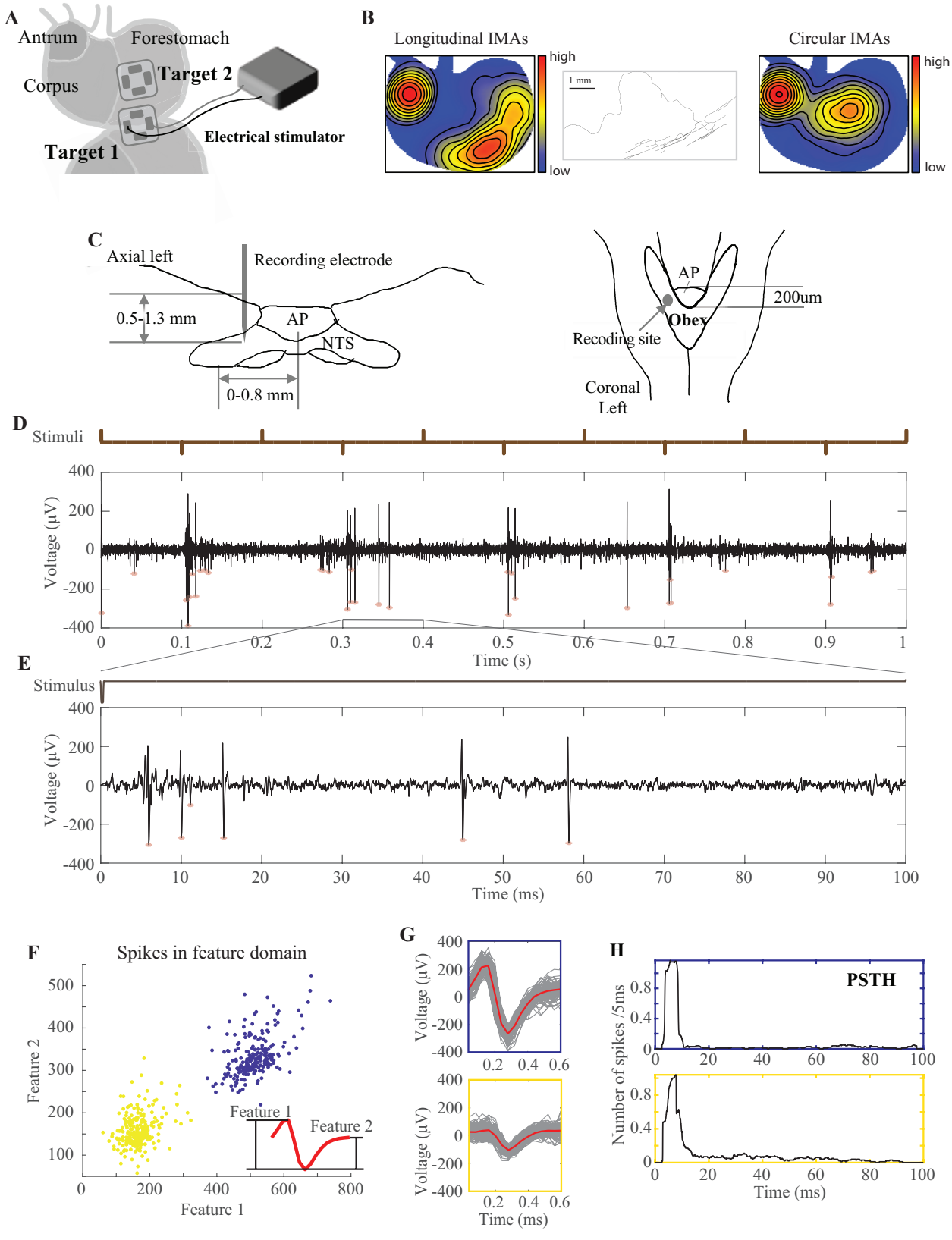
A
Antrum
Forestomach
Corpus
Target 2
Target 1
Electrical stimulator
B
Longitudinal IMAs
high
low
1 mm
Circular IMAs
high
low
C
Axial left
Recording electrode
0.5-1.3 mm
AP
NTS
0-0.8 mm
AP
200um
Obex
Recoding site
Coronal
Left
D
Stimuli
Voltage (μV)
Time (s)
E
Stimulus
Voltage (μV)
Time (ms)
F
Spikes in feature domain
Feature 2
Feature 1
Feature 1
Feature 2
G
Voltage (μV)
Voltage (μV)
Time (ms)
H
PSTH
Number of spikes /5ms
Time (ms)

Figure 2-1 Experiment protocol and analysis pipeline. *A shows the experimental setup to perform gastric electrical stimulation. B and C provide the location to record neural activity from the nucleus of the solitary tract (NTS) in axial view and coronal view respectively. D plots the time series of multi-unit activity. The detected spikes are marked with red stars. The timing of stimuli is plotted above the spiking activity. E is a zoom-in version of the time series. The stimulus is delivered at time 0. F provides an example of spikes feature domain. Each dot represents one spike. Yellow and blue marked the two clusters of spikes defined with the k-means cluster. The red curve on the lower right corner is a neural spike. The definition of spike features is illustrated in the spike. G plots the waveform of every spike shown in F. Grey curves are individual spikes, and red curves are the averaged waveform. H plots the post-stimulus time histogram (PSTH).*

We extended the above observation by performing quantitative comparisons across four orientations and two locations, which covered the non-overlapping "hotspots" of longitudinal and circular IMAs (Figure 2-1B). For Target 1, when a 1mA current stimulus was applied in 0^o (i.e., flowing in the longitudinal direction towards the proximal stomach), the stimulus induced multiple population spikes with spike timing highly consistent across repeated trials (Figure 2-2B). For an example MUA recorded from one channel, one spike occurred around 10 ms; a few spikes occurred from 40 to 60 ms. When the current stimuli were applied in other directions, fewer spikes were evoked and were less consistent across trials (Figure 2-2B). Beyond this example, the population response in NTS, in terms of the number of spikes per 100 ms averaged across channels and animals, was 4.09±0.50 (mean ± sem) for GES at 0^o, which was significantly higher than those for other orientations (2.52±0.45 for 270^o; 2.26±0.37 for 180^o; 1.88±0.34 for 90^o), as shown in Figure 2-2C. In summary, 1-mA GES at Target 1 evoked reliable population spikes in NTS when the stimulus was delivered in 0^o (longitudinal towards the proximal stomach).

Similarly for Target 2, we observed much stronger and more reliable population responses when 1-mA GES was applied in 270^o (circular towards the greater curvature) relative to other orientations. Given the preferred orientation, Figure 2-2E shows an example of the population spikes observed from one channel. The spike timing was highly consistent across repeated trials. The population spikes were fewer and much less consistent given GES in non-preferred

orientations. The mean firing rate was 3.83±0.39 per 100 ms (mean ± sem) for GES at 270°, which was significantly higher than those for other orientations (1.56±0.17 for 0°; 1.99±0.25 for 180°; 1.56±0.19 for 90°) (Figure 2-2F).

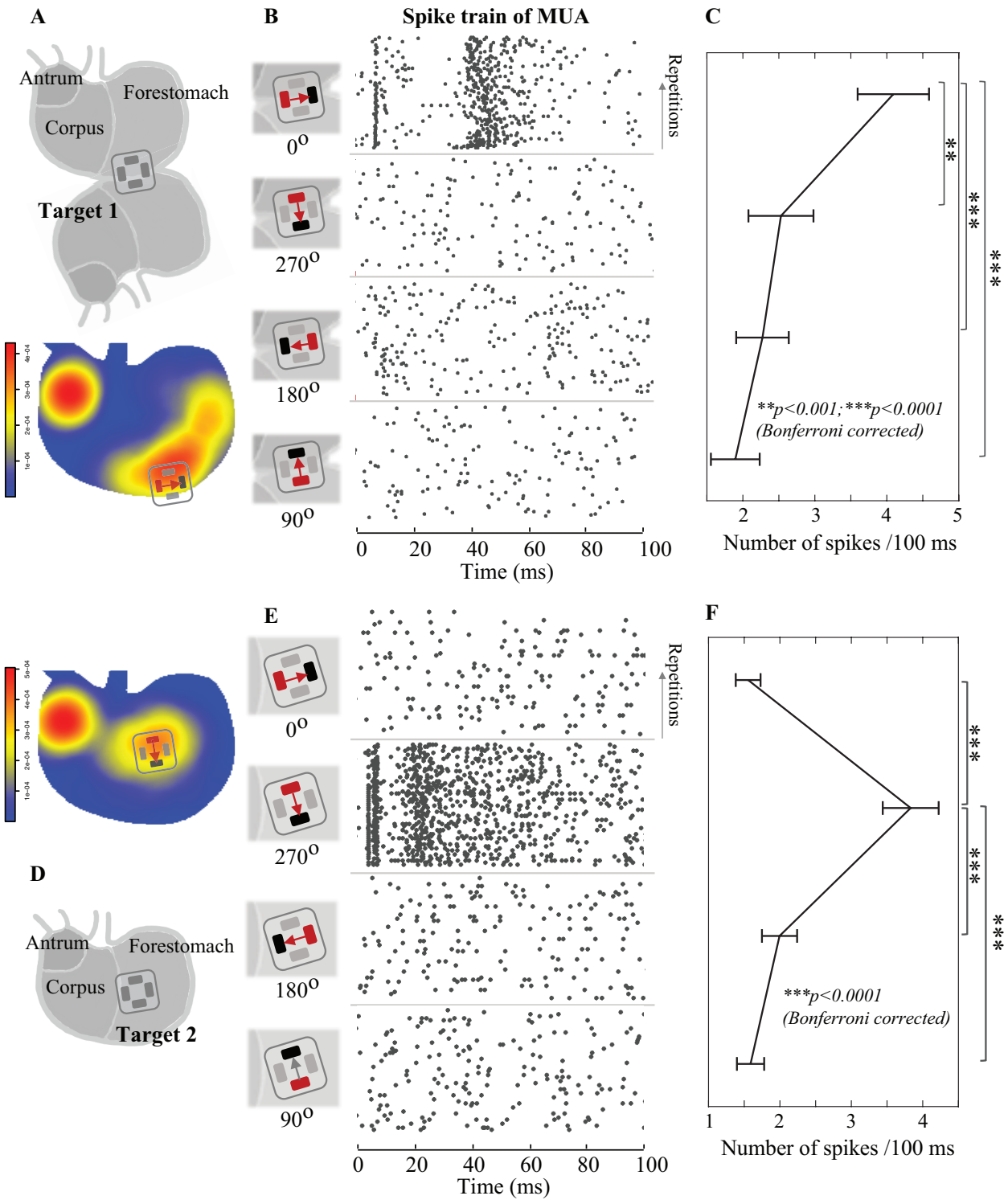

Figure 2-2 NTS neurons are tuned by gastric electrical stimulation at selected orientations. *A and D show locations of target 1 and target 2 on the stomach wall, respectively. B and E provide four pairs of anode and cathode for stimulation. The orientations of the four types of stimulation are 0º, 270º, 180º, and 90º. B and E also provide examples of neural activity after the four types of stimulation. The data is multi-unit activity (MUA) from one recording channel, but the data from B and E come from different channels. The black dots mark the time when spikes are identified. The dots in each row come from one trail. Time 0 is when stimuli are delivered. C and F plot the averaged number of spikes within 100ms after stimuli at each orientation, together with standard error. ** means p<0.001 with Bonferroni correction, and *** means p<0.0001.*

Effects of the current amplitude

We asked whether the orientation selectivity of NTS neurons observed with 1-mA GES was generalizable to GES with lower amplitudes. To address this question, we compared the neuronal population responses in NTS given GES with three different current amplitudes (0.6, 0.8, and 1 mA). For both Target 1 (Figure 2-3A) and Target 2 (Figure 2-3D), the time-averaged population responses in NTS were always greater when GES was applied in its preferred orientation (0º for Target 1, 270º for Target 2), despite the difference in the current amplitude used in this study (Figure 2-3B & E). In its preferred orientation, a stimulus with a higher amplitude tended to induce stronger population responses in NTS. Stimuli in other non-preferred orientations did not show significant amplitude-dependent effects in the resulting population responses.

We further calculated the orientation selectivity index (OSI) as the average difference in the neuronal response to GES between the preferred and non-preferred orientations. For both Target 1 and 2, increasing the current amplitude led to more pronounced orientation selectivity (i.e., increasingly higher OSI) (Figure 2-3C). For Target 1, the OSI at 0.6 mA was significantly lower than the OSI at 0.8 mA (p<0.005) or 1 mA (p<0.001) based on a permutation test with Bonferroni correction. Similar observations and statistics were found for Target 2 (Figure 2-3F). See Table 2-2 and Table 2-3 for more statistical results. In summary, orientation selectivity was generalizable across different current amplitudes (0.6, 0.8, and 1 mA).

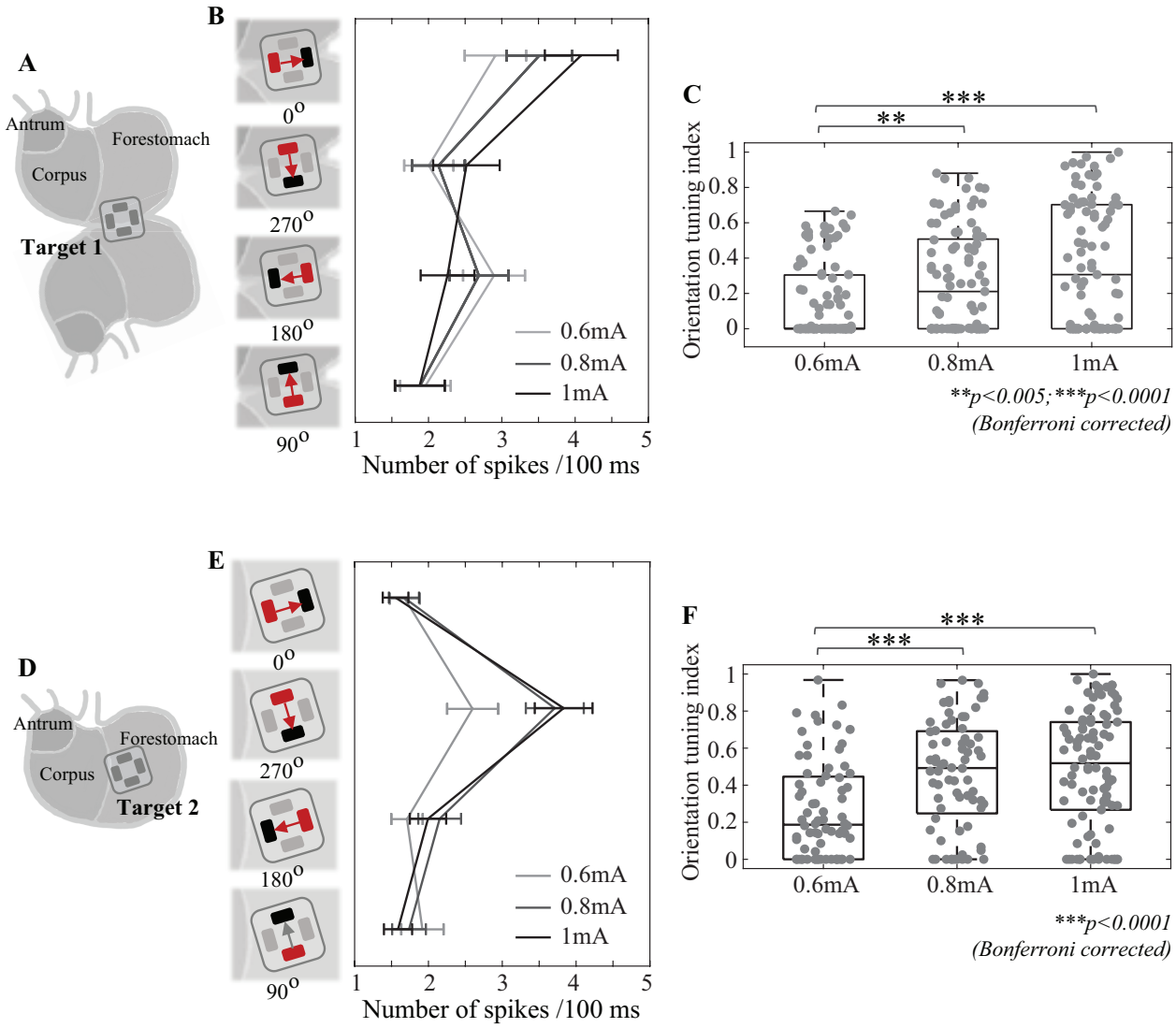

Figure 2-3 Effect of stimulating current on orientation tuning dependence. *A and D show locations of target 1 and target 2 on the stomach wall, respectively. B and E provide four pairs of anode and cathode for stimulation. The orientations of the four types of stimulation are 0°, 270°, 180°, and 90°. B and E also plot the averaged number of spikes, together with standard error, within 100ms after the stimulus with the current of 0.6mA, 0.8mA, 1mA. C and F show box plots of orientation-selectivity-index (OSI) for different types of stimulation. Grey dots represent individual samples. ** means p<0.005 with Bonferroni correction, and *** means p<0.0001.*

Table 2-2 Difference in the mean firing rate (i.e., the number of spikes per 100 ms) given GES applied to Target 1 with a preferred orientation (0^o) vs. other orientations (270^o, 180^o, 90^o)*. Each row corresponds to a different current amplitude. The statistics below are based on paired t-test with Bonferroni correction for multiple comparisons.*

current	Firing rate at 0^o	0^o vs 270^o	0^o vs 180^o	0^o vs 90^o
0.6mA	2.91±0.42 /100ms	t(91)=3.48; p=0.0023	t(91)=0.54; p=0.59	t(91)=3.56; p=0.0018
0.8mA	3.51±0.45 /100ms	t(92)=4.74; p=2.3e-5	t(92)=7.26; p=3.7e-10	t(92)=6.32; p=2.8e-8
1mA	4.09±0.50 /100ms	t(92)=3.82; p=7.2e-4	t(92)=6.93; p=1.7e-9	t(92)=7.63; p=6.2e-11

Table 2-3 Difference in the mean firing rate (i.e., the number of spikes per 100 ms) given GES applied to Target 2 with a preferred orientation (270^o) vs. other orientations (0^o, 180^o, 90^o)*. Each row corresponds to a different current amplitude. The statistics below are based on paired t-test with Bonferroni correction for multiple comparisons.*

current	Firing rate at 270^o	270^o vs 0^o	270^o vs 180^o	270^o vs 90^o
0.6mA	2.60±0.34 / 100ms	t(71)=4.62; p=5.0e-5	t(71)=4.60; p=5.4e-5	t(71)=4.57; p=6.0e-5
0.8mA	3.72±0.40 / 100ms	t(71)=7.19; p=1.6e-9	t(71)=6.98; p=3.9e-9	t(71)=7.45; p=8.3e-10
1mA	3.83±0.39 / 100ms	t(93)=7.49; p=1.2e-10	t(93)=6.39; p=1.9e-8	t(93)=7.86; p=2e-11

Orientation selectivity of single-unit responses

We further tested whether the orientation selectivity was applicable to the level of single neurons in NTS. We applied spike sorting to identify individual neurons activated by GES and analyzed their firing rates as a function of the stimulus orientation and location. In total, we identified 106 neurons activated by GES at Target 1 and 119 neurons by GES at Target 2.

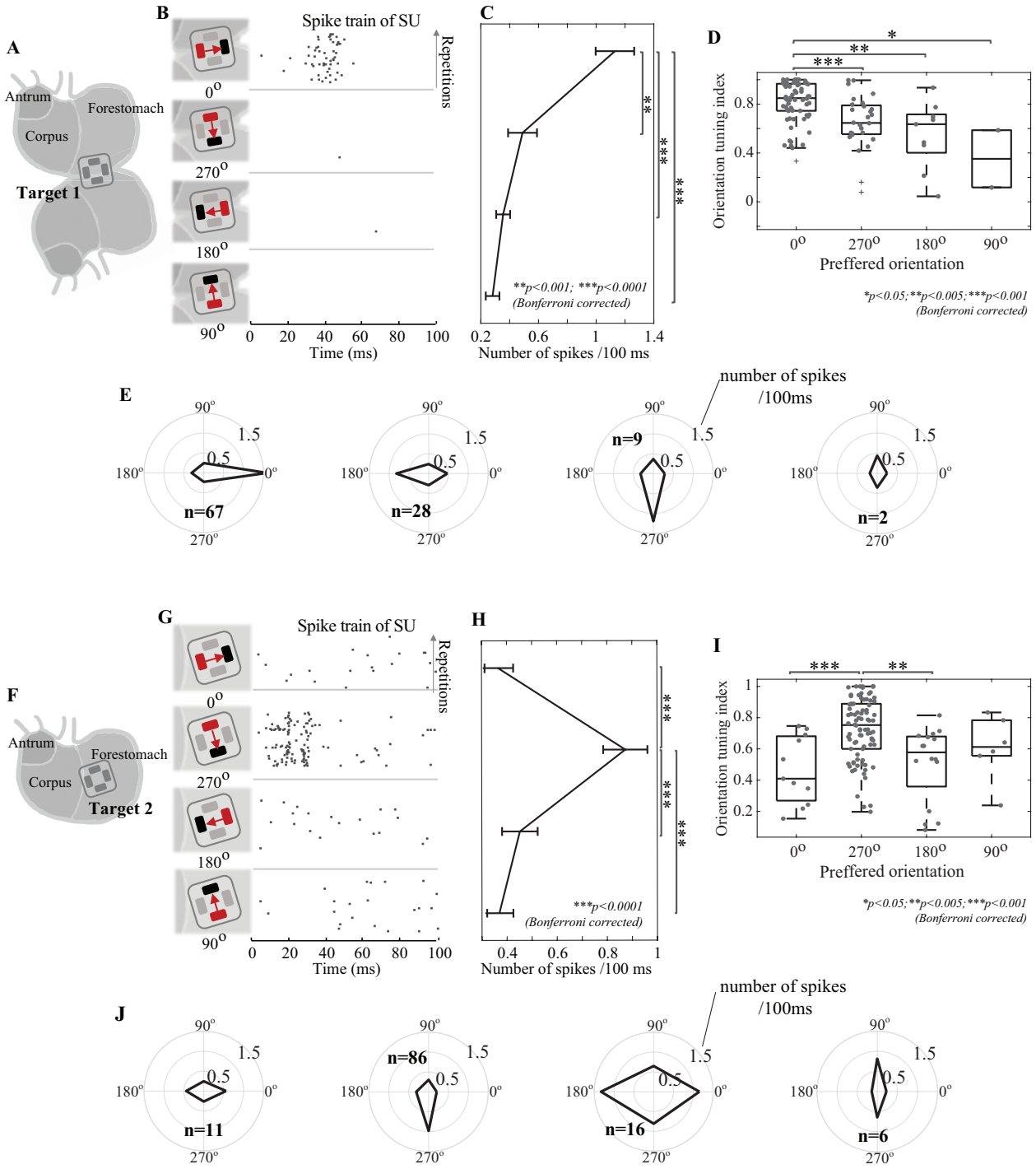

Figure 2-4 Orientation tuning dependence for individual neurons. *A and F show locations of target 1 and target 2 on the stomach wall, respectively. B and G provide four pairs of anode and cathode for stimulation with the orientation of 0º, 270º, 180º, and 90º. B and G also provide examples of neural activity after the stimulus. The data is SUA (SU) from two neurons in B and G respectively. The black dots mark the time when spikes are identified. The dots in each row come from one trial. Time 0 is when stimuli are delivered. C and H plot the averaged number of spikes within 100ms after the stimulus at each orientation, together with standard error. The result of the paired t-test is marked in the plot. ** means p<0.001 with Bonferroni correction, and *** means*

*$p<0.0001$. E and J show orientation tuning dependence for different groups of neurons. Neurons in one group share the same tuned orientation. The number of spikes within 100ms after the stimulus is marked for each orientation. D and I provide the box plots of the orientation-selectivity-index (OSI) for each group. Grey dots represent individual neurons. * means $p<0.05$ with Bonferroni correction, ** means $p<0.005$, and *** means $p<0.001$.*

Most neurons activated by GES manifested high selectivity for one stimulus orientation. In Figure 2-4B, an example neuron showed reliable responses only when GES at Target 1 was in 0^o, whereas virtually no responses were observed for other orientations. In total, 67 out of 106 neurons all shared the same preferred orientation (i.e., 0^o) and showed significantly higher firing rates given GES in 0^o than in other orientations (Figure 2-4C). Neurons that preferred other orientations (i.e., 270^o, 180^o, 90^o) were not only fewer but also less orientation selective (i.e., significantly lower OSI) (Figure 2-4D & E). Similarly for GES at Target 2, 86 out of 119 neurons were highly selective to the same preferred orientation of 270^o (Figure 2-4F through J). In summary, gastric neurons in NTS were selective to 0^o (longitudinal towards the proximal stomach) for GES at Target 1 and were selective to 270^o (circular towards the greater curvature) for GES at Target 2.

Orientation selectivity at different post-stimulus latencies

It was noticeable that GES evoked stronger and more reliable neuronal responses at some post-stimulus latencies than others (Figure 2-1). We asked whether the orientation selectivity was dependent on the response latency. To answer this question, we calculated the PSTH to resolve SUA in time and evaluated the time dependence of orientation selectivity in the level of single neurons (Figure 2-5). When Target 1 was stimulated in 0^o, the time-resolved firing rate (PSTH) of the activated gastric neurons was on average higher around 10 and 43 ms and around 20 ms, and at the baseline after 73 ms (Figure 2-5B). The neuronal responses to GES in other orientations did

not demonstrate similar time dependence, except that GES in 270° also showed a peak around 10 ms in the evoked SUA (Figure 2-5B).

According to the PSTH, we further divided the post-stimulus period into four periods (0-13, 13-29, 29-73, 73-100 ms) and evaluated the orientation selectivity of individual neurons separately for each period. Out of 106 neurons activated by GES at Target 1, 77 neurons were activated from 0 to 13 ms, 65 neurons from 13 to 29 ms, 79 from 29 to 73 ms, and 48 neurons from 72 to 100 ms. For two periods (0-13 ms and 29-73 ms), not only were more neurons activated, but most of the activated neurons were also selective to the same orientation (Figure 2-5C). The firing rate of each activated neuron manifested a stronger preference for GES in 0° during the periods of 0-13 ms and 29-73 ms, but much less so for other periods (Figure 2-5D). These results suggest that gastric neurons in NTS were selective to the orientation of GES at Target 1 with respect to their responses at two specific delays (about 8 ms and 43 ms) relative to the stimulus onset. For GES at Target 2, the firing rate averaged across all activated neurons was higher when the stimulus was in 270° at nearly all post-stimulus latencies (Figure 2-5F). The peak responses were noticeable in two periods (0-13 ms and 29-73 ms). In particular, the period from 29 to 73 ms showed that 77 out of 119 neurons were selective to the same orientation (270°), whereas slightly lower but comparable orientation selectivity was also noticeable for other periods. These results suggest that neurons activated by GES at Target 2 showed consistent selectivity to 270° for all post-stimulus periods, showing a lesser degree of time dependence compared to the responses to GES at Target 1. In summary, when Target 2 is stimulated, although more NTS neurons prefer the orientation of 270° within 29-73ms after the stimulus.

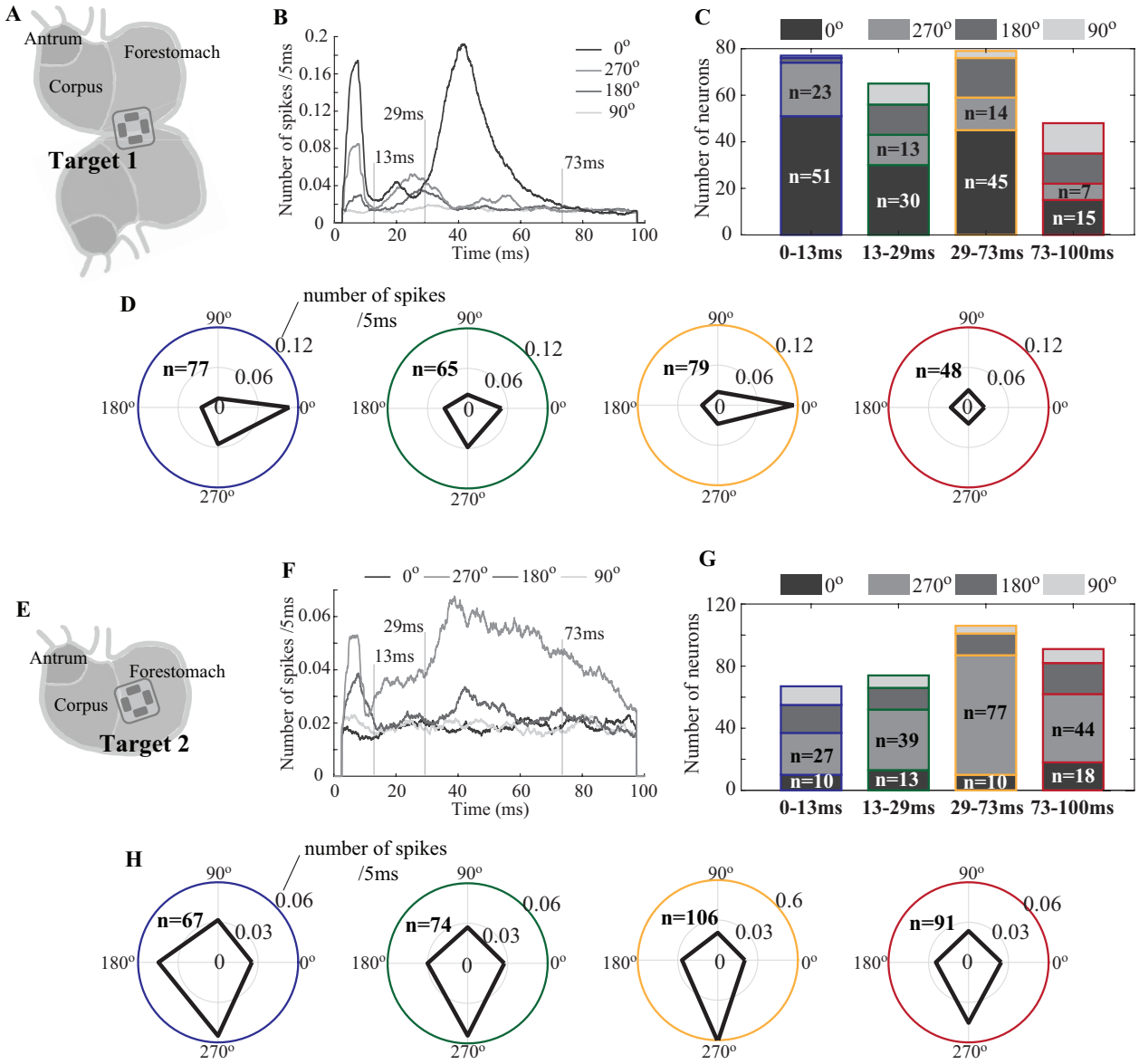

Figure 2-5 Orientation-selectivity during different post-stimulus periods. ***A*** *and* ***E*** *show locations of target 1 and target 2 on the stomach wall, respectively. B and F plot the averaged post-stimulus time histogram (PSTH) for stimulation with the orientation of 0°, 270°, 180°, and 90°, separately. C and G show the number of neurons with the preferred orientation at 0°, 270°, 180°, or 90°. D and H show the average number of spikes for each post-stimulus period. The number of neurons is presented together with the plots. I and J show the box plot of the orientation-selectivity-index (OSI) for each group. Dots represent individual clusters, and the color encodes the group to which dots belong. * means p<0.05 with Bonferroni correction, ** means p<0.01, and *** means p<0.001.*

Compare neural responses after the stimulus on different targets

We further asked whether stimulating different locations could activate the same neurons within NTS, and if yes, whether their responses were distinctive and dependent on the stimulus location. To answer these questions, we implanted electrodes to both Target 1 and Target 2 in four rats (Figure 2-6A). When applying 1-mA current stimuli in the preferred orientation (0^o for Target 1 or 270^o for Target 2), we identified the single units that responded to either or both of the locations.

In total, 100 neurons were identified: 88 for Target 1, 63 for Target 2 stimulation, and 51 for both. On average, the single-unit firing rate per 100 ms was 1.72±0.15 (mean ± standard error) for Target 1 and 0.91±0.10 for Target 2. For the 51 neurons responsive to both targets, their average firing rate was 2.12±0.21 for Target 1 and 0.92±0.10 for Target 2. The time-averaged neuronal responses were significantly higher for Target 1 than for Target 2 (paired t-test: t=7.35, p=1.7e-9, dof=50). Only 7 neurons showed higher responses to Target 2, whereas the majority showed higher responses to Target 1 (Figure 2-6C).

We further resolved the single-unit firing rate in time and averaged the response across the 51 neurons responsive to both targets. Figure 2-6B shows the firing of a single neuron across repeated stimuli. In this example, the neuron fired at different times in response to the stimulus at Target 1 vs. Target 2. Activation with Target 1 was mostly between 30 and 60 ms, whereas activation with Target 2 was later, especially around 80 ms (Figure 2-6B). We averaged the firing rate across neurons, and found that the average neuronal response was higher for Target 1 for the first 60 ms, whereas it was higher for Target 2 between 65 and 100 ms (Figure 2-6D).

These results suggest that gastric electrical stimulation selectively applied to longitudinal or circular IMAs at different locations may activate a common group of neurons in NTS but at

different times. This group of neurons is more responsive to stimulation applied to the longitudinal IMAs on the greater curvature at early times (within 60 ms) but is more responsive to the circular IMAs at later times (after 65 ms).

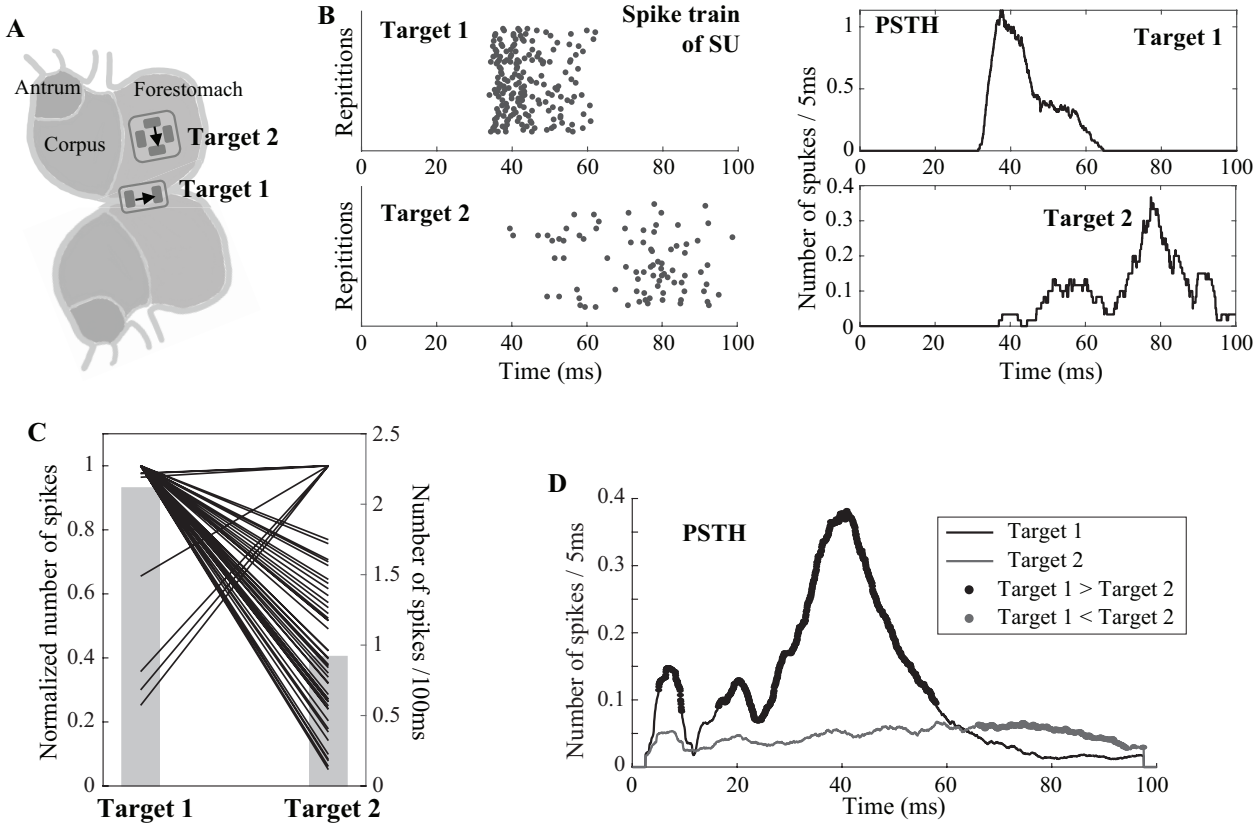

Figure 2-6 One neuron can respond to gastric electrical stimulation on different targets. *A shows the locations of the two stimulating targets together with their orientation. B plots the post-stimulus time histogram (PSTH) from a single neuron. The upper plot is PSTH after the stimulus on Target 1, and the lower plot is PSTH after the stimulus on Target 2. C plots the changes in the number of spikes after the stimulus on different targets for all neurons identified in this experiment. The number of spikes is normalized for each neuron. Each line represents the change from each neuron, and the corresponding scale is the left axis. Grey bars represent the averaged numbers of spikes, and the corresponding scale is on the right. D plots averaged PSTHs for both targets. The black curve is PSTH for Target 1, and the grey curve is PSTH for Target 2. The black dot means that, at that time point, the number of spikes is significantly higher for Target 1, and the grey dot means that the number of spikes is significantly higher for Target 2, according to paired t-test with* $\alpha = 0.05$.

Discussion

In this paper, we studied GES-evoked neural spiking activity in NTS and tested whether the neural activity was orientation-selective to gastric stimuli. We found that NTS neurons could respond to stimulation on the distal forestomach and be selectively activated by the specific orientation of electrical currents. The orientation-selectivity was generalizable for stimulation on different regions in the forestomach, but the preferred orientation depended on the layout of nearby IMAs. With the carefully designed orientation, the stimulus might selectively activate longitudinal or circular IMAs, and the same neuron in NTS would respond to stimuli on both targets.

Stimulus with the specified orientation can activate IMAs

IMA is a type of vagal afferent terminal on the stomach (Powley et al., 2016; Powley et al., 2019; Powley and Phillips, 2002). It is an elongated, narrow, and nearly-planar array with an average length of 4.3 mm, in conjunction with nearby smooth muscle fibers. Given this unique morphology, IMAs are hypothesized to detect the stretch of smooth muscle (Powley et al., 2016). Individual IMAs can either run longitudinally in the longitudinal smooth muscle layer or run circularly in the circular smooth muscle layer. This orientation property determines that individual IMAs can be activated by stretches in either direction. Stretch-induced activation can be sent to NTS, in which neurons can process such information and relay them to downstream nuclei. In this study, we observed that spiking activity in NTS could be modulated stimuli delivered to gastric regions with high IMA density. This stimulus-evoked spiking activity indicates that vagal innervated gastric receptors, likely IMAs, are modulated by GES and transmit the modulatory effect to NTS neurons.

NTS neurons selectively respond to different orientations of GES. More specifically, spiking activity in NTS is more likely to occur after one of the four GES orientations applied to

the stomach. The orientation-selectivity can be observed when the stimulus was delivered on two different sites. The first site, Target 1, is on the greater curvature and with a high density of longitudinal IMAs and a low density of circular IMAs (Powley et al., 2016). When the stimulus is on Target 1, most NTS neurons prefer the stimulation orientation paralleling to longitudinal IMAs. The second stimulating site, Target 2, is on the ventral forestomach and with a high density of circular IMAs and a low density of longitudinal IMAs (Powley et al., 2016). For Target 2 stimulation, the preferred orientation of most neurons aligns with the circular IMAs. In summary, the preferred stimulation orientation always follows the layout of IMAs, suggesting that the activation of IMAs dominates the stimulus-evoked neural activity and is also selective to the orientation of stimuli.

The orientation-selected spiking activity is not evoked by the activation from other sources Because stimulating electrodes are placed on the serosal surface of the stomach, the electrical current can influence gastric smooth muscle, gastric branches of the vagus nerve, and different gastric sensory receptors other than IMAs. Here, we would like to argue that the IMA activation dominates the post-stimulus spiking activity in NTS.

Although the stimulating current can run through gastric smooth muscles, the stimulation parameter used in this study may not be sufficient to activate smooth muscles. Activating smooth muscles requires the stimulus to have a pulse width longer than 1ms (Du et al., 2009; Li & Chen, 2010; Tomita, 1966). Given the low pulse width (0.3ms) used in this study, smooth muscle cells are unlikely to respond to these stimuli directly.

The stimulus-evoked activation in gastric vagal branches should not be the primary cause of the stimulus-evoked spiking activity in NTS. This conclusion is because the preferred stimulation orientation observed in this study (i.e., Target 2 stimulation) is more likely to block

the ascending propagation of action potentials along the vagus nerve. This blocking effect is the anode blockade, meaning that the stimulus can block the propagation of action potentials across the anode. In this study, the anode is on the side of the lesser curvature and in the ascending vagal pathway for the preferred orientation of Target 2 stimulation. This anode location makes action potentials hard to propagate to the brain. The contradiction between the outcome of stimulus-evoked vagal nerve activation and our observations suggests that gastric stimuli may not activate vagal branches directly.

We also argue that the spiking activity in NTS is dominated by stimulus-evoked responses from IMAs but not other gastric sensory receptors. The key evidence is that the preferred stimulation orientation changes with the distribution of IMAs and depends on the layout of IMAs (Powley et al., 2016). The varying orientation-selectivity is also independent of distributions from other sensory receptors. Therefore, the orientation-selected IMA activation is likely to be the major contributor to the stimulus-evoked spiking activity in NTS.

NTS neurons encodes the orientation of gastric smooth muscle activity

The orientation-specific electrical stimulation is highly likely to activate IMAs with the same orientation. This phenomenon can be utilized to selectively activate IMAs and illustrate how NTS neurons encode IMA activation, which represents the orientation of gastric smooth muscle activity. By selectively activating the longitudinal and circular IMAs, we observed that a single NTS neuron can respond to stimuli on different targets. Specifically, if one NTS neuron responds to the 0^{o} stimulus on Target 1 (targeting longitudinal IMAs along the greater curvature), the same neuron may still respond to the 270^{o} stimulus on Target 2 (targeting circular IMAs on the ventral stomach). This finding suggests that NTS neurons are not grouped based on their receptive fields in the stomach or orientations of their receptive IMAs. Instead, single NTS neurons may receive

inputs from IMAs at different gastric regions and targeting different orientations, thus integrating gastric sensory information from different IMAs at different locations. This integrating strategy is likely to be encoded by synaptic connections between the vagus nerve and NTS neurons. It can facilitate an overall sensation of gastric volume and promote efficient regulation of the digestive process but requiring a small number of neurons. These speculations align with the current understanding that individual gastric subnuclei of NTS do not have a precise topographic mapping of the stomach but receive and process both chemo and mechanical inputs parallelly, such that the vago-vagal reflex can be executed efficiently (Rogers et al., 1995; Travagli & Anselmi, 2016).

Although single NTS neurons could encode both longitudinal and circular IMAs, smooth muscle activity in longitudinal and circular directions might modulate the neural activity differently. Our result reveals that the firing rate of SUA is higher after the stimulus targeting longitudinal IMAs on the greater curvature than that targeting circular IMAs on the ventral stomach, suggesting that smooth muscle activity in the longitudinal directions have a more substantial impact on neural activity in NTS. Also, given the observation in PSTHs, stimulating longitudinal IMAs can evoke stronger neural activity within 60ms after the stimulus, while stimulating circular IMAs can evoke more vigorous neural activity after 60ms. Taken together, we presume that NTS neurons respond to gastric smooth muscle activity stronger and faster in the longitudinal direction and weaker and slower in the circular direction. This conclusion is in line with the volume changes of the forestomach. The forestomach has more distortion in the longitudinal direction than circular direction during volume changes (Schulze-Delrieu, 1983). Activity of the longitudinal IMAs can be a better indicator of gastric volume, while circular IMAs may play a facilitating role in sensing the stomach volume.

The clinical significance of the study

This study focuses on a new GES strategy, targeting a specific type of vagal terminals on the stomach, the IMA. This strategy requires the electrical current to run in a specific orientation based on the morphology and layout of targeted IMAs. With the carefully designed orientation, NTS neurons can effectively respond to stimuli innervated by prior-chosen IMAs. For example, the stimulation can be designed in the longitudinal direction and pointing to the proximal stomach if we need to activate longitudinal IMAs. Similarly, the stimulation should be in the circular direction and point to the greater curvature if circular IMAs are stimulating targets. This phenomenon is likely to make GES selective in activating IMAs and modulating spiking activity in NTS. In other words, the orientation-selected IMA activation sheds light on the precision control of GES.

Another potentially beneficial phenomenon is that single NTS neurons might respond to stimuli in various gastric regions. This observation indicates that a single-target stimulation is likely to modulate NTS neurons innervating different IMAs at different regions, thus achieving modulatory effects similar to the multi-target stimulation. In other words, instead of implanting multiple electrodes and delivering GES on multiple targets, a well-designed single-target stimulation has the potential to provide a comparable modulatory effect. This widespread stimulating effect could benefit clinical applications of GES since it can achieve sufficient responses and require fewer electrodes. Therefore, the proposed orientation-specific stimulation is propitious for clinical applications in various aspects.

It is also worth noting that stimulation targets in this study are not commonly used in clinical settings. The commonly used GES targets are within the corpus or antrum (Abell et al., 2003; Hasler, 2009). This choice can be traced back to early GES studies in the 1960s using direct

current (DC) for pacing gastric contractions (Kelly & La Force, 1972). Although yielding efficient modulatory effects, the DC stimulation has not been widely used due to its high-power consumption (Hasler, 2009; Yin, & Chen, 2008). Nowadays, given the new GES hypothesis involving the gut-brain neuroaxis, it is of interest to reconsider the stimulation target. New targets can be defined according to the anatomical distribution of gastric receptors innervating the brain and sensory neurons in the enteric nervous system.

Future steps

This study reveals that GES with specific orientation may activate IMAs and further modulate spiking activity in NTS neurons. Going beyond this study, it is of interest to compare the effect of electrical stimulation with gastric distention, which is a well-studied model for gastric volume changes (Carmagnola et al., 2005). The comparison between electrical and volumetric modulation will describe the similarity between the two in modulating IMAs and help design optimal stimulation paradigms for GES to activate NTS neurons and engage the stomach-brain neuroaxis efficiently.

Chapter 3 Gastric Electrical Stimulation Drives Fast and Strong fMRI Activity in the Brain [2]

Summary

Functional magnetic resonance imaging (fMRI) is commonly thought to be too slow to capture any neural dynamics faster than 0.1 Hz. However, recent findings demonstrate the feasibility of detecting fMRI activity at higher frequencies beyond 0.2 Hz, whereas the origin, reliability, and generalizability of fast fMRI responses are under debate and remain to be confirmed through animal experiments with fMRI and invasive electrophysiology. Here, we acquired single-echo and multi-echo fMRI, as well as local field potentials, from anesthetized rat brains given gastric electrical stimulation modulated at 0.2, 0.4 and 0.8 Hz. Such gastric stimuli could drive widespread fMRI responses at corresponding frequencies from the somatosensory and cingulate cortices. Such fast fMRI responses were linearly dependent on echo times and thus indicative of blood oxygenation level dependent nature (BOLD). Local field potentials recorded during the same gastric stimuli revealed transient and phase-locked broadband neural responses, preceding the fMRI responses by as short as 0.5 sec. Taken together, these results suggest that gastric stimulation can drive widespread and rapid fMRI responses of BOLD and neural origin, lending support to the feasibility of using fMRI to detect rapid changes in neural activity up to 0.8 Hz.

[2] Formatted for dissertation from the article published in NeuroImage. (Cao et al., 2019)

Introduction

Functional magnetic resonance imaging (fMRI) detects the blood oxygenation level dependent (BOLD) signal (Ogawa et al., 1990a, b) as a surrogate measure of neural activity (Bandettini et al. 1992; Kwong et al. 1992; Ogawa et al. 1992). Despite its wide use for cognitive sciences, fMRI is commonly recognized to only be sensitive to very slow (<0.2 Hz) fluctuations in neural activity. Faster neural signals are left undetected due to slow image acquisition and/or slow neurovascular coupling. As technical advances enable fMRI acquisition at increasingly higher sampling rates (<1 s), the bandwidth of the neural activity detectable by fMRI is primarily limited by the mechanism by which neural activity induces hemodynamic changes. Recent studies with fast sampling for fMRI have shown that the BOLD response can follow changes in neural activity as fast as 0.75 Hz (or even higher) either in the resting state (Lee et al., 2013) or given visual stimulation (Lewis et al., 2016, 2018). Although encouraging, the fast fMRI responses reported in those studies are barely above the noise level and maybe susceptible to artifacts from data acquisition or processing (Chen et al., 2017; Glover et al., 2000; LeVan et al., 2017). It remains controversial whether fast (>0.2Hz) fMRI responses are reliable across brain regions or states, or indeed indicative of neural activity. Addressing these questions is necessary for proper interpretation of relatively high-frequency fMRI signals in a broader range of imaging studies for cognitive and psychological sciences.

Here, we cast these questions in a new scenario - when the brain responds to electrical stimulation applied to the gut. The gut, unlike any other organ-system, contains the enteric nervous system (ENS) with complete neural circuits for complex and reflexive control of the digestive system (Furness and Stebbing, 2018). Being often referred to the “second brain”, the ENS interacts with the central nervous system (CNS) through reciprocal gut-brain communications, which

maintains gastrointestinal homeostasis and regulates emotion, motivation and intuition (or crudely coined as “gut feelings”) (Farmer et al., 2018; Naliboff et al., 2006; Mayer, 2011). As such, the gut-brain interaction is continuous and spontaneous to affect neural activity in CNS, regardless of the behavioral or cognitive state (Rebollo et al., 2018). Stimulating the gut can modulate a variety of CNS functions, including autonomic control, motivation and reward, emotional arousal, and affective behaviors (Mayer et al., 2009; Al Omran and Aziz, 2014). Thus, the gut is an intrinsic source of fluctuation that in part drives the brain’s spontaneous activity, and a potent target for visceral stimulation that may drive widespread neural responses across sensory, emotional, cognitive, and affective systems (Tillisch et al., 2018).

Furthermore, sensory information about the gut is encoded by afferent neurons, endocrine cells, or immune cells, and is transmitted to the brain through cranial nerves or circulating bloodstream (Furness et al., 2013). Neuronal signaling travels through peripheral vagal and spinal nerves and continues through central pathways, allowing the gut to rapidly communicate with the brain (Powley et al., 2011, 2014, 2015). Endocrine or immune-related signaling is relatively slower, since it primarily relies on systematic circulation (Psichas et al., 2015). These mechanisms of brain-gut interaction impose distinctive time scales, from milliseconds to seconds to minutes or even longer, by which the brain may respond to sensory or nutritional stimuli applied to the gut. Separating the gut-induced fMRI activity in frequency (reversely related to time scale) holds the potential to disentangle the CNS signature of gastric sensation transmitted through different mechanisms. We speculate that high-frequency responses arise from neuronal signaling, whereas low-frequency responses arise from endocrine or immune-related signaling.

Additionally, with the recent upsurge in attempts to identify optimal locations for electroceutical interventions for visceral disorders, considerable effort has been directed towards

comparing stimulation at different sites along nerves and in target tissues to locate particular loci for stimulation that maximize on-target effects and minimize off-target side effects. In the case of stomach disorders, local stimulation on the stomach wall is an obvious candidate, though conceivably such manipulations may be "too close" to the target. Specifically, local gastric stimulation might not only engage vagovagal reflex, but also, concomitantly, have unintended consequences involving other visceral afferent or sympathetic effects. Determinations of the central consequences of stimulation at particular sites are an obvious means of assessing the neural consequences of electroceutical manipulations.

The above considerations motivated us to investigate the frequency characteristics of the fMRI response to gastric stimulation. We focused on pushing the upper limit of the fMRI-detectable response spectrum, given our primary interest of probing the brain response to vagal or spinal neuronal input arising from the stomach. Specifically, we used anesthetized rats as a model for *in vivo* fMRI, gastric stimulation and neural recording. Gastric electrical stimulation (GES) was applied to the forestomach wall at a site known to be densely innervated by vagal sensory terminals that relay sensory information from the gut to the brain (Powley et al., 2016). When GES was modulated periodically with an increasing frequency (ranging from 0.2 to 0.8 Hz), the resulting fMRI and neural responses were recorded in separate sessions and analyzed for comparison. The data were used to address the following questions: 1) could GES evoke reliable fast (>0.2 Hz) fMRI responses in the brain; 2) if yes, were the evoked responses BOLD; 3) if further yes, what was the neurophysiological correlate to the response.

Materials and Methods

Subjects

A total of 14 Sprague–Dawley rats (male, weight: 250-400g; Envigo RMS, Indianapolis, IN) were used according to a protocol approved by the Purdue Animal Care and Use Committee (PACUC) and the Laboratory Animal Program (LAP). All animals were housed in a strictly controlled environment (temperature: 21±1°C; 12 h light-dark cycle with lights on at 6:00 AM and off at 6:00 PM). All animals were electrically stimulated at the forestomach, during which nine animals were scanned for fMRI and the other five animals were recorded for neural signals. In fMRI experiments, all of the nine animals went through single-echo EPI acquisition, eight of them went through multi-echo EPI acquisition.

Surgical implantation of stimulating electrodes

All animals underwent an abdominal surgery for implantation of a patch electrode on the forestomach. Each animal was briefly anesthetized with 5% isoflurane for 5 minutes, followed by 2% isoflurane to maintain a surgical plane of anesthesia. Following a toe-pinch test, a ~3 cm incision was made starting at 1 cm caudal to the xiphoid and moving 3 cm caudally. After separating and retracting the skin and muscle layers, the ventral stomach was exposed such that the intersection of the greater curvature and the limiting ridge could be identified. A pair of electrodes (Microprobes, Gaithersburg, MD, USA), which consisted of Pt/Ir foils adhered to a thin perylene substrate (a rectangular shape of 4mm-by-2mm size and 0.015 mm thickness), was directly sutured onto the forestomach wall. This patch electrode was placed along the greater curvature at about 4mm proximal to the limiting ridge (see Figure 3-1A). Next, the muscle and skin layers at the incision site were closed with sutures. The leads of the implanted electrodes were either routed out of the abdomen (for acute experiments with neural recording) or were tunneled

subcutaneously to the back (for chronic experiments with fMRI). The animals that underwent chronic experiments were allowed at least 1 week for post-surgical recovery. To minimize pain and inflammatory responses after the surgery, all animals were given Baytril (BioServ, Flemington, NJ) (one tablet per day, 2 mg/Tablet) two days before the surgery and buprenorphine hydrochloride (0.01 mg/kg, subcutaneous) immediately before the surgery. Then, they were given Baytril/Rimadyl (BioServ, Flemington, NJ) (one tablet per day, 2 mg/Tablet for Baytril and Rimadyl) for the first three days after the surgery and then were given Baytril (one tablet per day, 2 mg/Tablet) for the following three days.

Gastric electrical stimulation

For GES, the electrodes were connected to a current stimulator (model 2200, A-M Systems Inc, Sequim, WA, USA). The stimulator was controlled by an in-house program developed in MATLAB (Mathworks, Massachusetts, USA) and a Data Acquisition (DAQ) device (National Instruments, Austin, TX, USA). During fMRI experiments, the stimulator was placed outside of the MRI room and was connected to the animal through a twisted-wire cable.

As illustrated in Figure 3-1, gastric stimuli were delivered with a "nested block-design" paradigm. In a longer temporal scale, the paradigm included 30s STIM periods alternating with 30s REST periods. Stimuli were only delivered in every STIM period, whereas no stimulus was delivered in any REST period. However, stimuli were not continuous during each STIM period; instead, they were delivered as stimulus trains modulated by a periodic ON-and-OFF pattern. For example, a 2s-ON-3s-OFF pattern means that a 2s train of stimuli was delivered every 5s; in other words, the stimuli were modulated at 0.2Hz. In this study, stimuli were modulated in three periodic patterns: 2s-ON-3s-OFF, 1s-ON-1.5s-OFF, 0.5s-ON-0.75s-OFF, corresponding to 0.2, 0.4, and 0.8Hz of modulation, respectively. Each stimulus was a pair of charge-balanced biphasic pulses

(i.e., two pulses with opposite polarity). The pulse width was 0.3ms and the pulse amplitude was 6mA. The inter-stimulus interval was 50ms.

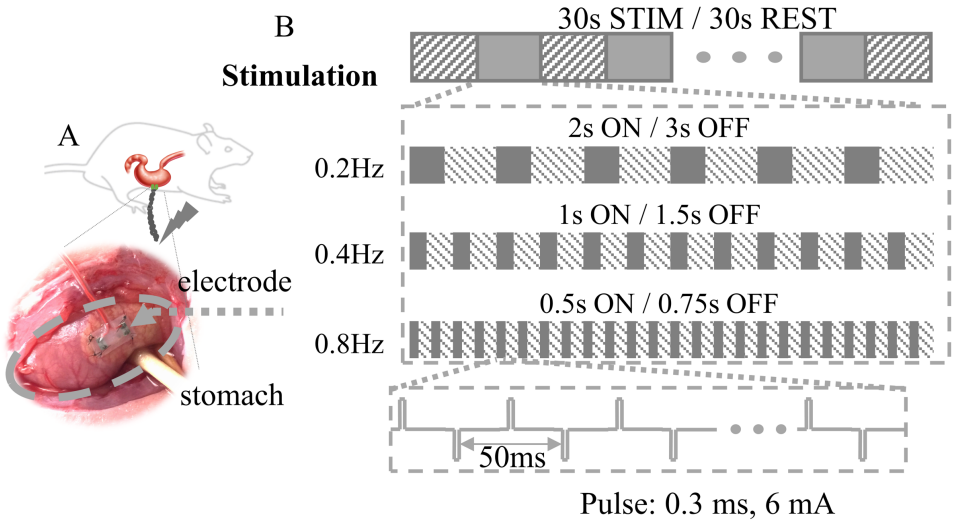

Figure 3-1 Schematics of experiment design. *Panel A shows the implantation procedure of the patch electrode. The electrode was implanted on the forestomach, aligning with the great curvature, and centered about the limiting ridge. The electrode had two contacts. Panel B describes the stimulation paradigm used for fast modulation. Every imaging session included ten 30s-STIM-30s-REST blocks. The fast modulation only occurred during the 30s-STIM period. Three modulatory frequencies were delivered during the 20s-STIM period: 0.2 Hz (2s-ON-3s-OFF), 0.4 Hz (1s-OF-1.5s-OFF), and 0.8 Hz (0.5s-ON-0.75s-OFF). The bipolar rectangular pulse was applied during the stimulation ON block (pulse width: 0.3ms, current: 6mA, inter-pulse interval: 50 ms).*

In each experimental session, the 30s-STIM-30s-REST pattern was repeated for 10 cycles, starting with a 20s rest period and lasted 620s in total; stimuli were modulated by the same frequency for every STIM period in the same session. For the fMRI experiment, every frequency setting was used for six sessions per animal, of which three sessions were used for single-echo fMRI and the other three for multi-echo fMRI (see ***MRI and fMRI Acquisition***). For the electrophysiological experiment, one session was sufficient for each frequency setting since neural signals have higher signal-to-noise ratios than fMRI signals.

This paradigm was designed with our intention to balance multiple considerations. In the longer temporal scale, the 30s-STIM-30-REST pattern was used because it allowed us to average the fMRI response across multiple STIM periods. The averaged response had a higher signal-to-noise ratio, readily allowing us to evaluate its temporal characteristics by visual inspection and its spectral characteristics by Fourier analysis. In the shorter temporal scale, the periodic ON-and-OFF pattern used a similar duration for ON vs. OFF and formed a square wave with a 40% duty cycle. Such a square wave was intended to approximate a sinusoidal waveform, which would be ideal for driving the fMRI response to fluctuate at a single frequency, if this frequency is within the detectable bandwidth of fMRI. In practice, the square-wave modulation was much easier to implement than a sinusoidal modulation and provided sufficient frequency specificity. Moreover, the ON-and-OFF pattern was intentionally designed to keep the same number of stimuli during the entire 30s STIM period, regardless of the frequency (0.2, 0.4, 0.8Hz) of modulation. The varying frequency only affected how the stimuli were distributed in time, whereas it did not change the average or total number of stimuli delivered in every 5, 10, 15, 20, 25, 30s. In other words, the dose of stimulation was kept constant across various frequency settings, allowing us to focus our analysis on the effect of the modulating frequency.

MRI data acquisition

The MRI and fMRI data were acquired with a 7-tesla small-animal MRI system (BioSpec 70/30, Bruker, Billerica, MA, USA) using an imaging protocol adopted from our previous study (Cao et al., 2017). Each animal was initially anesthetized with 5% isoflurane. After the animal was setup in the MRI scanner and placed in a prone position, 2-3% isoflurane mixed with oxygen was delivered to the animal through a nose cone. The head was restricted with a bite bar and two ear bars to avoid head motion. A bolus of dexdomitor (15 μg/Kg, Zoetis, NJ, USA) was then

administered subcutaneously. The dose of isoflurane was then lowered to 0.1-0.5% as soon as the animal's heart rate and respiration started to drop. About 15 to 20 minutes following the bolus injection, subcutaneous infusion of dexdomitor was administered at 15 μg/Kg/h, during which the isoflurane was maintained at 0.1-0.5%. The dose of dexdomitor was adjusted slightly every hour as needed to stabilize the animal's physiology. Respiration rate, heart rate, body temperature, and oxygen saturation level (SpO_2) were monitored in real-time and maintained throughout the experiment: respiratory rate from 30 to 70 breaths per minute, heart rate from 250 to 350 beats per minute, body temperature at 37 ± 0.5 °C, and SpO_2 >96%.

A volume coil (86 mm inner diameter) and a 4-channel surface coil were respectively used as the transmitter and receiver for image acquisition. After the localizer scans, T_2-weighted anatomical images were acquired using a rapid acquisition with relaxation enhancement (RARE) sequence with repetition time (TR)=5804.6 s, effective echo time (TE)=32.5 ms, echo spacing=10.83 ms, voxel size=0.125×0.125×0.5mm^3, RARE factor=8, and flip angle (FA)=90°.

Following the anatomical scan, T_2^*-weighted fMRI images were acquired with a 2-D single-shot gradient-echo (GE) echo-planar imaging (EPI) sequence with TE=16.5 ms, in-plane resolution=0.5×0.5 mm^2. The slice number, slice thickness, TR, and FA were set differently according to different stimulation frequencies to ensure that the fMRI acquisition was fast enough to capture the evoked response as the stimuli were modulated at an increasing frequency. Specifically, when GES stimuli were modulated at 0.2 or 0.4 Hz, TR=0.5 s, FA=45°, and slice thickness=1mm; when the stimuli were delivered at 0.8 Hz, TR=0.25 s, FA=33°, and slice thickness=1.5mm. In addition, multi-slice, multi-echo GE-EPI was performed to acquire fMRI images at four different echo times (10, 23.5, 37, 50.5 ms) with TR=0.5 s, FA=45°, in-plane resolution=0.5×0.5 mm^2, and slice thickness=1.5 mm.

fMRI preprocessing

The MRI/fMRI data were processed using FSL (Jenkinson, et al., 2012), AFNI (Cox, 1996), and in-house software developed in MATLAB. For single-echo fMRI data, head motion was first corrected by co-registering every volume to the first volume within each session (*3dvolreg*). Next, the slice timing in each volume was corrected (*slicetimer*). The fMRI images were then aligned with the anatomical images (*flirt*) and were further registered to a rat brain atlas (*fnirt*) (Valdes Hernandez et al., 2011). The fMRI data were spatially smoothed with a 3-D Gaussian kernel of 0.5-mm full-width-at-half maximum and were temporally detrended.

The preprocessing of multi-echo fMRI data was similar to that of single-echo fMRI. Image co-registration for motion correction and normalization to the atlas were based on the linear/nonlinear transformation functions estimated from the images acquired with TE=10ms, whereas the same functions were applied to images at other echo times. As such, the images at different TEs were all co-registered within and across sessions and animals.

Mapping fast fMRI responses

Following the preprocessing, we mapped the brain regions activated with gastric stimuli modulated at 0.2, 0.4 or 0.8 Hz. The analysis was done in three different levels: independent component, region of interest (ROI), and single voxel. Briefly, independent component analysis (ICA) was used to identify spatially independent functional networks in a data driven manner. This analysis aimed to address whether the temporal fluctuation of each identified "network" was able to follow a response pattern at the same frequency as was GES modulated. Similarly, the time series, either extracted from a single voxel or averaged across voxels within a pre-defined ROI, was evaluated and tested for frequency-specific fast fMRI response.

For the component-wise analysis, the fMRI data were separated by different frequency settings (i.e., 0.2, 0.4, and 0.8 Hz). For each setting, the voxel-wise time series was first demeaned and standardized to unit variance within every session, and then were concatenated across all sessions and animals. Infomax ICA (Bell and Sejnowski, 1995) was used to decompose the concatenated data into 40 spatially independent components (ICs). For each IC, the spatial distribution revealed a voxel pattern and shown as IC weights, and the temporal pattern reported the dynamics of that voxel pattern over the duration concatenated across all sessions and animals. To highlight the network (or regions) represented by each IC, its spatial pattern was thresholded based on the method described in (Beckmann and Smith, 2004). In brief, a two-Gaussian mixture distribution was modeled on the Z-statistics of each IC map: one Gaussian model representing the noise, the other representing the signal. The threshold was selected such that for each voxel, the probability of being a signal was as least three times higher than being noise.

The component-wise signal was further segmented based on the onset of each STIM period, i.e. the 30-s pulse trains modulated at a specific frequency. Specifically, each segment lasted 27.5 s, starting from 2.5 s after the onset of a STIM period (to avoid the period of transient effects) and ending at the offset of the same STIM period. After subtracting the mean from the signal within each segment, we averaged the signal across segments for each animal. As a result, the averaged signal indicated the animal-wise activity of each IC in response to the gastric stimuli. We further tested for each IC whether its averaged response showed an oscillatory pattern at the specific frequency as the frequency of gastric modulation, as later described in detail.

In the voxel-wise analysis, the signal at each voxel was divided by its mean during each session and was represented in terms of percentage change. Then the voxel time series were separated into 27.5s segments based on the onset and duration of every STIM period (as described

in the preceding paragraph). The segmented data were further averaged across segments, yielding the voxel-wise evoked response separately for each animal and each frequency setting.

In the ROI-wise analysis, multiple anatomical regions (the insula, cingulate cortex, somatosensory cortex, motor cortex, and thalamus), as predefined in the rat brain atlas (Papp et al., 2014; Valdes Hernandez et al., 2011), were selected because they are presumably involved in brain-gut interaction (e.g., Mayer, 2011; Tillisch et al., 2018). The voxel-wise signal was converted to and represented as the percentage change signal and then averaged across voxels within each ROI. Then for each ROI, the time series was segmented and averaged across repeated STIM periods.

It should be noted that the component, region, or voxel-wise time series signal was not filtered either before or after being averaged across repeated 30s STIM periods. For each component, region, or voxel of interest, the power spectral density of the evoked response was analyzed to evaluate the frequency specificity of the observed response.

A linear regression model was used to test the significance of the fast-fMRI response extracted from each component, ROI, or voxel. Specifically, a linear regression model was defined as a weighted sum of a sine signal and a cosine signal, both oscillating at the same frequency by which the stimuli were modulated. The weights (or regression coefficients) were estimated by least squares estimation (LSE). The F statistic was calculated and converted to a z statistic (*fift_t2z* in AFNI), indicative of how well the model fitted the time series. The regression model was applied to the averaged time series extracted from each component, ROI, or voxel, separately for each animal. Then, a random-effects group analysis was performed by applying one-sample t-test to the z values obtained from every animal. For the component analysis, the statistical significance was evaluated based on the t statistic with false discovery rate $q<0.01$. For the ROI-level analyses, the

statistical significance was evaluated based on the t statistic with $p<0.05$. For the voxel-wise analysis, the statistical significance was based on the t statistic with $p<0.05$, and a cluster-wise significance level $p<0.05$ with cluster size >10 mm^3 by using *3dClustSim* in AFNI (Cox et al., 2017). For those significantly activated voxels, we further averaged the voxel response to every cycle of stimuli and measured the peak-to-peak response amplitude in terms of percentage change.

Multi-echo ICA

It is established that the relative BOLD response is a linear function of echo time (TE) (Peltier and Noll, 2002). If an fMRI response is BOLD, it should depend linearly on TE; otherwise, it is unlikely to reflect any change in neural activity. Following this notion, we applied ICA to multi-echo fMRI data, as described in previous studies (Evan et al., 2015; Kundu et al., 2012, 2014), to evaluate the TE dependence of the GES-evoked fMRI response.

Specifically, TE was treated as the fourth spatial variable. In the spatial domain, the fMRI data at four different TEs were concatenated to expand the spatial dimension by four times. In the time domain, the data from different sessions and animals were concatenated after the voxel time series was demeaned and standardized to unit variance separately for each session. Spatially ICA was then applied to the concatenated data. Each of the resulting ICs was characterized by a spatial pattern and a time series over the duration concatenated over all sessions and animals. The time series was used to determine whether or not each IC was activated by GES modulated at a specific frequency (e.g., 0.2, 0.4, or 0.8 Hz) based on the same single-subject and group-level analyses as for single-echo fMRI data. The spatial pattern was used to map the activated regions and to assess the response dependence on TE. Specifically, the spatial pattern of each IC was separated into four maps, each corresponding to a specific TE. For each TE-specific IC map, the value of each voxel was converted to $\Delta S/S$ by multiplying a factor, which indicated the ratio of the standard deviation

to the mean of the original voxel time series before it was demeaned and standardized for ICA. The values ($\Delta S/S$) of all voxels were averaged and weighted by the Fisher transformed component weights for each TE-specific IC. The component-wise $\Delta S/S$ was modeled as a linear function of TE, as Equation 3-1

$$\Delta S/S = -\Delta R_2^* \times TE \qquad \textit{Equation 3-1}$$

where ΔR_2^* was estimated by using least squares estimation and indicated the change in susceptibility-weighted transverse relaxation time. The goodness-of-fit of this model was evaluated for statistical significance based on the F statistic with $p<0.05$.

Neural data acquisition and analysis

Five animals were prepared for acute neural recording immediately after a patch electrode was implanted to the forestomach. Each animal underwent a cranial surgery for a 32-channel linear electrode array (NeuroNexus Technologies, Ann Arbor, MI, USA) to be inserted into the right primary somatosensory cortex at a site that represents the forelimb (S1FL). Specifically, the animal's head was secured in the stereotaxic frame (Stoelting Co, Wood Dale, IL, USA). After adequate anesthesia/analgesia (2-3% isoflurane) was ensured, a midline incision was made through the scalp. Right S1FL was localized as anterior-posterior=0mm, medial-lateral=3.9mm relative to the bregma; from there, a 3x3mm^2 window through the skull was drilled. The recording electrode was inserted through the window by ~2 mm in depth. Micro-screws were secured above the olfactory bulb and were used as reference and ground. The recording electrode was connected to a broadband recording system (Tucker Davis Technologies, Alachua, FL, USA) that amplified and digitized (at 25 kHz) the voltage between the recording site and the reference site (i.e. a micro-screw secured over the olfactory bulb). The electrode localization was initially guided by the

stereotaxic frame and was then finalized on the basis of observable responses to electric stimuli applied to the left forepaw.

Following the implantation, the animal was switched to a low-dose anesthesia with continuous administration of 0.1-0.5% isoflurane and subcutaneous infusion of dexdomitor at 15 μg/Kg/h, keeping the same kind and dose of anesthesia as in fMRI experiments. Neural signals were recorded from S1FL while the forestomach was stimulated using the protocols described in the previous subsection (see ***Gastric Electrical Stimulation***).

The local field potential (LFP) was processed using in-house software developed in MATLAB. Firstly, stimulation artifacts were identified and removed; the removed data points were recreated by linear interpolation from the neighboring artifact-free data points. To visualize the GES evoked potentials over the periodically occurring ON-OFF blocks, the recorded LFP was segmented based on the onset/offset of every STIM period, starting from 1s before the onset of the STIM period and ending at 10 s following the offset of the STIM period. The segmented signals were averaged across segments. We also obtained the GES-evoked potential over a shorter duration corresponding to the stimulus train during a single ON block within the STIM period. To do so, the evoked potential over the longer (30s) STIM period was further segmented based on the onset of every ON block. A segment was defined from 0.1s before the onset of a ON block, included the duration of the ON block, and as well as the duration of the subsequent OFF block. As such, every segment covered a single cycle of the ON-OFF alternation and lasted 5s, 2.5s or 1.25s for 0.2, 0.4, and 0.8 Hz of gastric modulation, respectively. From the segmented LFP signal was subtracted the pre-stimulus baseline, i.e. the average amplitude during the pre-stimulus period. Then the signal was averaged across all the segments with the same frequency setting, yielding the GES evoked potential. The evoked potential was evaluated separately for different frequency

settings and different animals and was further averaged across animals. Note that no filtering was applied in order for us to focus on the broadband neural response, while avoiding any oscillation that would be otherwise artificially generated by bandpass filtering.

Results

We sought to answer whether fMRI could report relatively fast (> 0.2 Hz) modulation of neural responses to gastric stimulation. To address this question, the forestomach was electrically stimulated through a patch electrode chronically implanted along the greater curvature in 9 rats (Figure 3-1A). This gastric electrical stimulation was switched ON and OFF, effectively modulating the stomach at 0.2, 0.4, and 0.8 Hz for 30s followed by 30s of rest. While alternating this pattern for 10 cycles (Figure 3-1B), the brain was continuously scanned for fMRI by using either single-echo or multi-echo EPI.

Gastric stimuli induced fast fMRI responses

The fast-fMRI responses were examined at three different levels: spatially independent components, predefined anatomical ROIs, and single voxels. In the component level, ICA was applied separately to the whole-brain fMRI data acquired with different frequencies (0.2, 0.4 and 0.8Hz) of gastric modulation. As shown in Figure 3-2, 6 out of 40 ICs were activated at 0.2 Hz (FDR $q<0.01$), 3 out of 40 ICs were activated at 0.4 Hz (FDR $q<0.01$), and 4 out of 40 ICs were activated at 0.8 Hz (uncorrected $p<0.01$). Across the three frequency conditions, the activated components overlapped with the somatosensory cortex, motor cortex, cingulate cortex, visual cortex, auditory cortex, parietal association cortex, and thalamus. In particular, a large part of the somatosensory cortex was activated at all three frequency conditions.

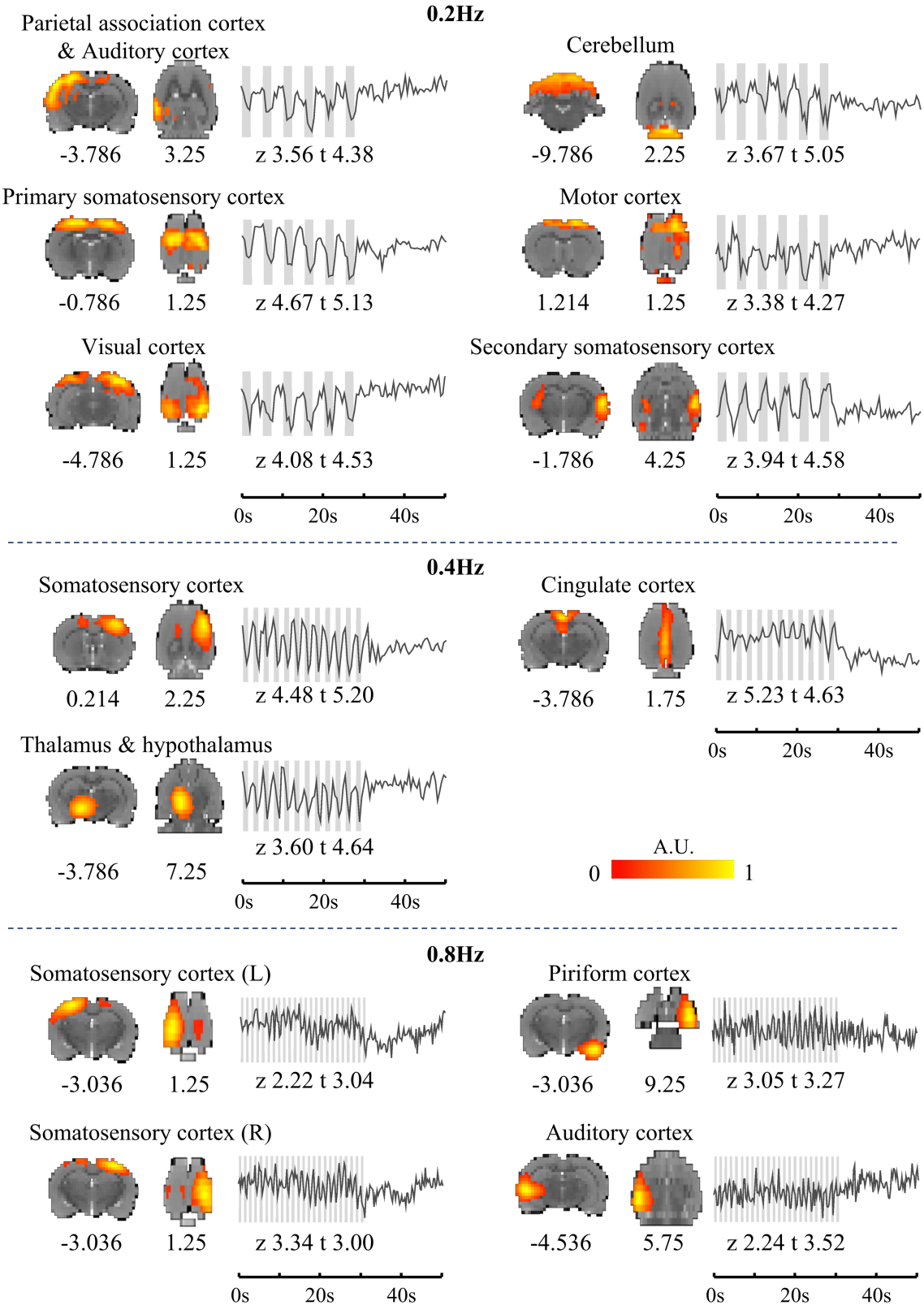

Figure 3-2 Independent component (IC) time series shows fast fMRI fluctuation. *The components with fast fMRI activity are presented in the figure. The time traces are the average*

time series of corresponding ICs. The statistical values are labeled for each component. For 0.2Hz modulation, 6 components had significant fast fMRI response (false discover rate q<0.01), including the visual cortex, primary and secondary somatosensory cortex, secondary motor cortex, auditory cortex, parietal association cortex, and cerebellum. For 0.4Hz modulation, 3 components had significant fast fMRI response (false discover rate q<0.01), including the primary somatosensory cortex, cingulate cortex, hypothalamus. For 0.8Hz modulation, 4 components were found to contain fast fMRI response (uncorrected p<0.01), including the primary somatosensory cortex (left and right side, short for L and R), piriform cortex, and auditory cortex.

As a result of data-driven component analysis, the activated components were found to be not precisely confined into predefined anatomical partitions. In a complementary ROI-level analysis, we examined the fMRI signal within anatomically predefined ROIs, including the somatosensory cortex, cingulate cortex, motor cortex, insular cortex, and thalamus, all of which have been shown or hypothesized to be directly or indirectly involved in communication with the gut (Mayer, 2011; Tillisch et al., 2018). The response time series averaged within each ROI showed a varying degree of oscillation at the same frequency as that of gastric modulation (Figure 3-3). The selected ROIs all showed notable oscillations at 0.2 Hz; the somatosensory cortex, cingulate cortex, motor cortex showed apparent oscillations at 0.4 Hz; the somatosensory cortex and cingulate cortex showed discernable oscillations even at 0.8 Hz. The power spectral density further confirmed the specificity to the frequency of gastric modulation, especially at 0.2 and 0.4Hz.

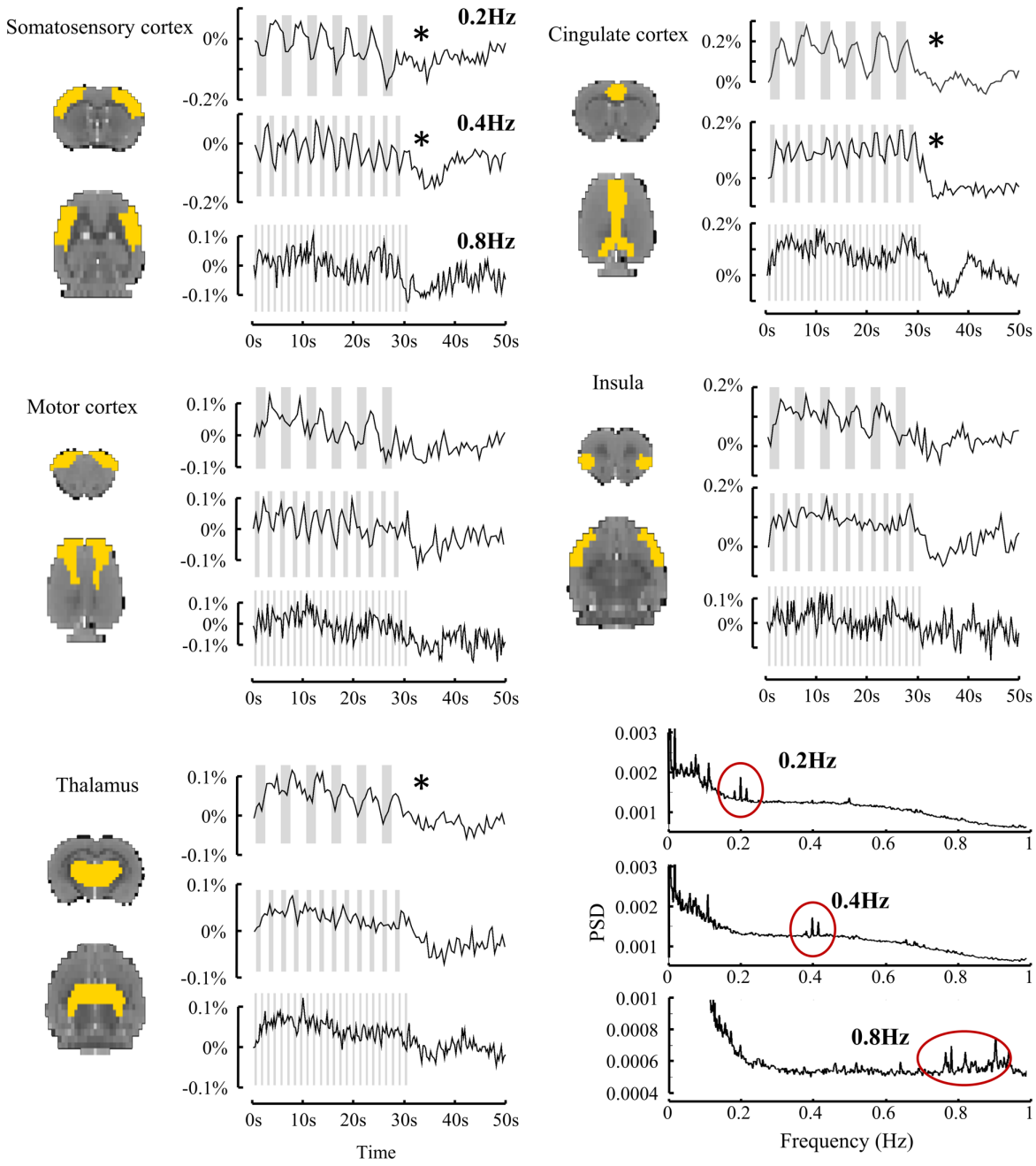

Figure 3-3 Network exhibits fast fMRI fluctuation. *The time series of percentage change in fast-BOLD response are presented for each anatomical region of interest. The regions of interest include the somatosensory cortex, motor cortex, thalamus, cingulate cortex, and insula. The mask used to define each region of interest is shown in yellow (see both axial and coronal views). The time series of percentage change are shown on the right for each frequency condition (i.e. 0.2, 0.4, and 0.8Hz). The time series are marked with * if the fMRI signal follows the fast-modulation ($p<0.05$). The power spectrum density (PSD) averaged across all regions of interest is displayed at the bottom right separately for each frequency condition. The frequency of interest is highlighted with a red circle.*

In addition, the voxel-wise analysis further confirmed the above finding with single-voxel resolution. Figure 3-4 shows the voxels that were significantly activated (cluster-wise $p<0.05$) given gastric modulation at 0.2 to 0.8 Hz. The fast-fMRI signal was mainly found in the somatosensory cortex, marginally present in the motor, visual, auditory, cingulate, parietal association cortex, as well as hippocampus, and thalamus. In response to a single train of gastric stimuli, the response amplitude (%) tended to be relatively lower at a relatively higher frequency. For example, the primary somatosensory cortex showed the peak-to-peak amplitude as high as 0.89% at 0.2 Hz, 0.8% at 0.4 Hz, or 0.33% at 0.8 Hz.

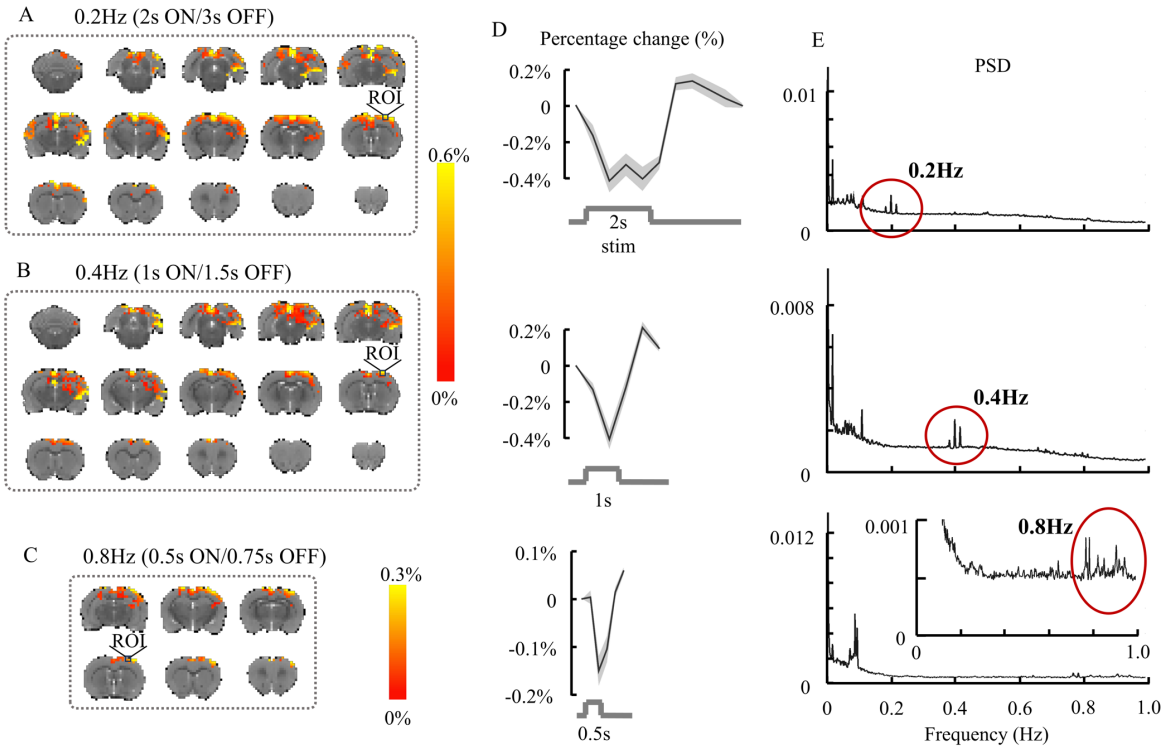

Figure 3-4 Percentage change of the fast-BOLD response. *Panel A-C show the percentage change maps that correspond to the 3 modulatory frequency conditions. The areas that exhibited significant fast-BOLD response are predominantly the primary somatosensory cortex and cingulate cortex. As the modulatory frequency increases, fewer regions could respond to the fast stimulation. Panel D shows example response time series from four selected voxels in the primary somatosensory cortex forelimb region (S1FL). The selected voxels are marked with a small box and labeled ROI. Panel E shows the averaged power spectrum density (PSD) in the responsive regions within each frequency condition. The frequency of interest is highlighted with a red circle.*

Fast fMRI responses were BOLD

We further asked whether the GES-evoked fast responses were blood oxygenation level dependent (BOLD) and thus likely of a neural origin. To address this question, we acquired multi-echo EPI data and evaluated the TE-dependence of the GES-evoked response. Specifically, the relative response amplitude (ΔS/S) was evaluated as a function of echo time (TE=10, 23.5, 37, 50.5 ms), separately for each IC obtained with multi-echo ICA (Kundu et al., 2012, 2014; Evan et al., 2015). As shown in Figure 3-5, when gastric stimuli were modulated at 0.4 Hz, 8 out of 40 ICs were found to be activated, showing an oscillatory response pattern at 0.4 Hz. For each of these 8 ICs, the relative response amplitude (ΔS/S) was linearly dependent on the echo time (Figure 3-5, *F*-test, $p<0.05$), a signature indicative of the BOLD response (Kundu et al., 2012; Peltier and Noll, 2002).

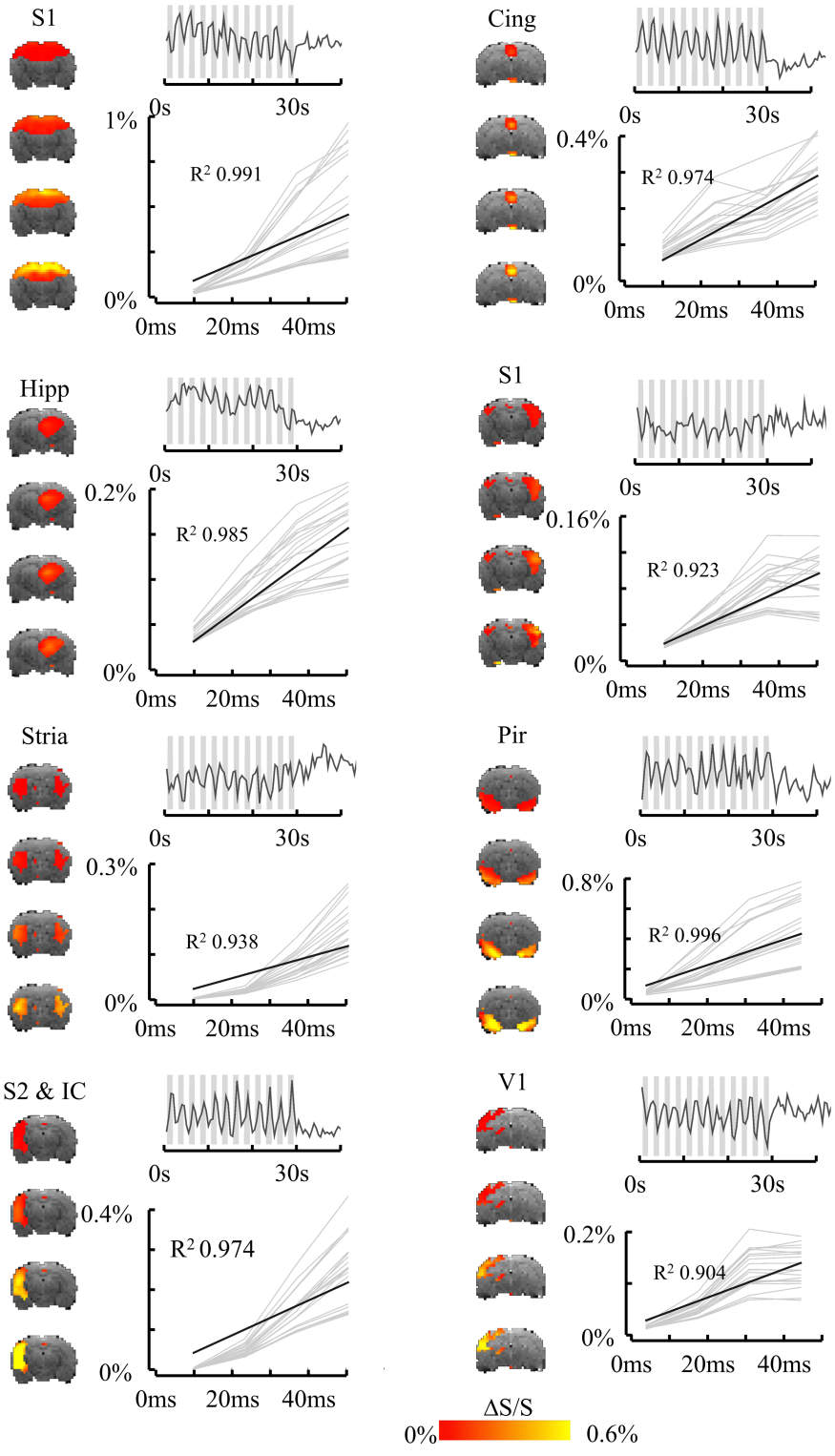

Figure 3-5 Fast fMRI response is echo-time dependent. *Multi-echo independent component analysis was used to test the echo-time dependence of the observed fast fMRI response. The activation maps and time series of eight independent components containing fast fMRI fluctuation*

are shown. These components include the primary and secondary somatosensory cortex (S1 & S2), cingulate cortex (Cing), hippocampus (Hipp), striatum (Stria), piriform cortex (Pir), visual cortex (V1), and insular cortex (IC). The map of each component is presented as the ΔS/S under different echo times (10, 23.5, 37, 50.5 ms), and the time series has unit variance. The linear relationship between the echo time and %ΔS/S is also presented for each component. The grey curves represent results from individual fMRI sessions, and the dark line shows the overall echo-time dependency.

Neural response to gastric stimuli

To confirm the neural origin of the observed fast BOLD responses, we recorded LFP from the primary somatosensory cortex in five animals under gastric stimuli modulated in the same way as in the fMRI experiment. We chose the somatosensory cortex because it was most reliably activated with gastric stimuli modulated at all three frequencies: 0.2, 0.4, and 0.8 Hz. Specifically, the electrode was inserted to the left S1FL, the cortical area representing the left forepaw, which was confirmed based on observable neural responses to electrical stimuli applied to the left forepaw. From the recorded signals, we extracted the evoked responses to periodically modulated (at 0.2, 0.4, or 0.8 Hz) gastric stimuli during the entire 30-s STIM period.

As shown in Figure 3-6A, a train of gastric stimuli only evoked a transient LFP response shortly after the beginning of the stimulus train, whereas no LFP response was observed for the rest of the stimulus train. Although the LFP response was not phase-locked to every single pulse of gastric stimulation, a transient LFP response was observed for every stimulus train. It was phase-locked to the onset of the stimulus train (or the ON block), reoccurring at the same frequency as the stimulus train was turned ON and OFF periodically. In short, the periodically modulated gastric stimuli induced periodically occurring transient neural responses in S1FL.

The transient LFP response were highly consistent across animals. See the gray lines in Figure 3-6B for the response in each animal. Whereas the response timing was consistent across different frequency settings, the amplitude of the transient LFP response was slightly lower as

gastric stimuli were modulated at an increasingly higher frequency: 355±154μV for 0.2Hz; 312±132μV for 0.4Hz; 227±107μV for 0.8Hz).

Although they were acquired in separate sessions, we further compared the neural and BOLD responses colocalized to S1FL. As shown in Figure 3-6C, the transient (~100ms duration) neural response corresponded to a much longer BOLD response, presumably reflecting the temporal smoothing due to neurovascular coupling. A greater amplitude in the neural response corresponded to a greater amplitude in the BOLD response, as observed across the different frequency settings.

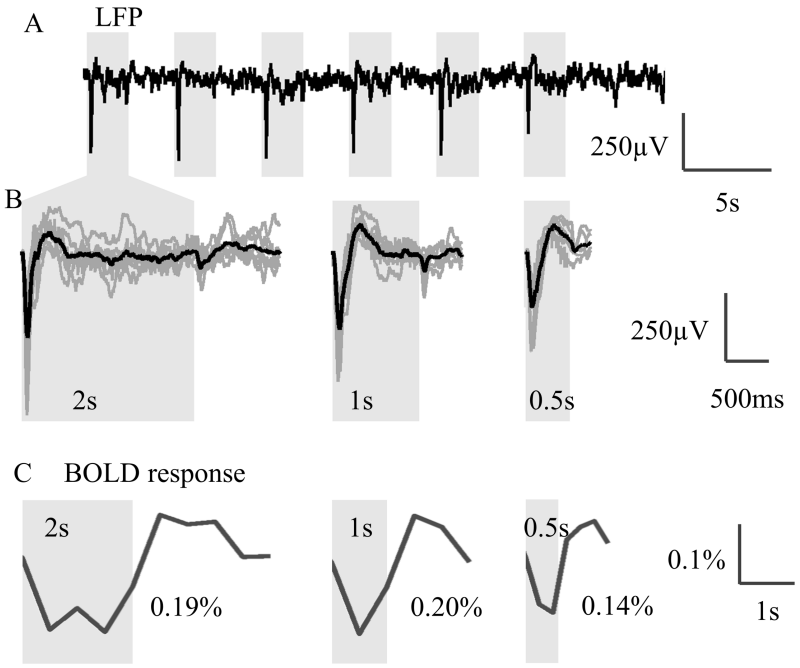

Figure 3-6 LFP and BOLD responses to gastric stimuli. Panel A *shows the LFP responses at S1FL given gastric stimuli modulated at 0.2 Hz during the 30-s STIM block. The dark line shows the LFP response averaged across animals. The light gray background indicates the ON period in which the stimulus train was delivered. Panel* ***B*** *is a zoomed-in view and shows the evoked LFP response during a single ON period. The gray curves represent the response for individual animals. The response averaged across animals is shown as the dark curve. The gray background indicates the period of the stimulus train. The responses during 2, 1, and 0.5s ON periods correspond to the 0.2, 0.4, and 0.8Hz modulation of gastric stimuli. In a similar format as* ***B****, panel* ***C*** *shows the average BOLD responses from S1FL given 0.2, 0.4, and 0.8Hz modulation of gastric stimuli. Scale bars are shown to the right.*

Discussion

In this study, we investigated the fMRI responses to gastric electrical stimulation in rats. We report that rapidly modulated gastric stimuli can drive fast fMRI responses up to 0.8 Hz in multiple brain regions, especially the somatosensory cortex. Such fast responses are linearly dependent on echo-time and are thus indicative of BOLD changes. The observed fMRI responses also accompany transient changes in broadband neural activity and are thus of neural origin. The reported findings corroborate that fMRI is capable of capturing higher frequency fluctuations in neural activity than is traditionally assumed or utilized. Whereas it is in line with recent studies with exteroceptive visual stimulation (Lewis et al., 2016, 2018), the conclusion from this study lends support to generalizing the feasibility of detecting fast fMRI response to interoceptive visceral stimulation, e.g. gastric electrical stimulation.

Fast fMRI responses to interoceptive visceral stimuli

Arguably, if the fast fMRI response could be used more broadly for neuroscience, its presence and basis need to be investigated in a broader and more diverse set of conditions, including visceral stimulation. It is very unusual to use gastric stimulation in fMRI studies. Gastric stimuli drive interoceptive sensory pathways and ascending modulatory pathways. They affect many brain regions in ways that are highly different from exteroceptive senses, e.g. vision, hearing, touch, taste. Interoceptive neural processes are always active in part for the purpose of maintaining homeostasis of the gut or other visceral organs, thereby contributing to spontaneous fluctuations of brain activity observed in the resting state (Fox and Raichle, 2007). Gastric stimulation can affect emotional, cognitive, and affective systems beyond activations with simple sensory stimuli (Van and Aziz, 2009). The profound and broad impact of gastric stimulation on the brain makes it a useful paradigm, distinctive from and complementary to existing sensory stimulation paradigms,

for investigating the characteristics of the fMRI signal beyond any single system, yet still in a controllable manner to address fundamental questions concerning, e.g., the feasibility and basis of fast fMRI signals.

The gut, as a sensory organ, communicates with the brain through fast electrical signals along cranial nerves or through slow acting hormones or cytokines circulated in the bloodstream. Depending on the mechanism of gut-to-brain signaling, brain responses to gastric sensation, whether mechanical or chemical in nature, emerge in a wide range of timescales, ranging from milliseconds, seconds, to minutes or even longer. It implies that brain responses arising from different signaling pathways (neuronal, endocrine, or immune systems) are likely to manifest themselves in distinct and potentially separable frequency ranges. Although this hypothesis remains speculative and provisional, identifying the upper limit of the fMRI detectable responses to gastric stimuli is a necessary first step towards exploring and utilizing the frequency properties to separately characterize gut-brain interactions of different mechanisms.

This study is focused on fast fMRI responses that occur within a few seconds following the modulation of gastric stimuli. In this temporal scale, the responses are most likely to arise from neuronal signaling from the gut to the brain, instead of endocrine or immune-related signaling (Mayer, 2011). Furthermore, the pattern of fMRI results indicates that the gastric electrical stimulation we delivered did effectively activate vagal afferent activity, thus potentially engaging vagovagal reflexes as well as the fast fMRI responses in the CNS. In particular, the stimulating electrodes were intentionally placed on the forestomach wall at a site that has been found to have a high density of vagal longitudinal intramuscular arrays (Powley & Phillips, 2011; Powley et al., 2016)—presumably a type of stretch receptor that transduces the mechanical information associated with eating and drinking into electrical signals propagating up the vagus to the

brainstem. The fact that both the BOLD signal in the "vagal neuroaxis" (vagus – nucleus of the solitary tract – parabrachial nucleus – thalamus – insula, etc.) and the multi-unit responses in the vagal complex were activated by direct gastric forestomach stimulation (Cao et al., 2019) indicate that "fast" GES does indeed activate "fast" neurovascular coupling in the vagal neuroaxis.

Though a full analysis is beyond the scope of the present investigation, the fMRI results also underscore the possibility that local stimulation of the stomach, i.e. forestomach, wall to engage vagovagal reflexes concomitantly activates dorsal root visceral afferents. While no detailed maps of visceral afferent innervation appear to exist, such afferents have clearly been described in the stomach (Spencer et al., 2016), and the present pattern of fMRI results reinforces the inference that local forestomach "fast" GES directed at the longitudinal intramuscular arrays may simultaneously activate the visceral afferents associated with sympathetic efferent projections. More specifically, the BOLD signal in the dorsal root lamina of the spinal cord and the conspicuous effects in the somatosensory cortex both suggest (see Jänig, 2006) the possibility of an early and "fast" BOLD activation by dorsal root visceral afferents.

Gut-associated brain regions

The gut sends neuronal afferent signals to the brain through sympathetic (spinal) and parasympathetic (vagal) pathways. Vagal afferents project to NTS, whereas spinal afferents project to the lamina I of the dorsal horn. The two pathways converge at the parabrachial nucleus, continue onto the forebrain or raphe nuclei and locus coeruleus, and further project to the cortex, especially for the cingulate cortex, insular cortex, prefrontal cortex, hippocampus, amygdala, and somatosensory cortex (Tillisch et al., 2018; Farmer et al., 2018). In the human brains, these regions interact as functional networks and have been found, at least in part, to respond to gastric

stimulation or exhibit brain activity correlated with spontaneous gastric activity (Mayer et al., 2009; Lee et al., 2016; Rebollo et al., 2018).

To the best of our knowledge, the gut-associated regions have been rarely mapped in the rat brain (Han et al., 2018; Wang et al., 2008), especially in the whole-brain scale observable with MRI (Johnson et al., 2010; Min et al., 2011). In this study, some rat brain regions activated by gastric stimuli appeared homologous to the putative gut-associated regions reported in human studies (Tillisch et al. 2018). However, the activated regions are not precisely confined to structurally defined regions but appear more diffuse than those reported in humans. On the basis of the results obtained with component (Figure 3-2), region (Figure 3-3), and voxel-wise (Figure 3-4) analyses, gastric electrical stimuli can activate the somatosensory cortex, cingulate cortex, insular cortex, as well as the motor cortex, thalamus, or even auditory cortex, in line with previous imaging studies in rats, e.g. (Wang et al, 2008). Speculatively, the diffuse responses are likely due to a widespread effect of visceral stimulation on brain activity (Cao et al., 2017).

We observed GES-induced activation in the sensorimotor network, including the somatosensory and motor cortex, is consistent with previous neuroimaging studies of brain-gut interactions (Aziz et al., 2000; Brüggemann et al., 1997; Rebollo et al., 2018; Strigo et al., 2003; Wang et al., 2008). Beyond the sensorimotor regions, the activation also covers, at least in part, the auditory and visual cortex. This finding has been rarely reported or discussed in literature, except (Rebollo et al., 2018; Wang et al., 2008). In Rebollo et al., 2018, gastric activity observed with body surface electrogastrogram (EGG) was found to be correlated with spontaneous brain activity at regions associated with touch, action, vision, as well as multi-sensory integration. In a plausible explanation, foraging, feeding or eating behaviors, which regulate gastric physiology, involve multiple sensory modalities and sensorimotor coordination (Rebollo et al., 2018).

Moreover, the lack of report for the visual and auditory involved gastric response is likely due to the differences in stimulation protocols (Wang et al., 2008). However, it is unclear whether multi-sensory and motor areas are necessarily engaged in response to gastric stimuli even in the absence of any sensory input or/and when the animal is anesthetized or sedated. In an alternative explanation, the broad activation of sensory areas does not reflect cortical processing of the sensory information from the gut, or certainly not the processing of any visual or auditory information. Instead, it likely reflects the change in cortical arousal, because the gut-innervating vagal and spinal afferents in part project to raphe nuclei and locus coeruleus complex, which provide input to ascending monoaminergic projections to the nearly entire cortex (Hulsey et al., 2017; Dorr and Debonnel, 2006).

In addition, our results reveal gastric stimulus-evoked activation in the midcingulate cortex and the insular cortex. The midcingulate activation includes its anterior and posterior parts. The insular activation, although less reliable as in a previous study (Mayer et al., 2009), is noticeable in the ROI analysis. Both the cingulate cortex (especially its anterior part) and the insular cortex are known to be involved in the gut-brain interaction, acting as the highest level of hierarchical homeostatic reflexes (Mayer, 2011) and regulating emotional arousal (Naliboff et al., 2006; Van Oudenhove and Aziz, 2009).

Given our focus on fast fMRI responses, it is noteworthy that the GES-activated regions reported herein are perhaps incomplete and may or may not be generalizable across gastric stimuli in different ways, at different sites, or with different parameters. Some subcortical areas (e.g. those in brainstem, hypothalamus, amygdala) are expected to be activated but are not shown in our results. It may be in part because of the fast-modulation paradigm used in our study design and in part due to the inter-regional difference in neurovascular coupling. The current stimulation

paradigm and analysis pipeline focus exclusively on the fast (>0.2Hz) BOLD response. It is likely that other regions were also activated by GES but showed responses at lower frequencies, and such regions would not be revealed as "activated" given our analyses. Subcortical areas tend to be less vascularized and thus more challenging to be detected with fMRI, especially when the frequency of interest is pushed toward the upper limit.

The origin of fast BOLD activity

Exteroceptive sensory stimulation is often used in studies that characterize the coupling between neural and hemodynamic responses in animals and humans. Previous animal studies have shown that the sensory stimulus-evoked hemodynamic response observed with fMRI can emerge as soon as 0.8s (Yu et al., 2012) and reach a peak at about 2.7s (de Zwart et al., 2005). Such onset and peak times are much faster than those in the canonical hemodynamic response function (Boynton et al., 1996). Therefore, the widely-held assumption that the fMRI signal is slow and primarily lower than 0.1Hz should be taken with caution and be revisited in future experimental and modeling studies.

However, the rapid change in impulse hemodynamic response does not necessarily lead to observable fMRI signal in a relatively high frequency range (e.g. 0.2 to 0.8Hz) (Hathout et al., 1999; Janz et al., 2001). This is because neurovascular coupling is not entirely linear but depends on the frequency (Lewis et al., 2016; Liu et al., 2010; Zhang et al., 2008), amplitude, and duration of neural response (Pfeuffer et al., 2003; Yeşilyurt et al., 2008). If neural response is relatively weak or short (likely due to strong adaptation), its cumulative (over time) effect is less likely to saturate the vascular response, allowing the vasculature to remain sensitive to changes in neural activity and respond within its dynamic range and thus capable of following faster modulation in neural activity. Indeed, our results suggest that a train of gastric stimuli only induce a transient

neural response (Figure 6), setting the system of neurovascular coupling to operate in a linear range such that the fast fMRI response is more likely observable.

Limitations and future directions

Although we conclude that the observed fMRI response is BOLD in nature and of neural origin, it is non-trivial to further pinpoint its neural origin and elucidate the precise relationship between neural and BOLD effects as a result of gastric stimuli. It remains unclear which types of neural processes drive the observed fast BOLD responses. It is likely that gastric stimuli may drive changes in ascending neuromodulation through vagal afferents and their extension in CNS (Cheyuo et al., 2011). It is also likely that gastric stimuli trigger the transmission and processing of sensory information at various brain regions through vagal as well as spinal afferents. Such neural processes are likely differentiable in terms of the response profile across different cortical layers, or across different frequency bands. Although it is beyond the scope of this study, it is of great interest to disentangle the various contributors to the fast fMRI responses to gastric stimuli.

The gut-brain circuitry is part of the autonomic nervous system. Therefore, stimulating the stomach could also affect the other components of the autonomic nervous system through projecting nerves and signaling molecules (Carabotti et al., 2015; Powley 2014). Such modulation of the autonomic nervous system may cause physiological variations in respiration and heart rate. To address the potential physiological effects on the fMRI signal, we recorded and compared the respiratory and cardiac activities between the stimulation ON and OFF periods but found no significant difference. Moreover, the fact that the observed fMRI response was found to be BOLD (Figure 3-4) and of neural origin (Figure 3-5) suggests that non-neuronal physiological fluctuation has a relatively minor contribution to the fast fMRI response to gastric stimulation. However, to

what extent the observed fMRI responses are specifically attributable to the gut, as opposed to the indirect effect on the other visceral organs, remains to be fully addressed in future studies.

The focus of this study was primarily on the spectral characteristics of the fMRI response to gastric stimuli. Given this focus, gastric stimuli were modulated in a periodic ON-OFF pattern as a square-wave approximate of a sinusoidal input – ideal for probing the frequency-specific response, while using a constant stimulation dose during the 30s STIM period regardless of the frequency of modulation. Such a paradigm is well suited for spectral characterization of the system underlying the steady-state response; however, it is not the ideal design for studying the event-related response. To note one limitation, the number of gastric stimuli during each ON period varied across different frequency settings (0.2, 0.4 and 0.8Hz), because the inter-stimulus interval was kept constant and the ON duration was longer for a lower frequency (e.g. 0.2Hz). For a single ON-OFF cycle, we delivered more gastric stimuli for 0.2Hz, relatively fewer for 0.4Hz, and the fewest for 0.8Hz. This variation might confound the direct comparison of the single-cycle response (peak-to-peak) amplitude across different frequency settings. Nevertheless, it should not diminish the single-cycle fMRI response observed at a higher frequency (e.g. 0.8Hz). Instead, it is reasonable to anticipate that the single-cycle response amplitude might be even higher than was shown in our results, if the stimulation dose with each ON period were kept constant across different frequency settings.

We only recorded neural responses from S1FL. Since other regions activated with gastric stimuli are not as easily accessible as S1, they are excluded from the full analysis in this study. In future studies, we will attempt to record both neural and fMRI responses, ideally simultaneously, at all regions involved in gut-brain interaction. Moreover, it is of interest to record the changes in specific types of neurotransmitters (e.g. norepinephrine and serotonin), in addition to fMRI and

electrophysiological responses. However, such multimodal recordings are challenging and not readily feasible with our existing experimental techniques.

Findings from this study are based on observations from anesthetized rats. All animals were anesthetized using dexdomitor and low-dose isoflurane (<0.5%) as in our prior study (Cao et al., 2017). It should be noted that anesthesia may weaken the BOLD response (Liang et al., 2015; Williams et al., 2010) and affect neurovascular coupling (Magnuson et a., 2014). To be more comparable to human studies, it is of great interest to acquire fMRI and neural signals from animals in fully awake or un-anesthetized conditions, as increasingly advocated (Gao et al., 2017).

Chapter 4 Vagus Nerve Stimulation Triggers Wide-Spread BOLD Responses in the Brain [3]

Summary

Vagus nerve stimulation (VNS) is a therapy for epilepsy and depression. However, its efficacy varies and its mechanism remains unclear. Prior studies have used functional magnetic resonance imaging (fMRI) to map brain activations with VNS in human brains, but have reported inconsistent findings. The source of inconsistency is likely attributable to the complex temporal characteristics of VNS-evoked fMRI responses that cannot be fully explained by simplified response models in the conventional model-based analysis for activation mapping. To address this issue, we acquired 7-Tesla blood oxygenation level dependent fMRI data from anesthetized Sprague–Dawley rats receiving electrical stimulation at the left cervical vagus nerve. Using spatially independent component analysis, we identified 20 functional brain networks and detected the network-wise activations with VNS in a data-driven manner. Our results showed that VNS activated 15 out of 20 brain networks, and the activated regions covered >76% of the brain volume. The time course of the evoked response was complex and distinct across regions and networks. In addition, VNS altered the strengths and patterns of correlations among brain networks relative to those in the resting state. The most notable changes in network-network interactions were related to the limbic system. Together, such profound and widespread effects of VNS may underlie its unique potential for a wide range of therapeutics to relieve central or peripheral conditions.

[3] Formatted for dissertation from the article published in PloS one. (Cao et al., 2017)

Introduction

Since the 1800s (Gaskell, 1886; Robinson & Draper, 1912), vagus nerve stimulation (VNS) has been studied as a potential way to treat various diseases, including epilepsy, depression, tinnitus, Alzheimer's Disease, and obesity (Ben-Menachem, 2002; Bodenlos et al., 2007; De Ridder et al., 2014; George et al., 2000; Peña et al., 2013; Sjögren et al., 2002). The therapeutic benefits apparently depend on the effects of VNS on the central neural system (CNS) mediated through neuroelectrical or neurochemical signaling (Henry, 2002). Studies have been conducted to evaluate the CNS responses to VNS with neural imaging or recording techniques. For example, invasive recordings of unit activity or field potentials have shown VNS-evoked neuronal responses in the nucleus of solitary tract (Beaumont et al., 2017), the locus coeruleus (Groves et al., 2005), and the hippocampus (Larsen et al., 2016). These techniques offer high neuronal specificity but only cover spatially confined targets. In contrast, electroencephalogram (EEG) has been used to reveal VNS-induced synchronization or desynchronization of neural oscillations in the macroscopic scale (Bartolomei et al., 2016; Chase et al., 1967), while being severely limited by its spatial resolution and specificity as well as its inability to detect activities from deep brain structures. However, sub-cortical regions are of interest for VNS, because the vagus nerves convey signals to the brain through polysynaptic neural pathways by first projecting to the brainstem, then subcortical areas, and lastly the cortex (Henry, 2002; Ressler KJ, Mayberg, 2007).

Complementary to conventional electrophysiological approaches, functional neuroimaging allows the effects of VNS to be characterized throughout the brain volume. Using positron emission tomography (PET) or single-photon emission computerized tomography (SPECT), prior studies have reported VNS-evoked responses in the thalamus, hippocampus, amygdala, inferior cerebellum, and cingulate cortex (Garnett et al., 1992; Ko et al., 1996; Henry et al., 1999; Zobel et

al., 2005); but these techniques are unable to capture the dynamics of the responses due to their poor temporal resolution. In this regard, functional magnetic resonance imaging (fMRI) is more favorable because it offers balanced and higher spatial and temporal resolution. Previous human VNS-fMRI studies have reported VNS-evoked blood oxygenation level dependent (BOLD) responses in the thalamus, hypothalamus, prefrontal cortex, amygdala, and hippocampal formation (Bohning et al., 2001,2003; Devous et al., 2002; Sucholeiki et al., 2002; Liu et al., 2001). However, the reported activation patterns are not always consistent (Chae et al., 2003), sometimes highlighting activations in different regions or even opposite responses in the same regions (Devous et al., 2002; Sucholeiki et al., 2002; Liu et al., 2001). What underlies this inconsistency might explain the varying efficacy of VNS in treatment of individual patients, or might be attributed to the analysis methods for activation mapping (Chae et al., 2003). Therefore, it is desirable to explore and evaluate various methodological choices in the fMRI data analysis, in order to properly interpret the VNS evoked activations for understanding the implications of VNS to neurological disorders.

Functional MRI not only localizes the CNS responses of VNS (Chae et al., 2003), it also reveals the patterns and dynamics of functional networks during VNS, which helps to characterize the network basis of VNS-based therapetutics. Findings from prior studies have shown that the therapeutic or behavioral effects of VNS may be compromised, when the underlying neuronal circuit is disrupted in terms of its critical node or receptor. For example, given a lesion in the locus coeruleus, VNS fails to suppress epilepsy (Krahl et al., 1998); given a blockade of the muscarinic receptor, VNS fails to promote perceptual learning (Nichols et al., 2001). However, how VNS affects the patterns of interactions among regions or networks (or functional connectivity) has

rarely been addressed (Fang et al., 2016), even though fMRI has become the primary tool for studying functional connectivity (Biswal et al., 1995; Van Den Heuvel & Pol, 2010).

In this study, we aimed to address the BOLD effects of VNS in the rat brain. The use of a rat model mitigated the inter-subject variation in genetics, gender, age, weight, and health conditions. It provided a well-controlled setting for us to focus on comparison of different analysis methods for mapping the activations with VNS. Specifically, we used the independent component analysis (ICA) to identify brain networks, and then used a data-driven analysis to detect the VNS-evoked activation separately for each network, as opposed to each voxel or region. In addition to the activation mapping, we also evaluated the effects of VNS on network-network interactions, against the baseline of intrinsic interactions in the resting state. As such, we attempted to address the effects of VNS on the brain from the perspectives of both regional activity and inter-regional functional connectivity.

Methods and Materials

Subjects

A total of 17 Sprague–Dawley rats (male, weight: 250-350g; Envigo RMS, Indianapolis, IN) were studied according to a protocol approved by the Purdue Animal Care and Use Committee (PACUC) and the Laboratory Animal Program (LAP). Of the 17 animals, seven animals were used for VNS-fMRI experiments; ten animals were used for resting state fMRI. All animals were housed in a strictly controlled environment (temperature 21±1°C and 12 h light-dark cycle, lights on at 6:00 AM, lights off at 6:00 PM).

Animal preparation

For the VNS-fMRI experiments, each animal was initially anesthetized with 5% isoflurane and maintained with continuous administration of 2-3% isoflurane mixed with oxygen and a bolus

of analgesic (Rimadyl, 5 mg/Kg, Zoetis) administrated subcutaneously. After a toe-pinch check for adequate anesthesia, a 2-3cm midline incision was made starting at the jawline and moving caudally. The left cervical vagus nerve was exposed and isolated after removing the surrounding tissue. A bipolar cuff electrode (Microprobes, made of platinum and with 1mm between contacts) was wrapped around the exposed vagus nerve. For resting-state fMRI experiments, animals were anesthetized with the same dose of anesthesia without the surgical procedures.

After the acute electrode implantation (for VNS-fMRI) or the initial anesthetization (for resting-state fMRI), each animal was moved to a small-animal horizontal MRI system (BioSpec 70/30, Bruker). The animal's head was constrained with a customized head restrainer. A bolus of dexdomitor (Zoetis, 7.5 μg/Kg for animals gone through electrode implantation, 15 μg/Kg for animals without surgery) was administrated subcutaneously. About 15-20 mins after the bolus injection, dexdomitor was continuously and subcutaneously infused at 15 μg/Kg/h; the dose was increased every hour as needed (Pawela et al., 2009). In the meanwhile, isoflurane was administered through a nose cone, with a reduced concention of 0.1-0.5% mixed with oxygen. Throughout the experiment, both the dexdomitor infusion rate and the isoflurane dose were adjusted to maintain a stable physiological condition with the respiration rate between 40 and 70 times per min and the heart rate between 250 and 350 beats per min. The heart and respiration rates were monitored by using a small-animal physiological monitoring system (Kent Scientific). The animal's body temperature was maintained at 37 ± 0.5 °C using an animal-heating system. The oxygen saturation level (SpO_2) was maintained above 96%.

Vagus nerve stimulation

The bipolar cuff electrode was connected to a current stimulator (model 2200, A-M system) placed outside of the MRI room through a twisted-pair of copper wire. Stimulation current was

delivered in 10s-ON-50s-OFF cycles. When it was ON, biphasic square pulses (width: 0.1 ms; amplitude: 1.0 mA; frequency: 10 Hz) were delivered. Each fMRI session included ten ON/OFF cycles. A resting (stimulation-free) period of at least one minute was given between sessions. Up to 4 sessions were scanned for each animal. Figure 4-1 illustrates the VNS paradigm.

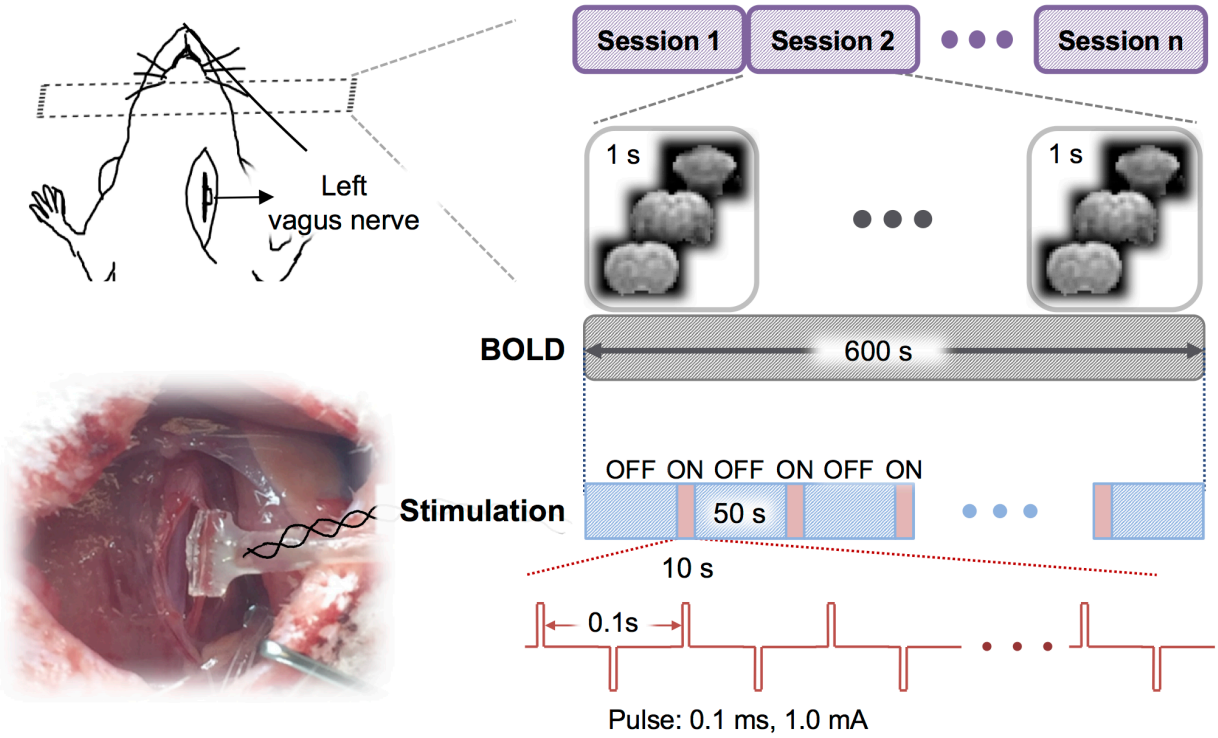

Figure 4-1 Experimental design for fMRI during VNS. *Each rat was stimulated at the left cervical vagus through a cuff electrode implanted in an acute surgery. Biphasic current pulses were delivered during a 10s "ON" period alternating with a 50s "OFF" period for 10 cycles. With this block design, the rat was scanned for fMRI with a repetition time of 1s.*

MRI and fMRI

MRI data were acquired with a 7-T small-animal MRI system (BioSpec 70/30, Bruker) equipped with a volume transmitter coil (86 mm inner diameter) and a 4-channel surface receiver array. After the localizer scans, T_2-weighted anatomical images were acquired with a rapid acquisition with relaxation enhancement (RARE) sequence (repetition time (TR)=5804.607s, effective echo time (TE)=32.5ms, echo spacing=10.83 ms, voxel size=0.125×0.125×0.5mm^3,

RARE factor=8, flip angle (FA)=90°). The BOLD-fMRI data were acquired by using a 2-D single-shot gradient echo echo-planar imaging (EPI) sequence (TR=1 s, TE=15 ms, FA=55°, in-plane resolution about 0.6×0.6 mm^2, slice thickness=1 mm).

Data preprocessing

MRI and fMRI data were preprocessed by using Analysis of Functional Neuroimages (AFNI) and custom-built functions in MATLAB. Within each session, the fMRI data were corrected for motion by registering every volume to the first volume using *3dvolreg*. After removing the first ten volumes, *retroicor* was used to correct for the motion artifacts due to respiratory and cardiac activity (Birn et al., 2006; Glover et al., 2000). Then, *slicetimer* was used to correct the timing for each slice. For each animal, we first registered the EPI image to its T_2 weighted structural images and then normalized to a volumetric template (Valdés-Hernández et al., 2011) using *flirt*. Motion artifacts were further corrected by regressing out the six motion-correction parameters. The fMRI data were then spatially smoothed with a 3-D Gaussian kernel with a 0.5-mm full width at half maximum (FWHM). The fMRI time series were detrended by regressing out a 2rd-order polynomial function voxel by voxel.

General linear model analysis

We used the conventional general linear model (GLM) analysis to map the activations evoked by VNS as in previous studies (Bohning et al., 2001; Kraus et al., 2007, 2013; Lomarev et al., 2002; Nahas et al., 2007). Specifically, we derived a response model by convolving the stimulation block (modeled as a box-car function) with a canonical hemodynamic response function (HRF) (modeled as a gamma function). For each session, the fMRI signal at every voxel was correlated with this response model. The correlation coefficient was converted to a z-score by using the Fisher's z-transform. The voxel-wise z-score was averaged across sessions and animals,

and the average z-score was evaluated for statistical significance with a one-sample t-test ($p<0.05$, uncorrected).

This analysis revealed the group-level activation map with VNS given an assumed response model. Since the validity of this response model for VNS was not established, we intentionally varied the response model by assuming three different values (3s, 6s, or 9s) for the peak latency of the HRF. We compared the activation maps obtained with the three different response models, to qualitatively assess the dependence of the model-based activation mapping on the presumed response characteristics.

Independent component analysis

In contrast to the voxel-wise GLM analysis, we used ICA to map networks and characterize their responses to VNS in a data-driven or model-free manner. For each session and each voxel, the fMRI signal during VNS was demeaned and divided by its standard deviation. The resulting fMRI data were then concatenated across all VNS-fMRI sessions. Infomax ICA (Bell et al., 1995) was used to decompose the concatenated data into 20 spatially independent components (ICs). Each of these ICs included a spatial map and a time series, representing a brain network and its temporal dynamics, respectively. In the spatial maps of individual ICs, the intensities at each given voxel represented the weights by which the time series of corresponding ICs were combined to explain this voxel's fMRI time series. The polarity of each IC was determined to ensure the positive skewness of its weight distribution. Such weights were converted to Z-statistics and then thresholded as described in a previous paper (Beckmann & Smith, 2004). The threshold was selected such that the false negative rate was three times as large as the false positive rate. To obtain the false negative and positive rates, the Z-statistics of all voxels in an IC map were modeled

as a two-Gaussian mixture distributions: one representing the noise, the other representing the signal.

Following ICA, we evaluated the VNS-evoked response separately for each IC, instead of each voxel. To do so, each IC's time series was segmented according to the timing of every VNS block. Each segment lasted 54 seconds, starting from 3 seconds before the onset of a VNS block to 41 seconds after the offset of this block, while the stimulus block lasted 10 seconds. To address whether an IC responded to the VNS, we treated each time point as a random variable and each segment as an independent sample. One-way analysis of variance (ANOVA) was conducted against a null hypothesis that there was no difference among all the time points (meaning no response). The ICs that were statistically significant (p<5e-6) were considered as activated by VNS.

For each activated IC, we further characterized its temporal response to VNS. Briefly, we identified the time points during or after the VNS block, where the signals significantly differed from the pre-stimulus baseline by using the Tukey's honest significant difference (HSD) test as a post-hoc analysis following the previous ANOVA test. Following this statistical test, the VNS-activated ICs were visually classified into three types (i.e. positive, negative, and mixed) of responses.

Functional connectivity analysis

We further addressed whether VNS altered the patterns of temporal interactions among functional networks identified by ICA. To do so, the voxel time series was demeaned and standardized for each fMRI session including both VNS and resting conditions. The fMRI data were concatenated across all sessions and were then decomposed by ICA to yield 20 spatially ICs or networks, along with their corresponding time series. The first IC was removed because it was

identified as the global component. The time series of the rest ICs were divided into the signals corresponding to the VNS sessions versus those corresponding to the resting-state sessions.

We defined the functional connectivity between networks as the temporal correlations between the ICs. The correlations were evaluated separately for the resting and VNS conditions and for every pair of ICs. Based on their temporal correlations, we grouped the ICs into clusters by applying k-means clustering method to ICs' temporal correlation matrix. As a result, the correlations tended to be stronger within clusters than between clusters.

We further evaluated the differences in functional connectivity between the VNS condition and the resting state. For this purpose, the functional connectivity between ICs was evaluated for each VNS session, as well as each resting-state session. Their differences between these two conditions were evaluated using unpaired two-sample t-test ($p<0.05$, uncorrected). The changes in functional connectivity were displayed in the functional connectogram (Irimia et al., 2012).

Results

Model-based VNS activations were sensitive to variation of the response model

Seven rats were scanned for fMRI while their left cervical vagus nerve was electrically stimulated in a (10s-ON-50s-OFF) block-design paradigm as illustrated in Figure 4-1. The BOLD response phase-locked to the VNS block appeared complex and variable across regions of interest (ROIs). For example, the BOLD responses were notably different across three ROIs, namely the retrosplenial cortex (RSC), brainstem (BS), and dorsal caudate putamen (Cpu) in a functional atlas (Ma et al., 2016) of the rat brain (Figure 4-2A). These responses were not readily explainable by a typical response model derived from a canonical HRF (Figure 4-2B, top). The GLM analysis with three different response models (by varying the HRF peak latency with 3s increments) yielded almost entirely distinctive activation maps (Figure 4-2B), each of which was only marginally

significant (p<0.05, uncorrected). Therefore, VNS-evoked BOLD responses were too complex and variable to be captured by a single response model. The GLM analysis likely leads to incomplete and inconsistent activations with VNS, which possibly accounts for the diverging findings reported in the related literature (Bohning et al., 2001,2003; Devous et al., 2002; Sucholeiki et al., 2002; Liu et al., 2001).

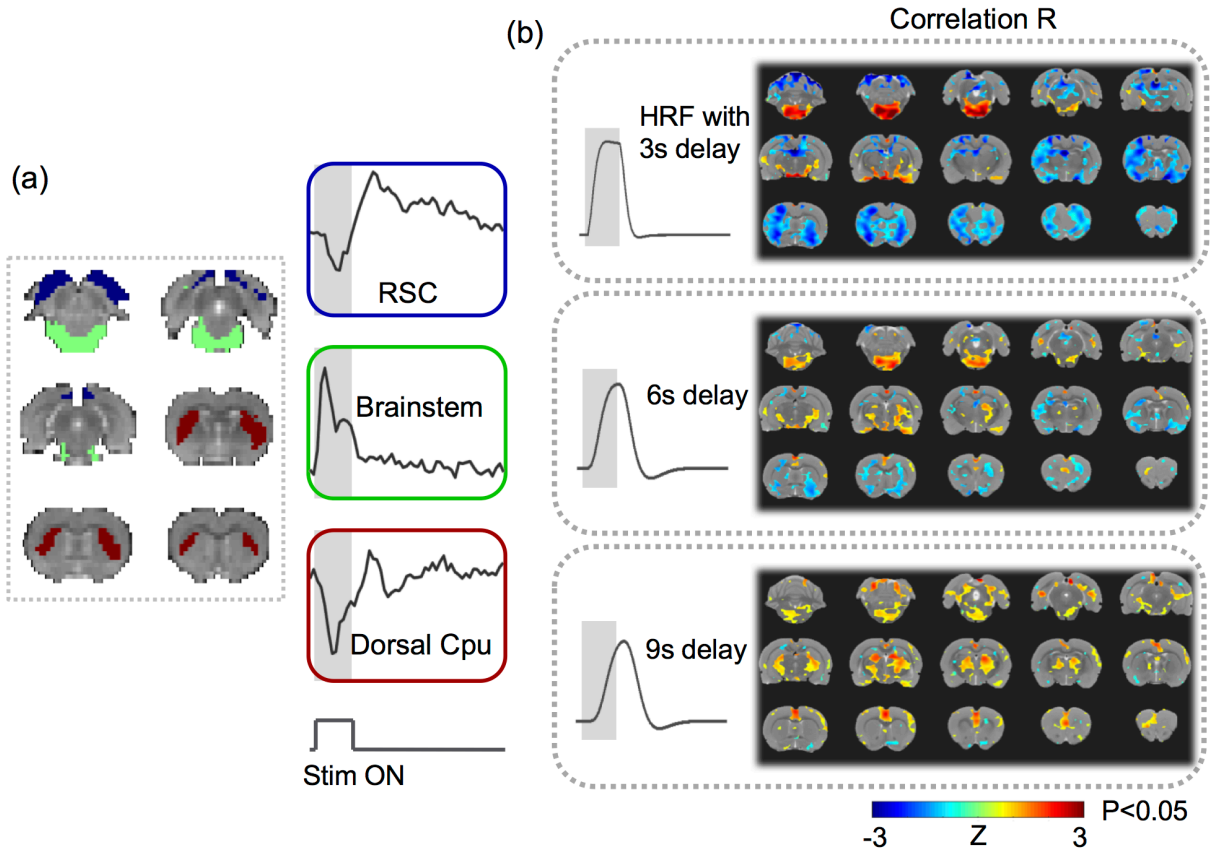

Figure 4-2 VNS-evoked responses varied across regions. *(A) shows the response time series averaged within each of the three regions of interest: the retrosplenial cortex (RSC) (blue), the brainstem (green), and the dorsal caudate putamen (Cpu) (red). (B) shows the highly different activation maps based on the response models derived with the HRF, for which the peak latency was assumed to be 3s, 6s, or 9s. The color shows the group average of the z-transformed correlation between the voxel time series and the modeled response. The maps were thresholded with p<0.05 (one-sample t-test, uncorrected).*

VNS induced widespread and complex network responses

With a data-driven method, we evaluated the VNS-evoked responses in the level of networks, where the networks were identified as spatially ICs. It turned out that 15 out of the 20 ICs were significantly activated by VNS (one-way ANOVA, p<5e-6, Fig 3A). Those activated ICs collectively covered 76.03% of the brain volume (Figure 4-3B). Among the activated regions, the brainstem and the hypothalamus exhibited relatively stronger responses than other areas.

The response time courses were also notably different across ICs. Figure 4-3A also highlights in red the time points, where the post-stimulus responses were significantly different from the pre-stimulus baseline (p<0.05, Tukey's HSD). It was noticeable that different ICs were activated at different times following VNS. The response time courses also showed different polarities and shapes, and could be generally classified as the positive, negative, or biphasic-mixed response. The negative response was shown in the amygdala, dorsal striatum, primary motor cortex, midbrain, left somatosensory cortex, and superior cerebellum. The positive response was shown mainly in the brainstem, thalamus, and hypothalamus. The mixed response was shown in the hippocampal formation, cingulate cortex, and prelimbic & infralimbic cortex. The ICs that appeared to exhibit similar responses to VNS were presumably more functionally associated with one another. From a different perspective, the network-wise response to VNS also seemed to be either stimulus-locked or long-lasting (i.e. sustained even 20-30 s after the end of VNS). The stimulus-locked response was most notable in the brainstem and hypothalamus, which receives more direct vagal projections with fewer synapses. The long-lasting response was shown in the hippocampal formation, prefrontal cortex, amygdala, all of which were presumably related to high-level cognitive functions, such as memory formation, decision making, and emotion regulation. Speculatively, the former was the direct effect of VNS; the latter was the secondary effect.

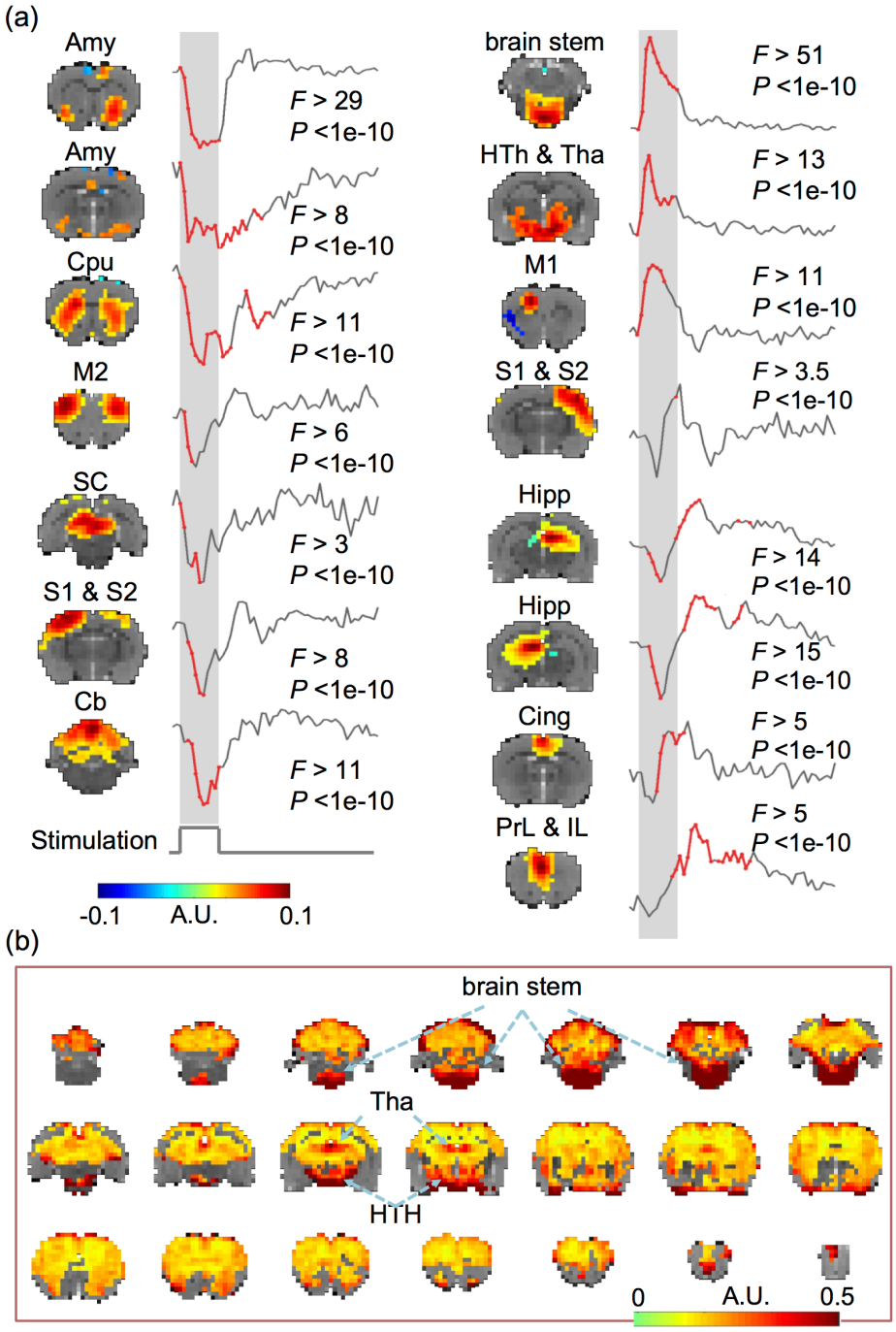

Figure 4-3 VNS evoked widespread and complex responses in the brain. *(A) VNS-evoked responses for different brain networks derived with ICA. The ICA-defined networks are labeled as: amygdala (Amy), caudate putamen (Cpu), hippocampus, (Hipp), cingulate cortex (Cing), prelimbic cortex (PrL), infralimbic cortex (IL), brain stem, hypothalamus (HTh), thalamus (Tha), superior colliculus (SC), cerebellum (Cb), primary and secondary motor cortex (M1, M2), and primary and secondary somatosensory cortex (S1, S2). For each network, the time points at which the responses were significant are shown in red. (B) The VNS-activated voxels cover 76.03% of the brain volume. The color represents the standard deviation of the voxel-wise response averaged*

across repetitions of VNS. The locations with the greatest responses are highlighted with arrows. Data relevant to the VNS-evoked network responses are available in the online Supplementary Information.

VNS altered functional connectivity

We further evaluated the network-network interactions during VNS in comparison with those in the resting state. The networks were captured as the ICs obtained by applying ICA to the data in both VNS and resting conditions. The matrix of pair-wise (IC-IC) correlations during VNS was overall similar to that in the resting state (Figure 4-4A). However, their differences in functional connectivity reorganized the clustering of individual networks (into Group 1, 2, 3) (Figure 4-4A). Group 1 covered the sensorimotor cortex, and it was mostly consistent between the VNS and resting conditions. Relative to the resting state, VNS reduced the extent of networks for Group 2, but increased the extent of networks for Group 3. For a closer investigation of the network reorganization, we found that VNS strengthened the correlations between the hippocampal formation and the retrosplenial cortex, but weakened the correlations between the prefrontal cortex and the basal ganglia. Beyond the difference in clustering, the significant changes in functional connectivity ($P<0.005$, t-test) are all shown in Figure 4-4B. The most notable changes were all related to the limbic system. During VNS, the cingulate cortex was less correlated with the ventral striatum; the hippocampal formation formed stronger functional connectivity between its left and right components, and with the retrosplenial cortex. The reorganization of functional connectivity was not only confined to the regions within the limbic system, but also between the limbic system and the sensorimotor cortex. VNS strengthened the interaction across the sensorimotor cortex with the hippocampal formation, retrosplenial cortex, and dorsal striatum, whereas it weakened the functional connectivity between the sensorimotor cortex and the cingulate cortex. In short, VNS

reorganized the functional connectivity within the limbic system and altered the interactions between the limbic system and the sensorimotor cortex.

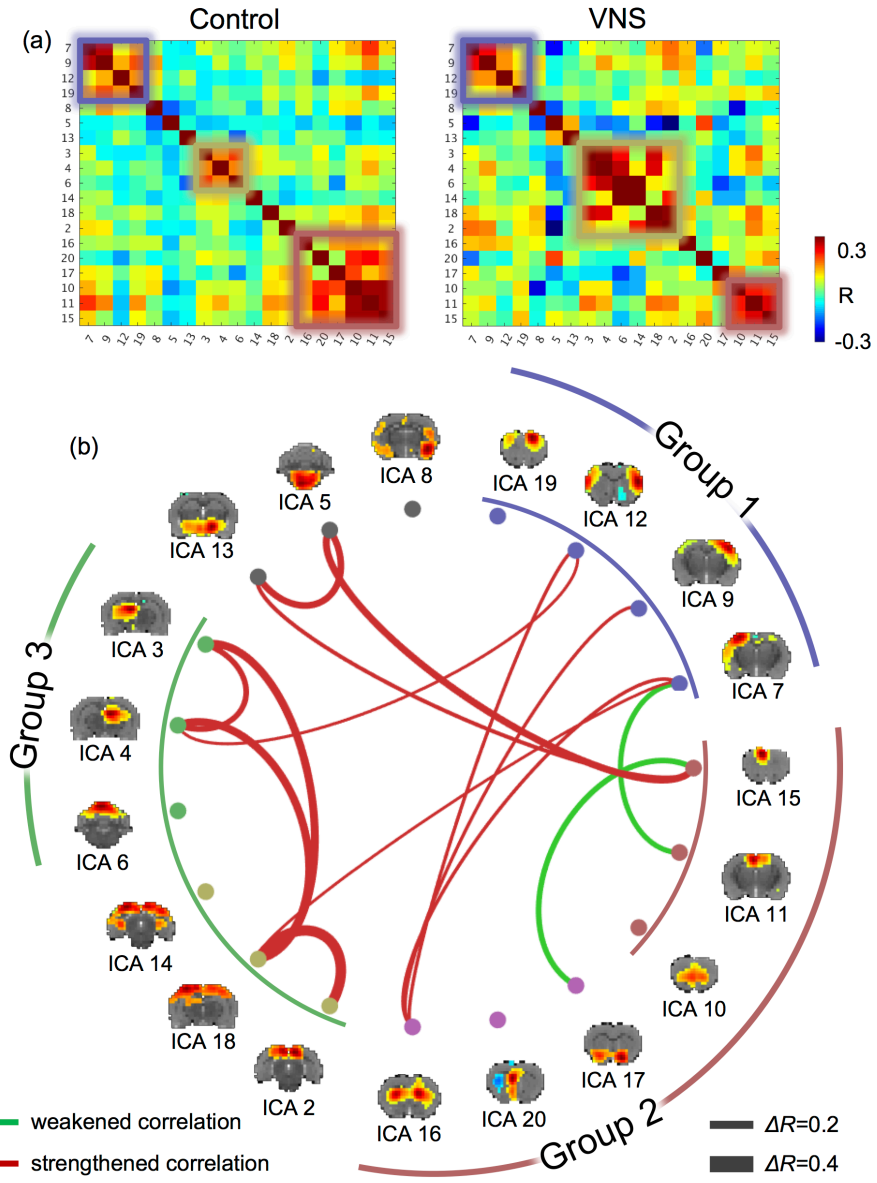

Figure 4-4 VNS altered the functional connectivity among functional networks. *(A) shows the correlations between independent components. The left shows the correlation matrix during the resting state (or the "control" condition). The right shows the correlation matrix during VNS (or the "VNS" condition). Smaller squares highlight the networks (or ICs) that were clustered into groups (based on k-means clustering). (B) shows the IC-IC functional connectivity that was significantly different between the VNS and control conditions (t-test, P<0.005). Red lines represent increases in functional connectivity, and green lines represent decreases in functional connectivity. The thickness of the lines represents the (VNS minus control) change in correlation. The brain maps show the spatial patterns of individual ICs. Corresponding to the squares in (A),*

the arc lines illustrate how the ICs were clusters into groups, for the VNS condition (inner circle) and the control condition (outer circle).

Discussion

Here, we report a model-free analysis method for mapping and characterizing the BOLD activations with VNS. Findings obtained with this method suggest that the repetitive and block-wise stimulation to the left cervical vagus nerve induces activations at widespread brain regions. The responses are complex and variable across regions, much beyond what can be described with conventionally assumed HRF. In addition, VNS also alters functional connectivity among different brain networks, and changes the brain's functional organization from its intrinsic mode as observed in the resting state. These findings suggest widespread and profound effects of VNS on the brain's regional activity and inter-regional interaction. Such effects are likely under-estimated by the model-based analysis in prior studies. This study also highlights the value of fMRI for addressing the large-scale and brain-wide effects of VNS, in order to understand and optimize its potential use for treatment of disease conditions in the brain or other organs, e.g. the gastrointestinal system.

VNS evoke brain-wide responses

A major finding in this study was that VNS evoked time-locked and widespread BOLD responses over most parts of the brain. This finding appeared surprising at the first glance, since the simulation was applied to the left cervical vagus – a seemingly narrowly-focused entry of neuromodulation. Nevertheless, previous studies suggest that neural activity may drive global fluctuations in resting-state fMRI activity (Irimia et al., 2010), and even simple (e.g., checkerboard) visual stimulation may evoke whole-brain fMRI responses (Gonzalez-Castillo et al., 2012). Common to those prior studies and this study is the notion that the brain is so densely wired and

interconnected that focal modulation may induce a cascade of responses through neuronal circuits. Such network responses may even have a global reach, if the stimulation innervates sub-cortical structures with distributed modulatory effects on the brain (Lee et al., 2010).

In this regard, widespread responses to VNS may be mediated through the diffusive neuromodulation triggered by VNS. Vagal afferents project to the parabrachial nucleus, locus coeruleus, raphe nuclei through the nucleus of solitary tract (Paxinos, 2014). From the parabrachial nucleus, locus coeruleus, and raphe nuclei, connectivity extends onto the hypothalamus, thalamus, amygdala, anterior insular, infralimbic cortex, and lateral prefrontal cortex (Van Bockstaele et al., 1999). In fact, the widespread VNS-evoked activations reported herein are consistent with the full picture gathered from piecemeal activations observed in prior VNS-fMRI (see reviews in Chae et al., 2003), transcutaneous VNS-fMRI (Frangos & Komisaruk, 2017), and EEG-fMRI studies (Bartolomei et al., 2016; Chase et al., 1967). In light of those results, the extent of the VNS effects on the brain has been under-estimated in prior studies, likely due to the use of simplified response models that fail to capture the complex and variable responses across all activated regions.

Origins and interpretation of different response characteristics

Results in this study suggest that VNS induces a variety of BOLD responses that vary across regions. In addition to coarse and qualitative classification of various responses as positive, negative, or mixed (first negative and then positive) (Figure 4-3), the responses at various regions or networks also differed in terms of transient vs. sustained behaviors during and following VNS. For example, the responses at the brainstem and the hypothalamus showed a very rapid rise around 2s and rapid decay around 5s following the onset of VNS. Although the generalizable origins of transient BOLD responses are still debatable (Renvall & Hari, 2009), we interpret the transient responses to VNS as a result of direct neuroelectric signaling through the vagal nerves. Nuclei in

the brainstem, e.g., NTS, contain neurons receiving direct projections from the vagus, and in turn connect to the hypothalamus. Such brain structures are thus well-positioned to respond rapidly to VNS. The rapid decay of the BOLD response in the brainstem and hypothalamus may indicate neuronal adaption, a factor of consideration for designing the duration and duty cycle of VNS. However, such interpretation should be taken with caution. The neurovascular coupling (modeled as the HRF) behaves as a low-pass filter through which the BOLD response is generated from local neuronal responses. Although the peak latency in HRF is 4 to 6s in humans, it is as short as 2s in rodents (Obata et al., 2004), making it relatively more suitable for tracking transient neuronal dynamics.

Another intriguing observation was the prolonged BOLD responses that sustained for a long period following the offset of VNS. In the striatum, hippocampus, as well as the prelimbic and infralimbic cortex, the VNS-evoked response lasted for 40s or even longer, while VNS only lasted 10s (Figure 4-3). Such prolonged responses suggest potentially long-lasting effects of VNS. This observation is also in line with clinical studies showing that the effects of VNS on seizure suppression are not limited to when stimulation is applied, but sustain during periods in the absence of VNS (Zabara et al., 1992). Moreover, those regions showing prolonged effects of VNS tended to be higher-level functional areas presumably involved in learning, decision-making, memory, and emotion-processing. Speculatively, it implies that the VNS-based modulation of cognitive functions or dysfunctions operates in a relatively longer time scale while imposing potentially therapeutic effects on a longer term.

VNS alters network-network interactions

This study highlights the importance of evaluating the effects of VNS on functional connectivity, which measures the degree to which regions or networks interact with each other. It

is widely recognized that brain functions emerge from coordination among regions (Anastassiou et al, 2016). However, prior studies address the effects of VNS in focal and target regions (Tian et al., 2010), whereas the effects of VNS on functional connectivity is perhaps more functionally relevant. In line with this perspective, a recent study has shown that transcutaneous VNS modulates the functional connectivity in the default mode network in patients with major depressive disorders, and the change in functional connectivity is related to the therapeutic efficacy across individual patients (Frangos & Komisaruk, 2017). Thus, VNS may reorganize the patterns of interactions among functional networks – a plausible network basis underlying VNS-based therapeutics.

Our results show that VNS reorganizes the functional connectivity with respect to the limbic system. Relative to the intrinsic functional connectivity in the resting state, VNS increases functional connectivity between the retrosplenial cortex and hippocampal formation, of which the functional roles are presumably related to memory, learning, and monitoring sensory inputs (Bush et al., 2000; Vogt et al., 1992). In addition, VNS increases functional connectivity between the sensory cortex and the striatum, of which the functional roles are presumably the integration of sensorimotor, cognitive, and motivation/emotion (Balleine et al., 2007). In contrast, VNS decreases functional connectivity between the cingulate cortex and the ventral striatum, which likely affect the emotional control of visceral, skeletal, and endocrine outflow (Parkinson et al., 2000). Collectively, these observations lead us to speculate that VNS biases the limbic system to shift its functional role from emotional processing to perceptual learning. Such speculation is consistent with the therapeutic effects of VNS in depression patients (Nemeroff et al., 2006; Sackeim et al., 2001) and the cortical plasticity of interest to perceptual learning and motor rehabilitation induced by VNS (Schwarz & Luo, 2015).

Model-free activation mapping in the level of networks

Central to this study is the use of model-free and data-driven analysis for mapping activations in the level of networks, instead of voxels or regions. This is in contrast to conventional GLM analysis used in previous VNS-fMRI studies, which assumes that neural responses sustain in the entire period of VNS, and the BOLD effects of neural responses may be modeled with a canonical HRF (Bohning et al., 2001; Lomarev et al., 2002; Nahas et al., 2007; Kraus et al., 2013; Kraus et al., 2007). Both of these assumptions may not be entirely valid. Neural responses may exhibit a range of non-linear characteristics. The typical HRF model is mostly based on data or findings obtained from the cortex during sensory stimulation (Friston et al., 1998), whereas no study has modeled the HRF for VNS. Moreover, the neurovascular coupling may also vary across regions in the brain, especially between sub-cortical and cortical areas due to their differences in local vasculatures(Li & Freeman, 2010). Thus, the GLM analysis with a single and empirical response model most likely falls short for explaining the complex and variable responses across all brain regions.

The model-free analysis allowed us to detect the VNS-evoked brain response in a data-driven way without assuming any prior response model. A similar strategy has been used to test for voxel-wise BOLD responses to visual stimulation in humans (Gonzales-Castillo et al., 2012). What was perhaps unique in this study was the use of the model-free analysis on the activity of spatially independent components, rather than that of single voxels. Each IC contained a set of voxels (or locations) that shared a common pattern of temporal dynamics. ICA utilized the fact that individual voxels were organized by networks, not in isolation, to extract the network activity as the time series of each IC, which reflected the (weighted) average activity of all the voxels that belonged to each IC. As such, the signal-to-noise ratio was higher for IC-wise activity than for

voxel-wise activity, providing better sensitivity for detecting activations at the network level. This model-free analysis method is thus arguably more favorable than conventional GLM analysis, especially when the response characteristics are complex and unclear, e.g., given VNS.

Potentially confounding cardiac and respiratory effects

The BOLD signal is an indirect measure of neural activity. Therefore, it may be affected by non-neuronal physiological fluctuations (Kundu et al., 2013). Previous studies have shown that VNS causes cardiorespiratory effects, e.g., variations in the heart rate, respiration rate, and SpO2 (Murray et al., 2001; Zaaimi et al., 2008). Such effects may potentially confound the interpretation of the VNS-induced BOLD responses in terms of neuronal activations. Such confounding effects were highlighted in a prior study, in which VNS was found to decrease the heart rate and in turn decrease the BOLD signal throughout the rat brain (Reyt et al., 2010). In this study, we were concerned about this potential confounding effect, and reduced to the pulse width of VNS to 0.1ms, instead of 0.5ms as in that study (Reyt et al., 2010). Such shortened pulse width largely mitigated the cardiac effects, as no obvious changes in heart rate were noticeable during experiments.

Moreover, the cardiac effects would manifest themselves as the common physiological response observable throughout the brain. This was not the case in this study. Despite wide-spread activations with VNS, the responses at individual regions exhibited different temporal characteristics, which could not be readily explained by a common confounding source (e.g., respiratory or cardiac). Instead, the regions with similar response patterns formed well-patterned functional networks, resembling intrinsic resting-state networks previously observed in rats (Sierakowiak et al., 2015). For these reasons, it was unlikely that the VNS-induced activation and functional-connectivity patterns were the result at non-neuronal cardiac or respiratory effects. Similar justifications are also applicable to the confounding respiratory effects. Nevertheless,

future studies are desirable to fully disentangle the neuronal vs. non-neuronal effects of VNS. Of particular interest is using multi-echo fMRI to differentiate BOLD vs. non-BOLD effects (Kundu et al., 2013), and combining electrophysiology and fMRI to pinpoint the neural origin of the fMRI response to VNS (Viswanathan & Freeman, 2007).

Chapter 5 The Stomach and the Brain are Intrinsically Phase-Coupled in Rats [4]

Summary

The stomach and the brain interact with each other intrinsically to maintain normal digestive function. The interaction is essential to the "gut feeling" and can influence cognition and emotion. However, neural circuits underlying the stomach-brain interaction remains poorly understood. This study aims to characterize the spontaneous stomach-brain interaction that manifests itself as the coupling between gastric and brain activities. We used electrogastrogram (EGG) to measure gastric activity and used fMRI to map brain activity. Simultaneous acquisition of EGG and fMRI was performed in rats in both the fasting and postprandial states. Our results suggest that gastric slow waves were phase-coupled with the BOLD signals from a broad set of brain regions, including the sensorimotor area, olfactory-related area, cingulate cortex, and insular cortex. The degree of phase-coupling was state-dependent, stronger in the postprandial state that the fasting state. Furthermore, the intact vagus nerve was central to this stomach-brain synchrony. These results were consistent with the finding from a recent human study (Rebello et al., 2018) and shed new lights on the role of the vagus in stomach-brain synchrony.

Introduction

The brain's representation of the stomach is an important topic and has been investigated for decades. Prior studies have identified the insular cortex as the critical brain region for gastric interoception (Craig, 2002, 2009). Beyond the insular cortex, several functional networks are also

[4] The contents of this chapter will be prepared for submission (Cao et al., in preparation)

involved, including the sensorimotor network, salience network, central executive network, default mode network, emotional arousal network, and central autonomic network (Aziz et al., 2000; Farr et al., 2016; Holtmann & Talley, 2014; Mayer et al., 2019; Van Oudenhove et al., 2004). Besides, both preclinical and clinical evidence suggests a strong correspondence between gastric disorders and psychological disorders, such as anxiety and depression (Drossman et al., 1999; Haug, et al., 2002; Klarer et al., 2014,2018; Levy et al., 2006; Mayer et al., 2000, 2001). It is increasingly recognized that the stomach has a profound implication to brain activity.

Understanding the stomach-brain interaction is not only necessary for brain studies but also crucial for the gastric system. The impaired stomach-brain interaction can cause severe gastric disorders, such as gastroparesis (Ali et al., 2007; Camilleri et al., 2018; Lacy & Weiser, 2005) and functional dyspepsia (Enck et al., 2017; Tack et al., 1998, 2004; Talley & Ford 2015). These disorders affect 20% of the general population and there are limited therapeutic options (Ford et al., 2020; Lacy et al., 2009; Stanghellini, 2016; Talley & Ford, 2015). Therefore, it is essential to map the stomach-brain interaction in health and disease with the overall goal of restoring the regular stomach-brain interaction.

So far, most studies utilize external stimulation to study the stomach-brain interaction. For example, one may apply mechanical, nutritional, and electrical stimulation to the stomach and use a food cue through visual stimulation. However, external stimulation is different from how the gut engages the brain under the intrinsic conditions. Mapping the intrinsic stomach-brain interaction is critical. Recent studies utilize electrogastrogram (EGG) to represent gastric activity and record EGG simultaneously with magnetoencephalography (MEG) or functional magnetic resonance imaging (fMRI) (Choe et al., 2021; Rebollo et al., 2018; Richter et al., 2017). These studies report that EGG is phase-coupled to neural activity, specifically in the insular cortex, visual cortex,

sensorimotor cortex, cerebellum, and the default mode network. These studies illustrate the intrinsic stomach-brain interaction and introduce a new avenue to this field. However, questions remain. Does intrinsic stomach-brain synchrony exist in animals, e.g., rodents? Is the synchrony dependent on the gastric state, e.g., fed vs. fasting conditions? What is the functional circuit that mediates this synchrony?

We attempted to address these questions with experiments in rats. Briefly, we recorded EGG and fMRI simultaneously in rats in an attempt to replicate and generalize the stomach-brain synchrony observed in humans (Rebollo et al., 2018). The experiment was performed in both the postprandial state and the fasting state to address the state dependence of stomach-brain synchrony. We further evaluated the effects of vagotomy to address the role of the vagus in the stomach-brain synchrony.

Methods and Materials

Subjects

This study used eight Sprague–Dawley rats (male, weight: 300–500 g; Envigo RMS, Indianapolis, IN) according to a protocol approved by the Institutional Animal Care and Use Committee (IACUC) and the Laboratory Animal Program (LAP) at Purdue University. Animals were housed in a strictly controlled environment (temperature: 21 ± 1 °C; 12 h light-dark cycle with lights on at 6:00 a.m. and off at 6:00 p.m. at Purdue University).

Animal training and feeding

The animal was trained to consume a fixed quantity of palatable dietgel (DietGel Recovery, ClearH2O, ME, USA) following a protocol published earlier (Lu et al., 2017). The training took 7 days. In the first 2 days, the animal was supplied with both regular rat chows and ~5g dietgel to accustom itself to the dietgel. In the following days, the animal was fasted for 18 hours (6PM to

12AM) and then fed with the dietgel only at 12AM. The animal was given 30 minutes to consume 5 dietgel; then regular meal was supplied to the animal afterwards. After the diet training (~2 to 3 repetitions), the animal could voluntarily consume the dietgel following overnight food restriction and was then used for the experiment.

Anesthesia protocol

The animal was anesthetized during the experiment. The animal was initially anesthetized with 5% isoflurane followed with 2.5% isoflurane to maintain the anesthesia depth. The animal was placed on a heating pad to maintain the body temperature. After a toe-pinch test, the animal was ready for abdominal surgery or the electrode placement. The dose of isoflurane was adjusted as needed to maintain the depth of anesthesia. The respiration rate, heart rate, oxygen saturation level (SpO2), and body temperature were monitored and maintained within the physiological range. The respiration rate was from 30 to 70 cycles per minute. The heart rate was from 250 to 350 cycles per minute. SpO2 was higher than 96%. The temperature was about 37± 0.5 °C.

For EGG and fMRI data acquisition, a different anesthesia protocol was used. Half an hour before data acquisition, a bolus of dexdomitor (15 μg/kg, Zoetis, NJ, USA) was administered subcutaneously. The dose of isoflurane was then lowered to 0.1-0.5% as soon as the animal's heart rate and respiration started to drop. About 15 to 20 mins after the bolus injection, subcutaneous infusion of dexdomitor (0.05mg/ml) was administered at a rate of 15 μg/Kg/h, during which the dose of isoflurane was kept below 0.5%. The dose of dexdomitor and isoflurane were adjusted as needed to maintain the depth of anesthesia and keep the respiration rate, heart rate, oxygen saturation level (SpO2), and body temperature within the corresponding physiological range (see the paragraph above).

Brain fMRI acquisition and signal preprocessing

The MRI and fMRI data were acquired with the 7-tesla small-animal MRI system (BioSpec 70/30, Bruker, Billerica, MA, USA). A volume coil (76 mm inner diameter) and a single-channel surface coil were used as the transmitter and receiver for image acquisition. During MRI, the animal's head was restrained with a bite bar and two ear bars to avoid head motion. The animal's torso was gently taped to the animal holder to avoid body motion. After localizer scans, T_2-weighted anatomical images were acquired using a 2-D rapid acquisition with relaxation enhancement (RARE) sequence with the repetition time (TR)=5,804.6 ms, effective echo time (TE)=32.5ms, echo spacing=10.83ms, voxel size=0.125×0.125×0.5mm^3, RARE factor=8, number of slices=50, and flip angle (FA)=90. Following anatomical scans, T_2*-weighted fMRI images were acquired with a 2-D single-shot gradient-echo (GE) echo-planar imaging (EPI) sequence (TE=16.5ms, in-plane resolution=0.5×0.5 mm^2, slice thickness=1mm, TR=1s, number of slices=25, and FA=55°).

The MRI/fMRI data was pre-processed using FSL (Jenkinson, et al., 2012), AFNI (Cox, 1996), and in-house software developed in MATLAB. Head motion was first corrected by co-registering every volume to the first volume within each session (3dvolreg). Next, the slice timing in each volume was corrected by (slicetimer). The fMRI images were then aligned with the anatomical images (flirt) and further registered to a rat brain atlas (Valdes Hernandez et al., 2011) (fnirt). Lastly, the fMRI signal is spatially smoothed with a 3-D Gaussian kernel of 0.5-mm full-width-at-half maximum (FWHM), the linear trend in time is regressed out from the fMRI signal.

Placement of the EGG recording electrode

For EGG recording, electrodes were placed on the abdominal surface. The fur on the animal's abdomen was carefully removed to expose the abdominal skin. A multi-channel EGG

array was attached and sutured onto the skin. The placement of electrodes was carefully designed to cover the stomach (as shown in Figure 5-1A). In brief, the xiphoid was first identified as the reference. Then, the electrode on the second row and third column was placed on top of the xiphoid. The electrodes were placed as a grid with columns in parallel with animal's central line. The reference electrode was attached to the skin 5mm above the xiphoid. The ground electrode was attached to the left hind limb.

EGG recording

The multi-channel body-surface EGG was recorded through a broadband recording system (Tucker Davis Technologies, Alachua, FL, USA). The recording electrode was connected to the head-stage for pre-amplification near the animal and then to the amplifier in which the DC-signal was also recorded to achieve broad-band acquisition. The amplifier was placed closed to the scanner to achieve good signal quality. The amplifier also digitized the EGG signal with the sampling rate of 24kHz and transmitted the digital signal to the data acquisition system outside the scanner room through an optical fiber. To synchronize EGG and fMRI signals in time, a TTL trigger, reporting the timing of MR acquisition, was recorded together with EGG. Both EGG and MRI trigger signals were stored for off-line analyses. The stored data was pre-processed to remove artifacts caused by MRI acquisition. For each channel, the signal was first demeaned and then detrended by regressing out the 5th-order polynomial function. Then, a low-pass filter was applied to the signal with the cut-off frequency at 0.45Hz. Finally, the EGG signal was down sampled to 1s and ready for further analyses.

Coherence analysis between EGG and fMRI signals

Coherence was calculated to evaluate the phase synchrony between EGG and fMRI signals. In brief, we first ran a power spectrum analysis on EGG from the selected channel and identified

the dominant frequency indicative of the gastric slow wave. We then applied the cross-spectral analysis between EGG from the selected channel and fMRI signals from individual voxels and only focused on the identified frequency. The cross-spectral density at the frequency of interest was then normalized for each spectrum as described in the following equation,

$$C_{xy}(f) = \frac{|G_{xy}(f)|^2}{G_{xx}(f)G_{yy}(f)} \qquad \textit{Equation 5-1}$$

in which x and y represent EGG and fMRI activity from each voxel, respectively, G_{xy} is the cross-spectral density between x and y, G_{xx} and G_{xy} is the spectral density of x and y respectively, C_{xy} is the coherence between x and y, and f represents the frequency. The normalized cross-spectral density reported the frequency-specific synchrony between EGG and fMRI activity.

Because the dominant frequency of gastric slow waves could vary over time, the coherence was calculated for every ~4 min segment with respect to the dominant frequency identified in each segment. First, EGG signals were divided into segments with 256 and 196 time points, respectively. The dominant frequency of gastric slow waves was located for each data segment using the power spectrum analysis. Specifically, the dominant frequency was identified as the frequency with the highest power within 0.06-0.13Hz. Then, the coherence between each EGG segment and the corresponding fMRI segment was calculated at the dominant frequency. The resulting coherence was averaged across every segment within each animal and then across animals.

To test the statistical significance, coherence was converted to the z-score before statistical tests. Specifically, EGG and fMRI signals were first shuffled in phase and then used for calculating the coherence. This shuffling and coherence calculation process was performed once for individual data segments and brain voxels. These coherences were used to build the null distribution for every frequency in the spectrum. According to the null distribution, coherence from each voxel and data segment was converted to the z-score for further statistical analyses.

To map coherence, we performed the one-side t-test on the voxel-wise z-score of coherence across animals. The statistical significance was based on $p<0.01$ while only keeping clusters of significant voxels greater than 2 mm^3 (8 voxels). In the coherence analysis of regions of interest (ROIs), we defined 156 ROIs based on rat brain anatomy (Papp et al., 2014; Paxinos & Watson, 2006; Valdes Hernandez et al., 2011), including both cortical and subcortical regions. Coherence z-scores were first averaged within each ROI for each animal. One-side t-test was then performed on the averaged z-scores across animals. The statistical significance was based on the t statistic with $p<0.01$ with Bonferroni correction for the number of ROIs.

Functional connectivity

We evaluated the temporal correlation between brain regions or between a seed region and other brain regions. In the seed-based correlation, a seed covered the left and right NTS. The functional connectivity to the seed region was calculated as the temporal correlations of the fMRI time series between NTS and other voxels. The correlation coefficient was converted to a z-score using the Fisher's z-transform and then averaged within each animal. The one-sample t-test ($p<0.05$) was performed on the z-scores across animals for the group-level analysis. Similarly, the correlations between parcellated brain regions were evaluated.

Results

This study aimed to check whether gastric slow waves were synchronized with the BOLD activity in the brain and whether the vagus nerve was essential to the synchronization. We recorded EGG during brain fMRI on eight rats and assessed the phase-coupling in both the postprandial and fasting states and tested whether the vagus nerve mediated the synchronization.

Phase-coupling between gastric slow waves and fMRI signals

Inspired by a prior human study (Rebollo et al., 2018), we hypothesized that a gastric network existed in the rat brain and exhibited spontaneous BOLD activity phase-locked to the gastric slow wave that paced the stomach for meal digestion. To test this hypothesis, we performed brain fMRI in eight SD rats simultaneously with EGG recording after rats consumed 5g diet gel. We applied coherence analysis to the fMRI and EGG signals and assessed their phase-locking effects at gastric phase-making frequency (4-6 CPM). According to the voxel-wised analysis, the BOLD signals in multiple brain regions were phase-coupled to gastric slow waves. The brain regions included the anterior cingulate cortex, insula, medial prefrontal cortex, sensorimotor cortex, visual cortex, and cerebellum (Figure 5-1C). The additional ROI-based analysis further confirmed the wide-spread phase-locking effects. The first 15 regions with the highest coherence were the left ectorhinal cortex, left and right entorhinal cortex, right hippocampal formation, left superior colliculus, left granular insular cortex, left olfactory ball, left cerebellum, right auditory cortex, right motor cortex, and right somatosensory cortex barrel region and hind limb region (Figure 5-1E). This result confirms the phase-coupling between gastric pace-making activity and BOLD activity in the rat brain, suggesting that the stomach and the brain are intrinsically synchronized.

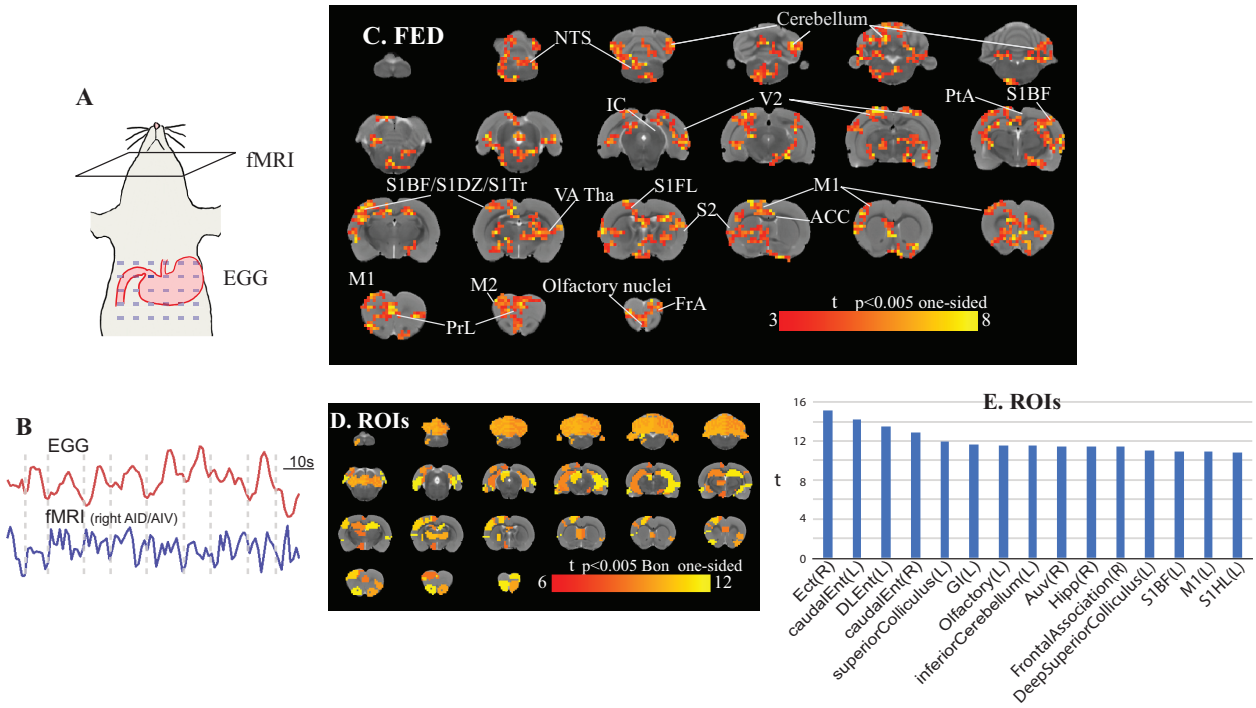

Figure 5-1 The coherence between gastric slow waves and fMRI signals in the postprandial state. *A shows the placement of the skin-surface EGG electrodes. The one selected for analysis is marked with darker blue.* ***B*** *provides an example of EGG and fMRI signals.* ***C*** *&* ***D*** *show the voxel-wised and ROI-wised phase-coupling map in the brain, respectively. The color encodes t statistics with p<0.005.* ***E*** *lists the top 15 regions with the highest coherence between EGG and fMRI signals.*

Phase-coupling between the stomach and the brain is state-dependent

The previous section confirmed the intrinsic phase-coupling between the stomach and brain in the postprandial state. Here, we assessed whether the phase-coupling also existed in the fasting condition. To answer this question, we repeated the experiment with five rats to simultaneously record EGG and fMRI after fasting the animal. As shown in Figure 5-2, the stomach-brain synchrony was also observable but covered fewer regions. At the fasting stage, the phase-coupling was more pronounced in the prelimbic cortex, anterior cingulate cortex, insular cortex, striatum, olfactory ball, primary somatosensory cortex, visual cortex, amygdala, and cerebellum (Figure 5-2AC). The overlap between the fed and fasting conditions was only partial, in the anterior cingulate cortex, striatum, primary motor cortex, visual cortex, and amygdala etc. (Figure 5-2B). The phase-

coupling at the fasting stage was also weaker than that at the fed stage. Most brain regions showed stronger phase-coupling at the fed stage (Figure 5-2E). The top-ten regions with the most notable difference included the right nucleus of the solitary tract, right dorsolateral orbital cortex, right auditory cortex, right parabrachial complex, left frontal association, right posterior parietal cortex, the left and right primary somatosensory cortex (hind limb and trunk regions), and left ventral thalamus. In particular, the difference was significant in the left primary motor cortex, left primary somatosensory cortex, left olfactory ball, left ventral thalamus, right insular cortex, and septal nucleus (Figure 2-2D, $p<0.05$). This result confirms that the phase-coupling exists in the fasting condition but it is weaker than in the fed stage, suggesting that the stomach-brain synchrony is dependent on the gastric state.

Comparing the fed and fasting conditions revealed the lateralization in the phase-coupling between the stomach and the brain. In the primary somatosensory cortex, motor cortex, and insular cortex, brain regions in the left hemisphere had higher coherence than the right hemisphere (Figure 2-3). This preference was more pronounced in the fed stage for the somatosensory cortex and motor cortex and was more pronounced in the fasting stage for the insular cortex. Similarly, the striatum in the right hemisphere had higher coherence than the right hemisphere, and this preference was more observable in the fed stage. The preference for one hemisphere could also be observed in the brainstem nuclei. In the nucleus of the solitary tract (NTS) and parabrachial complex (PBC), the right nuclei were more synchronized with the gastric slow wave than the left nuclei at the fed state (Figure 2-4D). This lateralization in phase-coupling suggests different engagement of the left vs. right hemispheres in the stomach-brain synchronization.

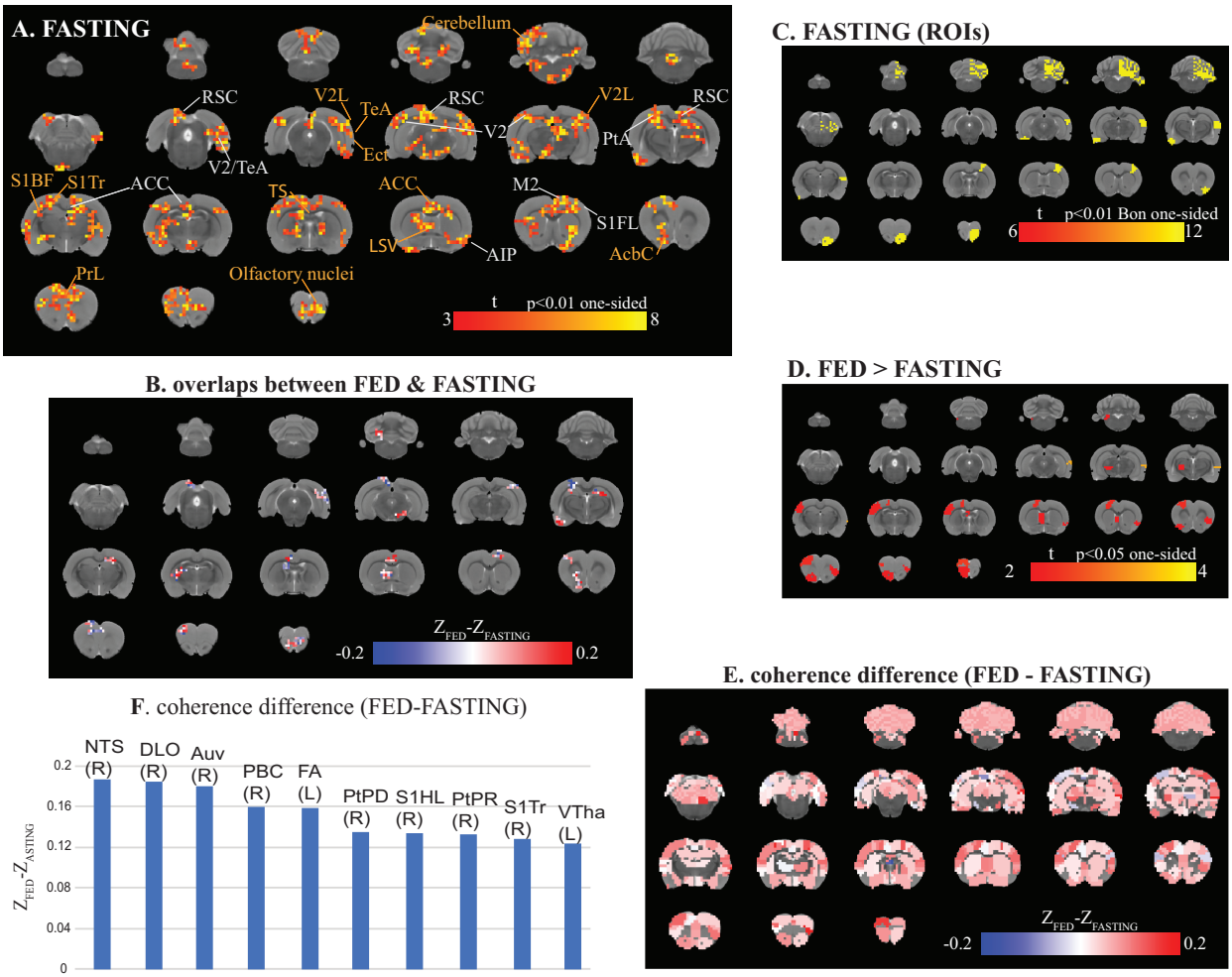

Figure 5-2 The coherence comparison between the postprandial (fed) and fasting stages. *A & C shows the fasting-state voxel-wised and ROI-wised phase-coupling map in the brain, respectively. The color encodes t statistics with p<0.01. B highlights the overlaps in the voxel-wised phase-coupling map between the fed and fasting states. The color represents the difference of coherence Z-score between the fed and fasting states. D provides the phase-coupling comparison between the fed and fasting states according to the ROI-based coherence z-score. The color gives t statistic with p<0.05. E also shows the phase-coupling comparison, but the color represents the difference in coherence z-score between the fed and fasting states. F plots the first ten brain regions with the highest coherence difference between the two conditions.*

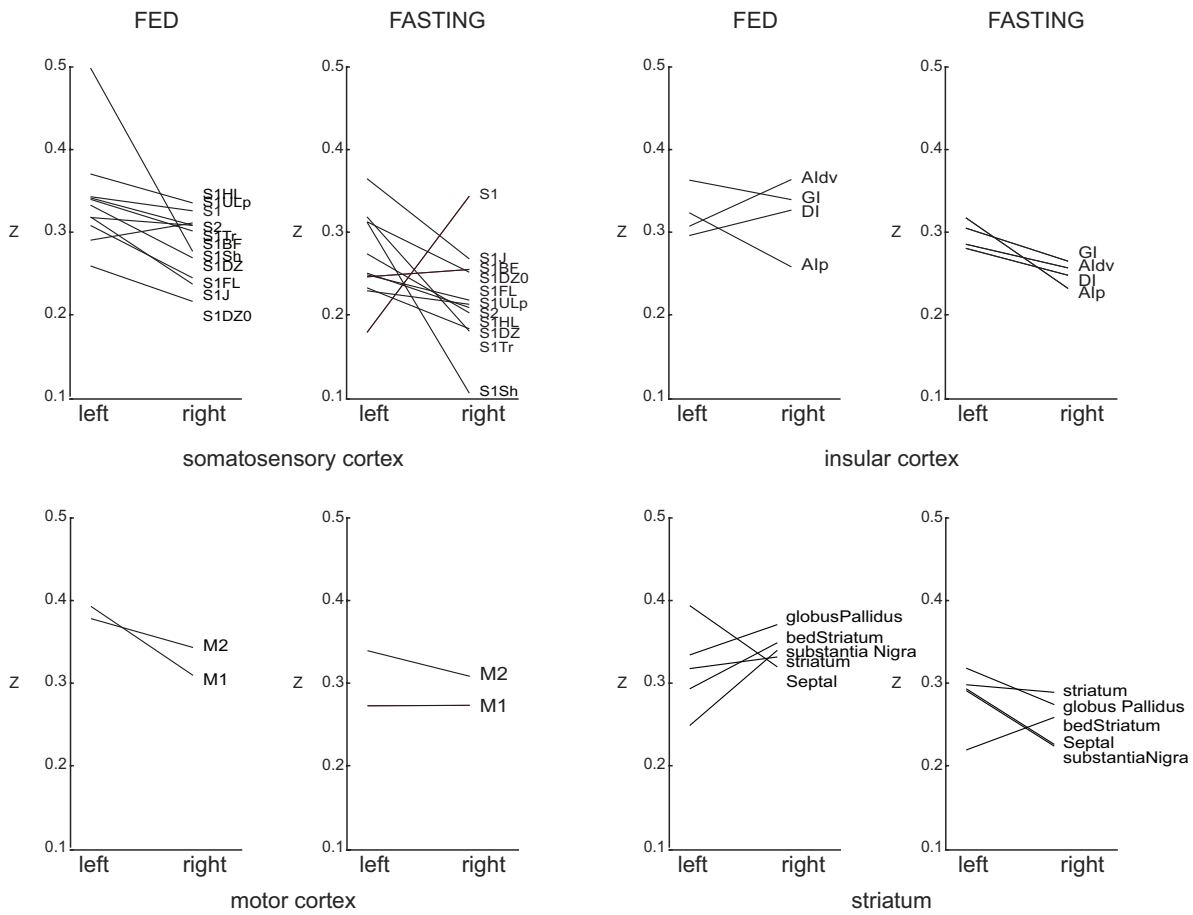

Figure 5-3 Coherence different between the left and right hemispheres. *The eight plots show the coherence difference between the left and right brain regions in the fed and fasting conditions. These plots include the regions in the somatosensory cortex, motor cortex, insular cortex, and striatum.*

Functional connectivity in the gastric network

To understand the information exchange within the gastric phase-coupling network, we further investigated the information flow involving the nucleus of the solitary tract (NTS), the essential relay between the stomach and the brain. We defined left and right NTS as two regions of interest and applied seed-based correlation and parcel correlation to map the functional connectivity between NTS and the rest of the brain. The functional connectivity was compared between the fasting and fed states to demonstrate its condition dependency. At the fasting state, both the left and right NTS-seeded functional network involved the periaqueductal gray,

somatosensory cortex, motor cortex, medial prefrontal cortex, and insular cortex (Figure 5-4AE). In contrast, the NTS-seeded functional network largely diminished at the fed state. The left-NTS-seeded network did not show significant involvement in the forebrain, and the right-NTS-seeded network only engaged the anterior cingulate cortex, medial prefrontal cortex, and insular cortex (Figure 5-4BE). The difference between the fasting and fed states was more significant in the somatosensory cortex, motor cortex, and insular cortex in the left-NTS seeded functional network (Figure 5-4C). In summary, NTS has stronger functional connectivity with the forebrain in the fasting state than the fed state. Also, the left and right NTS connect to the forebrain differently in the fed state.

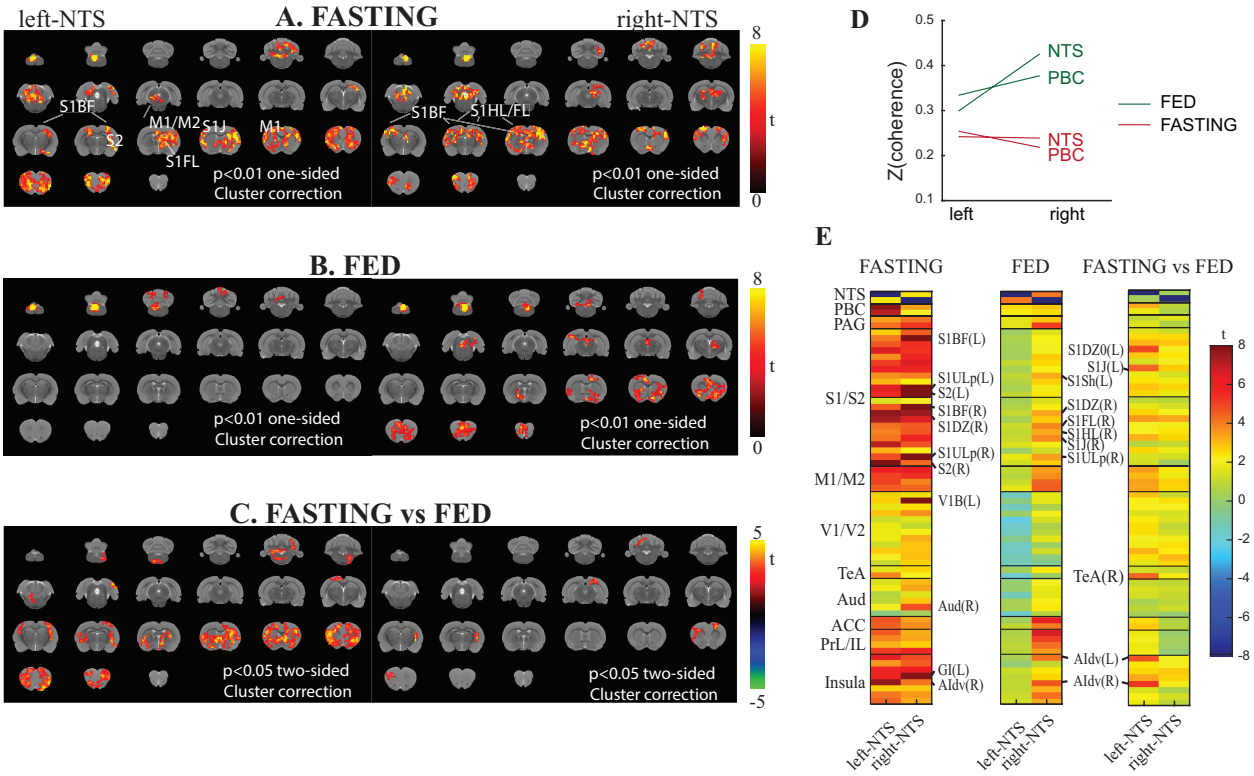

Figure 5-4 Functional connectivity between NTS and the forebrain. *A shows the seed-based correlation at the fasting state with the seed as the left and right NTS separately. B shows the seed-based correlation at the fed state and the seed as the left and right NTS. C shows the difference in the seed-based correlation between the fasting and fed conditions. D plots the coherence z-score in the left and right NTS and PBC at both the fed and fasting conditions. E plots the parcel correlation at both the fasting and fed conditions and correlation difference between the two conditions. In all the maps and plots, color encodes t-statistic.*

Phase-coupling is partially mediated by the vagus nerve

As mentioned in the previous section, NTS was the critical relay between the stomach and the brain. Here, we hypothesized that the vagus nerve, as the parasympathetic nerve innervating NTS, played an essential role in mediating the stomach-brain synchrony. We repeated the simultaneous EGG-fMRI recording experiments at the postprandial condition on five rats after bilateral cervical vagotomy. We applied the coherence analysis to assess the phase-coupling after cutting the vagus nerve and compared the coherence to the group with the intact vagus nerve. As illustrated in the voxel-wised analysis, only a few brain regions preserved after cutting the vagus nerve (Figure 5-5A), including a small portion of the somatosensory cortex, motor cortex, and insular cortex, with a slight overlap with phase-coupling map from the vagus nerve intact group in the primary somatosensory cortex, hindlimb and forelimb regions (Figure 5-5B). The coherence in the vagotomy group was also weaker than the group with the vagus nerve intact (Figure 5-5D). The difference was most significant in the right insular cortex, septal nucleus, thalamic nuclei, motor cortex, and visual cortex (Figure 5-5C). However, a few regions showed stronger coherence after vagotomy. The first six regions were the right primary somatosensory cortex (jaw region), left and right perirhinal cortex, left primary somatosensory cortex, right posterior thalamic nucleus, and right agranular insular cortex (Figure 5-5E). These results suggested that the vagus nerve is the primary, but not only, pathway that mediates the stomach-brain synchrony.

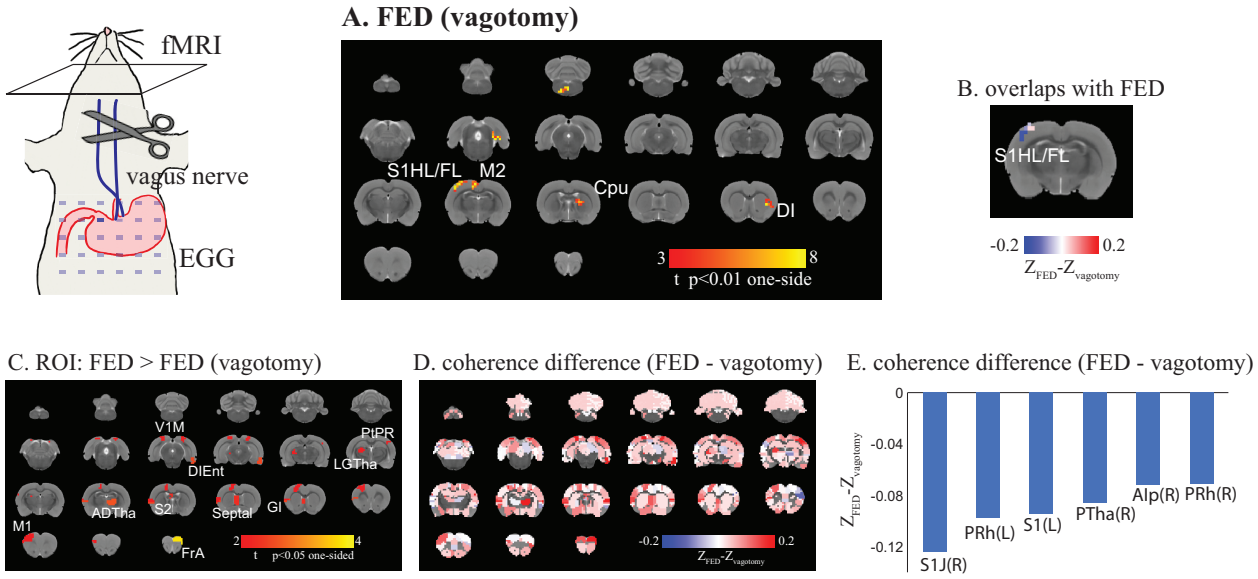

Figure 5-5 The role of vagus nerve in maintaining the phase-coupling at the postprandial (fed) stage. *A shows the voxel-wised phase-coupling map at the fed condition after bilateral cervical vagotomy. The color encodes the t statistic with $p<0.01$. B highlights the overlapped region between the vagotomy group and the group with the vagus nerve intact. The color encodes the difference in coherence z-score between the vagal-intact and vagotomy groups. C highlights the ROIs with the coherence z-scores significantly higher in the vagal-intact group than the vagotomy group. The color encodes the t statistics with $p<0.05$. D maps the difference in the coherence z-scores in all ROIs. The color encodes the coherence difference between the vagal-intact and vagotomy groups. E plots the first six regions in which the coherence is higher in the vagotomy group than the group with vagus nerve intact.*

Discussion

This study reported a gastric network, in which BOLD activity was phase-coupled to gastric pace-making activity. The gastric network was state-dependent, with a more extensive brain coverage and stronger coherence in the postprandial state than the fasting state. Within the gastric network, NTS, as the primary relay between the stomach and the brain, had a significant BOLD correlation with the somatomotor and prefrontal area. This correlation also showed state-dependency, with a higher correlation at the fasting state. Last, the gastric network was primarily mediated by the vagus nerve, with diminished phase-coupling after bilateral vagotomy.

The wide-spread coverage of different regions

Anatomical evidence

Anatomical connections between the stomach and brain have been increasingly mapped. Two major neural pathways connect the stomach with the central nervous system, including the vagus nerve and thoracic nerve (Browning & Travagli, 2011; Furness et al., 2014, 2020; Rogers et al., 1995). The thoracic nerve connects to the spinal cord, which further projects to the several brain nuclei, including the amygdala, lateral hypothalamus, periaqueductal gray, parabrachial complex, and nucleus of the solitary tract. The vagus nerve mainly connects to the nucleus of the solitary tract and further projects to the forebrain relayed by parabrachial complex and periaqueductal gray. Therefore, many brain regions are connected with the stomach within three or four synapses and form a central gastric network. These regions include the insular cortex, striatum, amygdala, medial prefrontal cortex, anterior cingulate cortex, hypothalamus, thalamus, and hippocampus (Browning & Travagli, 2011; Suarez et al., 2018). Recent studies also report that the somatomotor cortex and hippocampus are engaged in the gastric network through the thoracic nerve and the striatum, respectively (Levinthala and Strick, 2020; Suarez et al., 2018). This knowledge of neuronal connections provides anatomical support for most brain regions in the gastric phase-coupling network reported in this study.

The involvement of visual and auditory cortex

This study reveals that BOLD activity in the visual and auditory cortex is phase-coupled with EGG. A similar result is also reported in the EGG-fMRI study conducted in humans (Rebollo et al., 2018). However, the involvement of the visual and auditory cortex is hard to be explained. One speculation is that the visual cortex is essential in food-seeking (Rebollo et al., 2018). It logically makes sense but is with limited literature support. One indirect support is the motion

sickness that a specially designed visual stimulation can cause nausea and vomiting. The motion sickness experiment suggests a functional relationship between the visual system and the stomach (Griffin & Newman, 2004; Kennedy et al., 2010).

The involvement of the insular cortex

The insular cortex is the well-recognized region in the stomach sensation, but the previous studies on the synchronization between EGG and brain activity do not strongly support the synchronization in the insular cortex (Choe et al., 2021; Rebollo et al., 2018). Unlike what has been reported in the human literature, this animal study suggests that BOLD activity in the insular cortex is phase-coupled with EGG. In this result, the insular cortex is not primarily involved, only with engagement of the right agranular insular cortex (AI), right dysgranular insular cortex (DI), and left granular insular cortex (GI) at the postprandial state. Although different from human studies, this occurrence of the insular cortex is consistent with the hypothesis that the right insular cortex is the stomach region of the interoceptive cortex (Craig, 2003, 2009). Besides, the magneto-encephalographic study reports a similar finding that the amplitude of neural activity in the right insular cortex is coupled with EGG. Therefore, it is likely that there is an involvement of the right insular cortex in the gastric phase-coupling network.

The state-dependency of the gastric network

This study reveals that the phase-coupling between the stomach and brain is gastric-state-dependent. Dynamics of the stomach-brain interaction are essential to regulate gastric activity and form gastric sensations given different physiological conditions. For example, during the fasting state, the stomach has continuous gastric slow waves but lacks regular gastric contractions. In contrast, during the postprandial state, the corpus and antrum have regular rhythmic contractions, with stronger contractions occurring once a while for gastric emptying. Given significant dynamics

of gastric activity, the brain may respond to the stomach differently. Yet, not many studies target the dynamics of the stomach-brain interaction. The study with EGG and fMRI allows us to perform experiments under varying gastric phases and provides an opportunity to assess the dynamics of the stomach-brain interaction. State-dependency in the phase-coupling serves as a piece of solid evidence that the intrinsic stomach-brain interaction changes with gastric conditions.

Asymmetry in the gastric phase-coupling network

The gastric phase-coupling network reported in this study is asymmetric for both the postprandial and fasting states. Asymmetric networks have been reported in other gastric studies. For example, in the gastric network revealed by EGG-fMRI simultaneous recording in humans, only the right primary somatosensory cortex is found to be phase-locked to EGG (Rebollo et al., 2018). Similarly, in a rewarding study conducted on rodents, only the right vagal ascending pathway is involved in the gut-induced reward pathway (Wenfei Han et al., 2018). Lateralization is also commonly occurred in other functional systems, such as the visual system and somatomotor system. Speculatively, lateralization may also exist in the interoceptive system, hypothetically stating that the right insula is associated with energy expenditure and arousal. In contrast, the left insular cortex is associated with energy nourishment and appetitive behavior (Craig, 2009, 2014). Thus, different functions of the insular cortex in two hemispheres are likely to cause lateralized phase-coupling with gastric slow waves.

Causality in the stomach-brain interaction

Based on the prior knowledge of the stomach-brain interaction, it is more likely that the brain listens to the stomach. This stomach-to-brain ascending direct direction is supported by anatomical and functional evidence (Sanders et al., 2006). In brief, the gastric slow waves originate from the ICC network, a network of pace-making cells in the stomach. Gastric slow waves

propagate in the stomach, allowing the stomach to contract in a coordinated fashion. The gastric rhythms always exist even after cutting the neural connection with the brain. Therefore, the monitoring position of the brain is highly possible for the gastric phase-coupling.

However, it is also possible that the brain can adjust gastric rhythm. Efferent projections can be found targeting ICC cells, making the downstream regulation of gastric rhythm possible. The downstream regulation is also supported by functional evidence. For example, patients with brain death, injury, comma, or Parkinson's disease show alternated gastric rhythms (Bor et al., 2016; Krygowska-Wajs et al., 2000; Naftali et al., 2005; Thor et al., 2003;). Besides, visually induced motion sickness can cause gastric dysrhythmia (Cheung & Vaitkus, 1998). Furthermore, dysrhythmic activity can also be improved through deep brain stimulation (Krygowska-Wajs et al., 2016). Taken together, it is possible that the brain plays a supportive role in regulating gastric rhythms.

Limitation and the future direction

This study focuses on skin surface recording of gastric slow waves, which is a rough representation of gastric slow waves. In the actual scenario, gastric slow waves from different stomach segments are not perfectly synchronized. Single-channel EGG cannot well delineate the spatial information of gastric slow waves from various stomach segments, thus cannot fully reveal the phase-coupling between the stomach and the brain. Besides, EGG as the skin surface potential can be affected by other physiological signals, such as respiration, heart rats, and intestinal activity. Therefore, it is of great interest to investigate the stomach-brain synchronization with gastric slow waves recorded on the stomach wall.

Chapter 6 Gastric Myoelectrical Activity is Synchronized with BOLD Activity in the Brain at the Intrinsic State [5]

Summary

The stomach-brain interaction is critical in maintaining normal gastric activity. Recent studies tackle this problem and use the simultaneous recording of electrogastrogram (EGG) and functional magnetic resonance imaging (fMRI) to assess the problem and report the synchronization between the stomach and brain. However, EGG is not a direct measurement of gastric activity and can be confounded by various issues, such as high noise level, geometry of the stomach, and stomach fullness. It is of interest to reassure the stomach-brain synchronization with a more direct measurement of gastric activity. In this study, we implanted wire electrodes on the serosal surface of the stomach in rats and recorded gastric myoelectrical activity (GMA) simultaneously with fMRI. We confirmed the phase-coupling between the stomach and the brain and found that the corpus has stronger phase-coupling with BOLD activity compare to the antrum. Besides, the phase-coupling showed lateralization in the brain, with the corpus showing stronger phase-coupling with the right hemisphere and the antrum showing stronger phase-coupling with the left hemisphere. Besides the rhythmic activity, GMA power was also correlated with BOLD activity in the brain. Power of GMA in the corpus showed more significant correlation with BOLD activity at gastric pace-making frequency (5 cycles per minute) and low frequency (3.5 cycles per minute), while antrum correlated with BOLD activity only at the low frequency (3.5 cycles per

[5] The contents of this chapter will be prepared for submission (Cao et al., in preparation)

minute). This study confirms the phase-coupling between the brain and different segments of the stomach and reports the brain representation of gastric contractional power for the first time.

Introduction

The brain intrinsically interacts with the stomach to maintain the daily gastric function (Furness et al., 2014, Rogers et al., 1995). The impaired interaction yields both gastric and brain disorders, such as functional dyspepsia (Enck et al., 2017; Tack et al., 2004; Talley & Ford 2015), gastroparesis (Ali et al., 2007; Camilleri et al., 2018; Lacy & Weiser, 2005), anxiety, and depression (Drossman et al., 1999; Haug et al., 2002; Haug et al., 2002; Levy et al., 2006; Mayer, 2000). Gastric stimulation is often used to study the stomach-brain interaction, that requires a balloon or an infusion line to be inserted into the stomach to deliver pressure or nutrient stimuli (Ladabaum et al., 2001; Min et al., 2011; Wang et al., 2008). These stimuli can cause unpleasant sensations and may not trigger normal neural responses in the brain. Therefore, it is of great interest to study the stomach-brain interaction without external stimuli.

In the past few years, the intrinsic stomach-brain interaction has become a topic of interest. Unlike traditional study design requiring external stimulation to activate the gastric network, the new study paradigm uses electrogastrogram (EGG) to represent gastric activity and assess the relationship between EGG and the functional activity in the brain (Cheo et al., 2021; Rebollo et al., 2018; Richter et al., 2017). Given this new study design, the gastric phase-coupling network is reported in both humans (Choe et al., 2021; Rebollo et al., 2018) and animals (Chapter 5). However, EGG is a noninvasive measurement of gastric activity and can be contaminated by noise. It is of great interest to investigate the stomach-brain interaction with a direct measurement of gastric activity.

Besides the functional mapping, the neural anatomy has been better mapped in recent years. The vagus nerve is the primary pathway connecting the stomach and the brain, with the left gastric vagal branch innervating the ventral stomach and the right gastric vagal branch innervating the dorsal stomach (Furness et al., 2014, 2020; Rogers et. al., 1995). The left and right vagus nerve further project to the left and right nucleus of the solitary tract (NTS), respectively. However, the stomach does not have a clear topographic organization in NTS (Rogers et al., 1995; Travagli & Anselmi, 2016). NTS further projects within and across hemisphere and connects to forebrain regions (Browning & Travagli, 2011; Levinthal & Strick, 2020; Suarez et al., 2018). The complicated connection leaves the gastro-topic mapping largely unknown.

To address these questions, we implanted electrodes on the stomach surface and recorded gastric myoelectrical activity (GMA) simultaneously with brain fMRI. We focused on gastric activity at two different locations on the stomach (i.e., corpus and antrum) and further verified the stomach-brain synchrony given GMA from the corpus and antrum separately.

Methods

Subjects

This study used four Sprague–Dawley rats (male, weight: 300–500 g; Envigo RMS, Indianapolis, IN) according to a protocol approved by the Institutional Animal Care and Use Committee (IACUC) at University of Michigan. All animals were housed in a strictly controlled environment (temperature: 21 ± 1 °C; 12 h light-dark cycle with lights on at 5:00 a.m. and off at 5:00 p.m.). Animals underwent surgical implantation of wire electrodes for gastric myoelectrical activity recording.

Animal training and feeding

The animal was trained to consume a fixed quantity of palatable dietgel (DietGel Recovery, ClearH2O, ME, USA) following an established training protocol (Lu et al., 2017). The training process took 7 days. In the first 2 days, the animal was supplied with both regular rat chows and ~5g dietgel to accustom itself to the dietgel. In the following days, the animal was fasted for 18 hours (6PM to 12AM) and then fed with the dietgel only at 12AM. The animal was given 30 minutes to consume 5 dietgel; then regular meal was supplied to the animal afterwards. After the diet training (~2 to 3 repetitions), the animal was able to voluntarily consume the dietgel following overnight food restriction and was ready for participating the experiment.

Anesthesia protocol

The animal was anesthetized during the experiment. The animal was initially anesthetized with 5% isoflurane followed with 2.5% isoflurane to maintain the anesthesia depth. The animal was placed on a heating pad to maintain the body temperature. After a toe-pinch test, the animal was ready for other procedures including the surgery and electrode implantation. The dose of isoflurane was adjusted during the procedure to maintain the depth of anesthesia. Throughout the procedure, the respiration rate, heart rate, oxygen saturation level (SpO2), and body temperature were monitored and maintained in the safe range, in which respiration rate was from 30 to 70 breaths per minute, heart rate was from 250 to 350 beats per minute, SpO2 was higher than 96%, and the body temperature was within 37± 0.5 °C.

During the data acquisition, a different anesthesia protocol was applied to minimize the effects of isoflurane on homeostasis. Half an hour before the recording, a bolus of dexdomitor (15 μg/Kg, Zoetis, NJ, USA) was administered subcutaneously. The dose of isoflurane was then lowered to 0.1-0.5% as soon as the animal's heart rate and respiration start to drop. About 15 to

20 minutes following the bolus injection, subcutaneous infusion of dexdomitor was administered with the dose of 15 μg/Kg/h, during which the dose of isoflurane is maintained below 0.5%. The dose of dexdomitor and isoflurane were adjusted throughout the experiment to maintain the depth of anesthesia as needed. Respiration rate, heart rate, oxygen saturation level (SpO2), and body temperature were monitored and maintained in the safe range as described in the previous paragraph.

Brain fMRI acquisition and signal preprocessing

The MRI and fMRI data were acquired with the 7-tesla small-animal MRI system (Agilent, Varian medical system, Palo Alto, CA, USA). A 90 mm volume coil and a four-channel surface coil were respectively used as the transmitter and receiver for image acquisition. During the scanning, the animal's head was constrained with a bite bar and two ear bars to avoid head motion, and the animal's torso was gently taped to animal holder to avoid body motion. Localizer scans were first applied to locate the animal's brain. After localizer scans, T2-weighted anatomical images were acquired using a rapid acquisition with fast spin echo sequence (TR=6500ms, effective TE=33.35ms, echo spacing =11.12ms, voxel size=0.125×0.125×0.5mm^3, RARE factor=8, and flip angle (FA)=90°). Following anatomical scans, T2*-weighted fMRI images were acquired with a 2-D single-shot gradient-echo (GE) echo-planar imaging (EPIP) sequence (TE=18ms, in-plan resolution =0.5×0.5 mm^2, slice thickness=1mm, TR=1.2s, and FA=90°).

The MRI/fMRI data was pre-processed using FSL (Jenkinson, et al., 2012), AFNI (Cox, 1996), and in-house software developed in MATLAB. For single-echo fMRI data, head motion was first corrected by co-registering every volume to the first volume within each session (3dvolreg). Next, the slice timing in each volume was corrected by (slicetimer). The fMRI images were then aligned with the anatomical images (flirt) and further registered to a rat brain atlas

(Valdes Hernandez et al., 2011) (fnirt). Lastly, the fMRI signal was spatially smoothed with a 3-D Gaussian kernel of 0.5-mm full-width-at-half maximum (FWHM), the linear trend in time was regressed out from the fMRI signal.

Implantation of recording electrodes

To record the gastric myoelectrical activity (GMA) on the stomach wall, the electrode was chronically implanted prior to the experiment. The animal was fasted 18 hours before the surgery. To start the surgery, the fur on the animal's abdomen was shaved to expose the skin. A ~3 cm incision was made starting at the xiphoid and moving 3 cm caudally. The skin and muscle were retracted to expose the ventral stomach. The liver covering the stomach was gently pushed away until the greater curvature, the corpus, and the antrum were clearly identified. Two pairs of electrodes were sutured onto the serosal layer of the stomach wall along the stomach (as illustrated in Figure 6-1A). Leads of the implanted electrode were routed to the back of the animal, and connectors at the end of leads were exposed outside for future connection with the recording system. Next, the muscle and skin layers at the incision site on the abdomen were closed with sutures. The animal was given at least one week to recover from the surgery. After recovery, the animal was ready for the diet training and recording experiment. To minimize pain and inflammatory responses after the surgery, the animal was given Baytril (BioServ, Flemington, NJ, USA) (one tablet per day, 2 mg/Tablet) two days before the surgery and Rimadyl (5 mg/Kg, SC, Zeotis, Parsippany, NJ, USA) immediately before the surgery. Then, the animal was given Baytril/Rimadyl (one tablet per day, 2 mg/Tablet for both Baytril and Rimadyl, BioServ, Flemington, NJ, USA) for the first three days after the surgery and then was given Baytril (one tablet per day, 2 mg/Tablet) for the following three days.

GMA recordings

GMA was recorded through an EGG recording system (MP160, Biopac Systems, Inc., Goleta, CA, USA). Each pair of recording electrodes was first connected to the RF filter and then to differential amplifiers (EGG100C, Biopac Systems, Goleta, CA, USA). Signals were band-pass filtered with the low and high cutoff as 0.005 Hz and 1 Hz. The filtered signal was sampled at 100 Hz, and the digitized signal was stored in the hard disk for offline analysis. Together with GMA, Z-gradient from the MR scanner was also recorded to synchronize GMA and fMRI signals in time. In the preprocessing step, the stored GMA data went through a 0.45Hz low-pass filter and down-sampled to 0.833 Hz to match the sampling rate of fMRI signals.

Coherence analysis between GMA and fMRI signals

Coherence was used to evaluate the phase synchrony between GMA and fMRI signals. In brief, we first ran a power spectrum analysis on GMA from the selected channel and identified the dominant frequency representing gastric slow waves. We then applied the cross-spectral analysis between GMA from the selected channel and fMRI signals from individual voxels and only focused on the frequency of gastric slow waves identified previously. The cross-spectral density at the frequency of interest was then normalized for each spectrum as described in the following equation,

$$C_{xy}(f) = \frac{|G_{xy}(f)|^2}{G_{xx}(f)G_{yy}(f)} \qquad \textit{Equation 6-1}$$

in which x and y represent GMA and fMRI activity from each voxel, respectively, G_{xy} is the cross-spectral density between x and y, G_{xx} and G_{xy} is the spectral density of x and y respectively, C_{xy} is the coherence between x and y, and f represents the frequency. The normalized cross-spectral density was coherence and could describe the phase-synchrony between GMA and fMRI activity quantitatively.

Because the dominant frequency of gastric slow waves could vary over time, the coherence was calculated for every ~4 min segment to match the varying frequency. First, GMA signals were divided into segments with 256 and 196 time points, respectively. The dominant frequency of gastric slow waves was located for each data segment using the power spectrum analysis. Specifically, the highest peak within 0.06-0.13Hz was identified in the spectrum, and the corresponding frequency was the dominant frequency of gastric slow waves. Then, the coherence between each GMA segment and the corresponding fMRI segment was calculated at the dominant frequency. Coherences from all the segments were averaged within each animal, followed by statistical analysis across animals.

Coherence was converted to the z-score before statistical tests. Specifically, GMA and fMRI signals were first shuffled in phase and then used for calculating the coherence. This shuffling and coherence calculation process was performed once for individual data segments and brain voxels. These coherences were used to build the null distribution for every frequency in the spectrum. According to the null distribution, coherence from each voxel and data segment was converted to the z-score for further statistical analyses.

To map the voxel-wised coherence network, we performed the one-side t-test on coherence z-scores across animals. The statistical significance was based on the t statistic with $p<0.01$, and a cluster-wise error correction was executed to remove any cluster less than 2 mm3 (8 voxels). In the coherence analysis of regions of interest (ROIs), we defined 156 ROIs based on rat brain anatomy (Papp et al., 2014; Paxinos & Watson, 2006; Valdes Hernandez et al., 2011), including both cortical and subcortical regions. Coherence z-scores were first averaged within each ROI and for each animal. One-side t-test was then performed on the averaged z-scores across animals. The

statistical significance was based on the t statistic with $p<0.01$ with Bonferroni correction for the number of ROIs.

Relationship between fMRI and power of GMA

The relationship between GMA power and BOLD activity was also confirmed in this study. GMA power was calculated using the wavelet analysis, with the wavelet containing 9 ripples at the dominant frequency of GMA. The time series of GMA were then convolved with the predefined wavelet, and the power fluctuations were the squared value after convolution. The power fluctuations were then used to assess the relationship with BOLD activity. A general linear model was built to describe the relationship between GMA power and fMRI signals in each voxel, as shown in the following equation.

$$y = p \otimes h + \epsilon \qquad \textit{Equation 6-2}$$

in which y represents fMRI time series, p is the GMA power fluctuations, h is the hemodynamic response function, and ϵ is the noise. The hemodynamic response function was estimated with two gamma functions, with the training data from three animals. The estimated hemodynamic response function was then used to estimate the fMRI activity from the other animal (i.e., testing dataset). The correlation between the estimated fMRI and real fMRI in the testing dataset was used to evaluate whether estimation of the hemodynamic response function was successful or not. This estimation process was repeated four times with different selection of the testing and training dataset and generated four correlation maps. The correlation was converted to z scores using fisher z transform function. For voxel-wised analysis, z scores from individual voxels were tested for statistical significance using one-sample t-test with one-side $p<0.05$ and a cluster-wise error correction to remove any cluster less than 2 mm^3 (8 voxels). For ROI-wised analysis, z scores were first averaged within each ROI and then applied t-test with one-side $p<0.05$.

Results

This study aimed to check whether the gastric slow waves recorded on the stomach surface could still demonstrated the stomach-brain synchronization and whether gastric slow waves on different segments of the stomach synchronize with the brain differently. Four rats were implemented with two pair of recording electrodes on the stomach wall with one pair in the corpus and the other pair in the antrum. We recorded GMA during brain fMRI to simultaneously monitor gastric pace-making activity and BOLD activity in the brain. We assessed the synchronization between gastric pace-making activity and fMRI signals at both the postprandial and fasting stages.

Stomach-brain coherence validated with gastric myoelectrical activity recording

Previous studies demonstrated that gastric slow waves recorded through electrogastrogram were phase-coupled with the BOLD activity in the rat brain. In this study, we further validated the phase-coupling but with the gastric slow waves directed recorded from the stomach surface. Besides, due to the different functional roles of the proximal and distal stomach, we hypothesized that different stomach segments were phase-coupled with the brain differently. To test this hypothesis, we recorded gastric myoelectrical activity (GMA) from both corpus and antrum on four rats simultaneously with brain fMRI acquisition at both the postprandial (fed) and fasting states. We calculated the coherence between fMRI signals and GMA from corpus and antrum separately and compared the coherence at the two locations. As shown in Figure 3-1ABEF and Figure 6-2ABFG, both the ROI-wised and voxel-wised analyses revealed stronger phase-coupling between GMA and fMRI signals at both the fed and fasting conditions in various brain regions, including the somatosensory cortex, motor cortex, visual cortex, auditory cortex, insular cortex, striatum, thalamic nuclei, and nucleus of the solitary tract. The coherence was stronger with GMA in the corpus than antrum (Figure 6-1D & H and Figure 6-2) for both the fed and fasting conditions.

In particular, as illustrated in the ROI-based analysis, the difference was significant in the left parabrachial complex, right entorhinal cortex, posterior cingulate cortex, and bilateral pretectum at both the fed and fasting conditions. The right agranular insular cortex was significant only at the fasting condition (Figure 6-1C & G). A few exceptions also existed, including the left primary somatosensory cortex (for both the fed and fasting states) and right primary visual cortex (for the fed states), in which the difference was significant in the right primary visual cortex ($p<0.05$). The voxel-wised analysis revealed a similar difference. As shown in Figure 6-2DEIJ, at both the fed and fasting states, fewer voxels were involved in the voxel-wised network for the coherence with antrum than corpus. The averaged coherence z-score was also weaker for the phase-coupling with antrum than corpus. In summary, GMA further demonstrates the phase-coupling with fMRI activity in the brain. Also, the corpus, the origin of the pace-making activity, has stronger synchrony with the brain than the antrum.

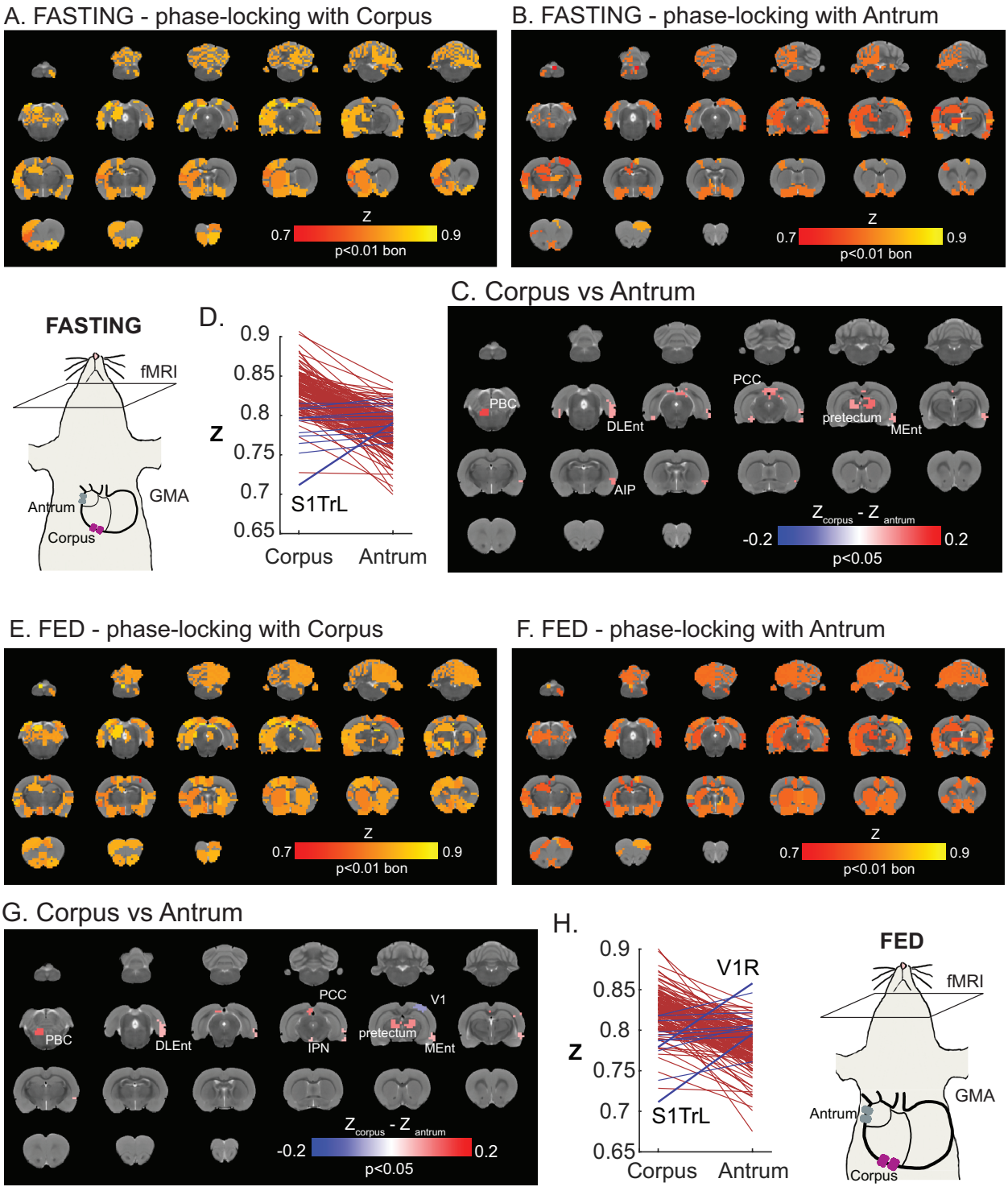

Figure 6-1 ROI-wised phase-coupling between brain fMRI and gastric myoelectrical activity (GMA) in the corpus and antrum separately. *A & B show the ROI-wised phase-coupling between fMRI and GMA at the fasting state in the corpus and antrum respectively. The color encodes the coherence z-scores with Bonferroni correct p<0.01. C highlights the regions with significant different coherence between the corpus and antrum. The color encodes the difference in coherence z-score between the corpus and antrum with p<0.05. D plots the coherence difference for all ROIs.*

Red lines mark the ROIs with coherence higher in the corpus; blue lines mark the ROIs with coherence lower in the corpus. EFGH show similar results at the fed state.

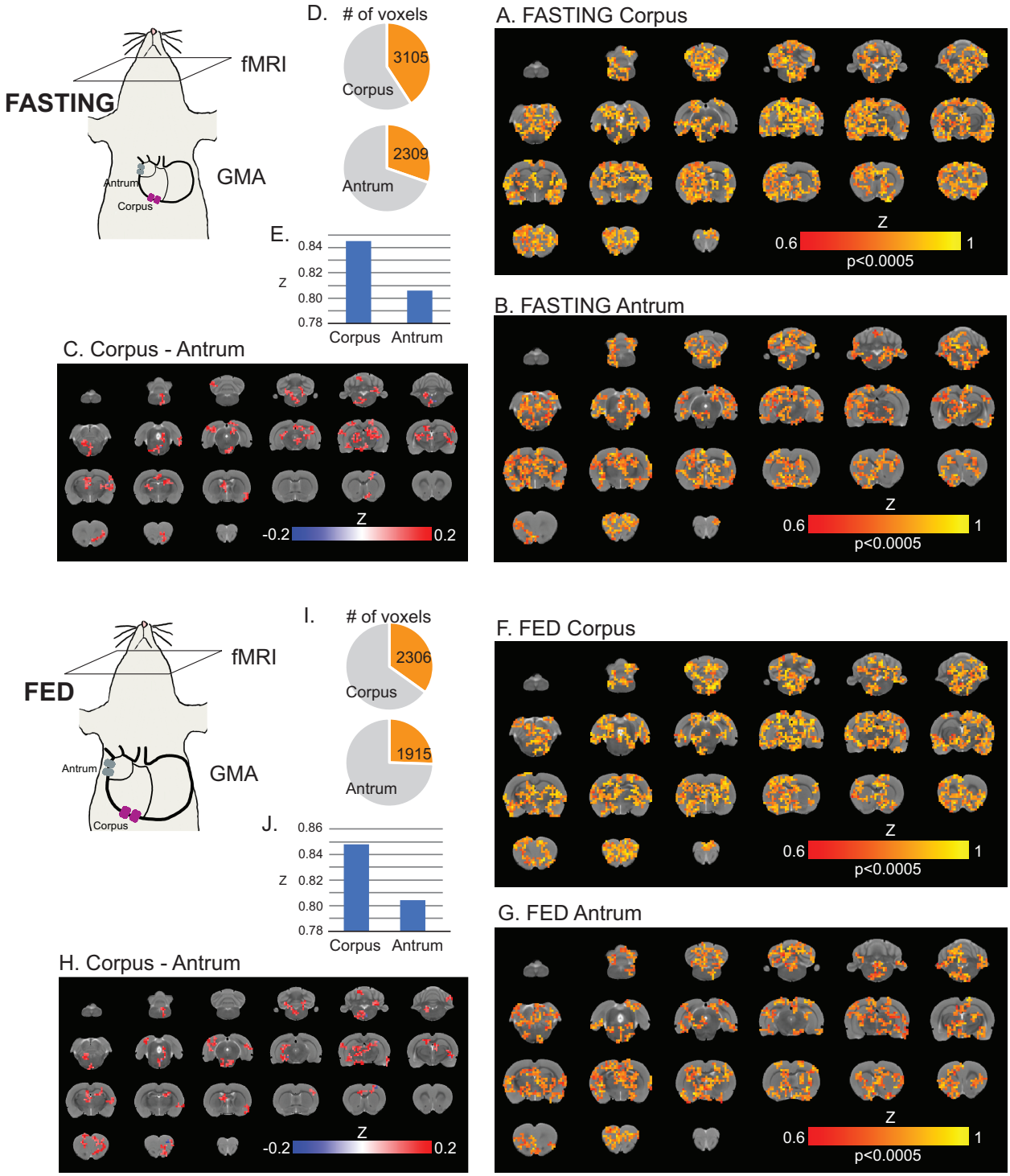

Figure 6-2 Voxel-wised phase-coupling between brain fMRI and gastric myoelectrical activity (GMA) in the corpus and antrum separately*. A & B show the fasting-state voxel-wised phase-coupling map between fMRI and GMA in the corpus and antrum, respectively. The color encodes*

the coherence z-score with p<0.0005. C highlights the regions having big coherence difference. The color encodes the coherence z-score. D illustrates the number of voxels with significant coherence between fMRI and GMA signals in the corpus and antrum separately. E plots the averaged coherence z-score for corpus and antrum separately. FGHIJ show similar results at the fed state.

Lateralization in the phase-coupling involving the corpus and antrum

The previous section illustrated the coherence difference with GMA from the corpus and antrum. Because of the different functional roles for corpus and antrum, we hypothesized that gastric slow waves in corpus and antrum were synchronized with BOLD activity in different brain regions. In particular, we assessed whether the literalization existed for the phase-coupling with GMA from the corpus and antrum. To answer this question, we identified 77 brain regions covering both the left and right hemispheres and calculate the coherence difference between the two hemispheres. The same dataset from the previous section was used here. As shown in Figure 6-3B & F, GMA from the corpus had stronger coherence with the brain regions from the right hemisphere, particularly in the insular cortex, striatum, olfactory ball, and hypothalamus for both the fasting and fed states. The regions with the largest difference between the right and left hemispheres included the primary somatosensory cortex trunk region, agranular, dysgranular, and granular insular cortex, posterior cingulate cortex, and superior colliculus for both gastric conditions (Figure 6-3DH). In contrast, GMA from the antrum had generally stronger coherence with the left hemisphere (Figure 6-3A & E). This lateralization was most observable in the somatosensory cortex, motor cortex, entorhinal cortex, and nucleus of the solitary tract. For both gastric conditions, the regions with the largest difference between the two hemispheres included the primary somatosensory cortex shoulder region, nucleus of the solitary tract, perirhinal cortex, parietal association cortex, posterior cingulate cortex, dorsal lateral and caudal entorhinal cortex, and inferior colliculus (Figure 6-3C & G). To summarize, GMA in the corpus has stronger phase-

coupling with the right hemisphere, particularly for the insular cortex and striatum. In contrast, GMA in the antrum is more phase-coupled with the left hemisphere, particularly for the sensorimotor cortex, parahippocampal regions, and nucleus of the solitary tract.

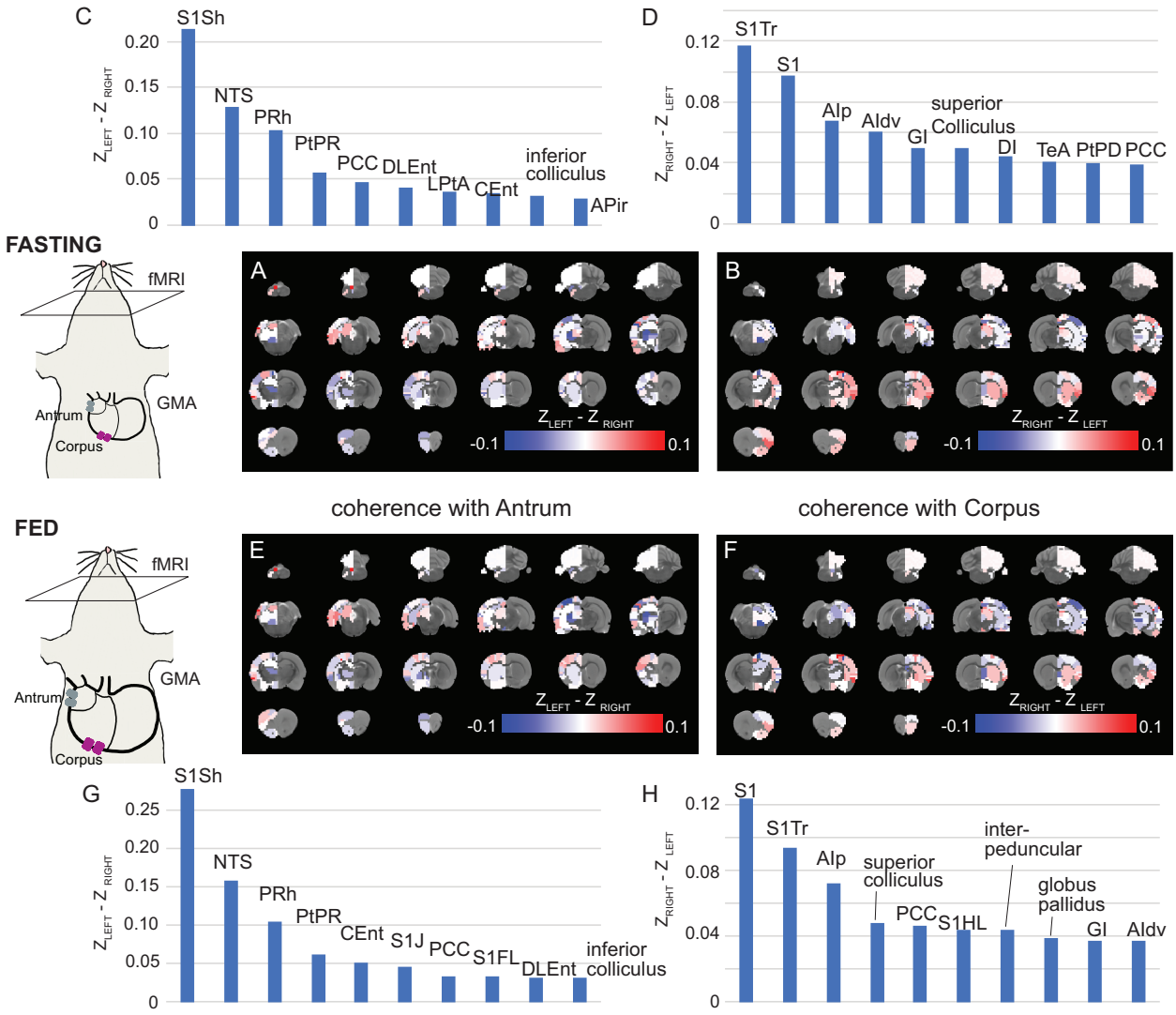

Figure 6-3 Lateralization in the phase-coupling with gastric myoelectrical activity (GMA) from the corpus and antrum. *A & E show the coherence different between the left and right hemisphere given GMA from antrum at the fasting and fed states respectively. The color encodes difference of the coherence z-score between the left and right hemispheres. C & G plot the first ten regions with the largest coherence difference across hemisphere with GMA from antrum for the fasting and fed states respectively. B & F show the coherence difference between the right and left hemisphere give GMA from corpus at the fasting and fed states respectively. The color encodes difference of the coherence z-score between the right and left hemispheres. D & H plot the first ten regions with the largest coherence difference across hemisphere with GMA from corpus for the fasting and fed states respectively.*

Gastric-condition-dependency of the phase-coupling between the stomach and brain

In the study described in chapter 5, we observed that the stomach-brain synchrony depended on gastric states. This section further investigated this state-dependency given gastric slow waves from the antrum and corpus separately. We first chose GMA from the antrum and calculated its coherence with fMRI signals at both the fed and fasting states. The coherence difference was presented for individual voxels and ROIs separately. With GMA from the antrum, the coherence was stronger at the fed state than the fasting state. According to the voxel-wised comparison, the difference was strongest in the left primary motor cortex, left somatosensory cortex, left lateral thalamus, right amygdala, left auditory cortex, and a small portion of the striatum (Figure 6-4A). The ROI-based comparison revealed similar results (Figure 6-4C), with the largest difference observed in the left somatosensory cortex (shoulder, forelimb, and jaw regions), right visual cortex, right interpeduncular nucleus, left frontal association cortex, right bed striatum, and right parietal association cortex (Figure 6-4E). We also chose GMA from the corpus and applied the same analysis. With GMA from the corpus, the coherence was generally weaker at the fed state than the fasting state, such as the anterior cingulate cortex, right lateral thalamus (as shown in Figure 6-4B), but with exemptions in the left primary motor cortex and a small portion of striatum having stronger coherence at the fed state, same with the coherence with antrum. Regions with the largest coherence difference included the right nucleus of the solitary tract, right primary and secondary visual cortex, posterior cingulate cortex, bilateral perirhinal cortex, right lateral geniculate thalamus, and medial parietal association cortex (Figure 6-4F). In general, GMA from the antrum has stronger phase-coupling with fMRI signals at the fed state, while the corpus has stronger coherence at the fasting state, suggesting an opposite state-dependency with the brain.

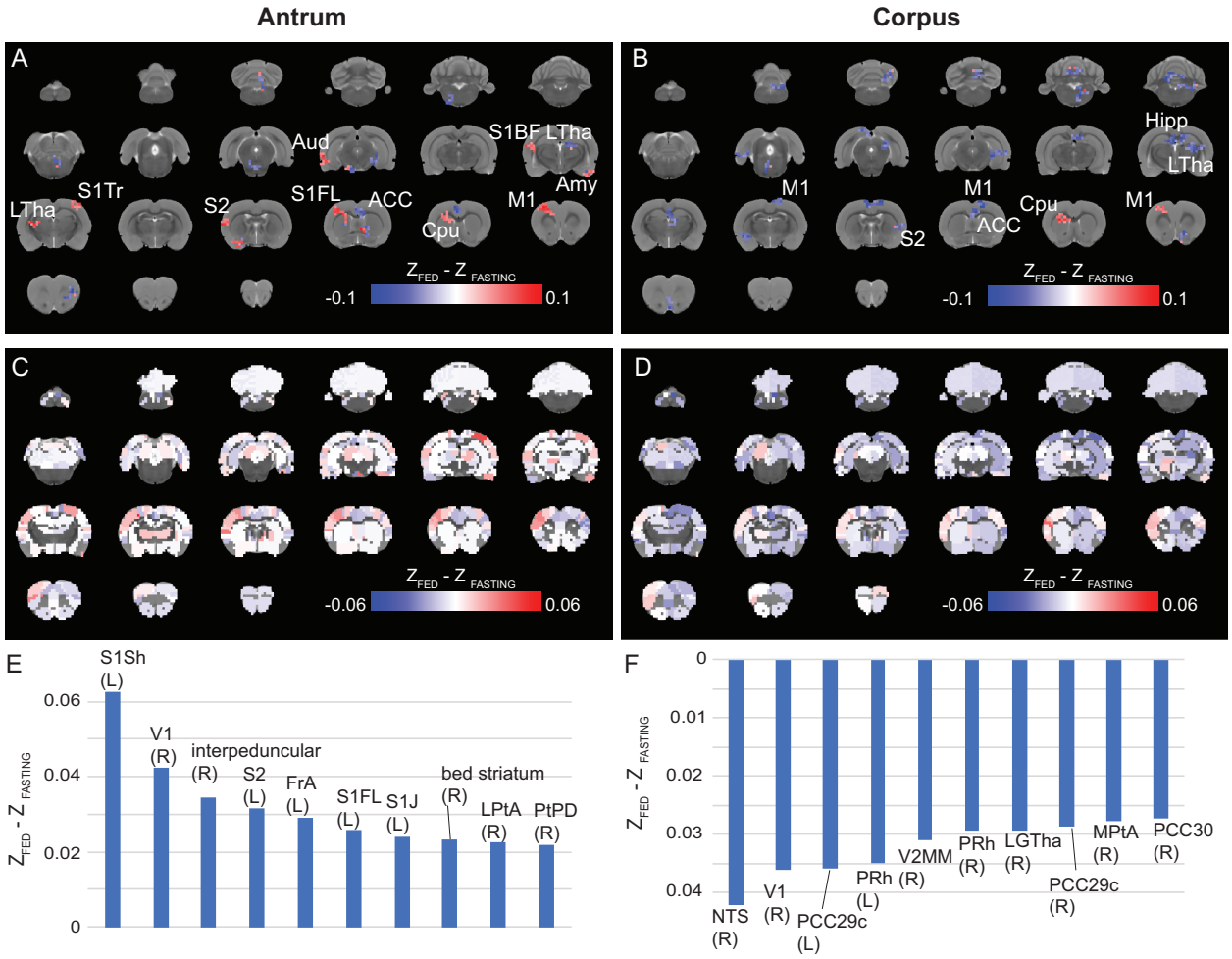

Figure 6-4 State-dependency of the phase-coupling between the stomach and the brain*. A & B show the coherence difference comparing the fed state with the fasting state at voxel and ROI level respectively with gastric myoelectrical activity from the antrum. C & D show similar results but with gastric myoelectrical activity from the corpus. For ABCD, the color encodes the difference of coherence z-score. E & F plot the first ten regions having the largest coherence difference between the fed and fasting states with gastric myoelectrical activity from the antrum and corpus respectively.*

Correspondence between fMRI and power of gastric myoelectrical activity

Besides gastric slow waves, the strength of gastric contraction is also a critical feature of gastric function that can be modulated through the stomach-brain neuroaxis. Because of the correspondence between the power of GMA and gastric contractions, we hypothesized that BOLD activity in the brain also correlated with the power fluctuations of GMA. To test this hypothesis,

we extracted the power fluctuations of GMA using wavelets with the frequency at 5CPM and assessed the correlation between the power fluctuations with fMRI signals to map the gastric power networks. As illustrated in Figure 6-5AF, the power fluctuated over time at both the fasting and fed states but with distinct patterns. Besides, the power fluctuation did not match well given GMA from the corpus and antrum, either. The gastric power networks also covered different brain regions. At the fed state, the network generated by GMA in the corpus covered a broad brain region, including the somatosensory cortex, motor cortex, insular cortex, anterior cingulate cortex, hippocampal formation thalamus, and visual cortex (Figure 6-5GI, $p<0.05$). In contrast, the gastric power network with GMA in the corpus covered fewer regions at the fasting state, including only the motor cortex and a small portion of the visual cortex (Figure 6-5BD, $p<0.05$). Compared with corpus, gastric power networks with GMA in antrum only involved a small portion of the motor and somatosensory cortex at both the fasting and fed states and covered part of the hippocampal formation and parietal cortex at the fasting state (Figure 6-5CEHJ, $p<0.05$). In summary, the power fluctuations from the corpus have a larger impact on BOLD activity in the brain, especially at the postprandial state.

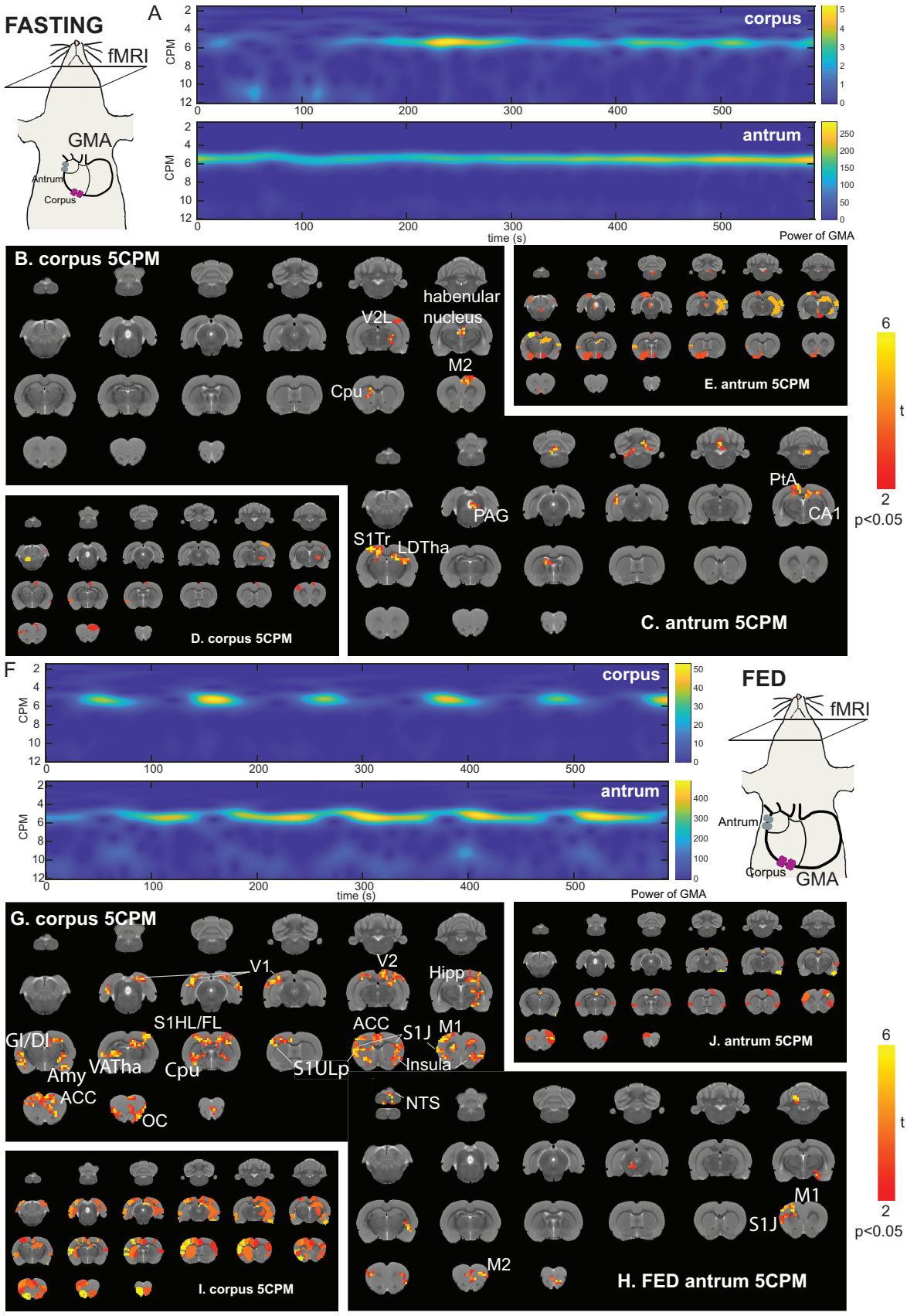
FASTING
fMRI
GMA
Antrum
Corpus
A
corpus
antrum
CPM
time (s)
Power of GMA
B. corpus 5CPM
habenular nucleus
V2L
M2
Cpu
E. antrum 5CPM
PtA
CA1
PAG
S1Tr
LDTha
C. antrum 5CPM
D. corpus 5CPM
t
2
p<0.05
F
FED
fMRI
Antrum
Corpus
GMA
G. corpus 5CPM
V1
V2
Hipp
S1HL/FL
GI/DI
Amy
VATha
Cpu
ACC
S1ULp
S1J
M1
Insula
OC
J. antrum 5CPM
NTS
M2
S1J
M1
H. FED antrum 5CPM
I. corpus 5CPM

Figure 6-5 Gastric power networks at the pacing-making frequency*. A & F plot an example the GMA power fluctuations over time with the frequency ranging from 1.5 CPM to 12 CPM at the fasting and fed states respectively. The color encodes the power. B & C show the voxel-wised gastric power networks at the fasting state given gastric myoelectrical activity (GMA) from the corpus and antrum respectively. D & E highlight the regions with significant correlation between power of GMA and fMRI signals given GMA from the corpus and antrum respectively. For BCDE, the color encodes t statistics with p<0.05. GHIJ show the same result at the fed state*

Occurrence of dysrhythmia in GMA is also an essential feature of gastric function with clinical relevance with nausea and vomiting. In this section, we further hypothesized that the brain fMRI signals were correlated with the power fluctuations of GMA at lower and higher frequencies. We repeated the same power analysis but used wavelets with frequencies of 3.5 CPM (low frequency) and 8 CPM (high frequency) to generate the gastric power networks. The gastric power networks covered limited brain regions with the power at 8CPM (Figure 6-6CDGH and Figure 6-7CDGH). This limited coverage held true for both the fasting and fed states and with GMA from both the corpus and antrum. In contrast, more brain regions responded to the power at 3.5CPM as the lower frequency for GMA. Broad coverage in the gastric power network could be observed with GMA in the corpus at the fasting state (Figure 6-6AE, $p<0.05$). The network included the somatosensory cortex, motor cortex, insular cortex, thalamus, visual cortex, and auditory cortex. The same network covered fewer regions at the fed state but still included the thalamus, somatosensory cortex, periaqueductal gray, and hippocampus (Figure 6-7AE, $p<0.05$). Like corpus, the gastric power network generated with GMA in antrum also showed extensive brain coverage but only at the fed state (Figure 6-6BF and Figure 6-7BF, $p<0.05$). The network at the fed state involved the somatosensory cortex, motor cortex, thalamus, hippocampus, and periaqueductal gray. In summary, BOLD activity in the brain is more sensitive to low-frequency activity but not high-frequency activity. Also, the low-frequency activity in the antrum has a more

significant impact on the brain at the fed state, and the low-frequency activity in the corpus has a more significant impact on the brain at the fasting state.

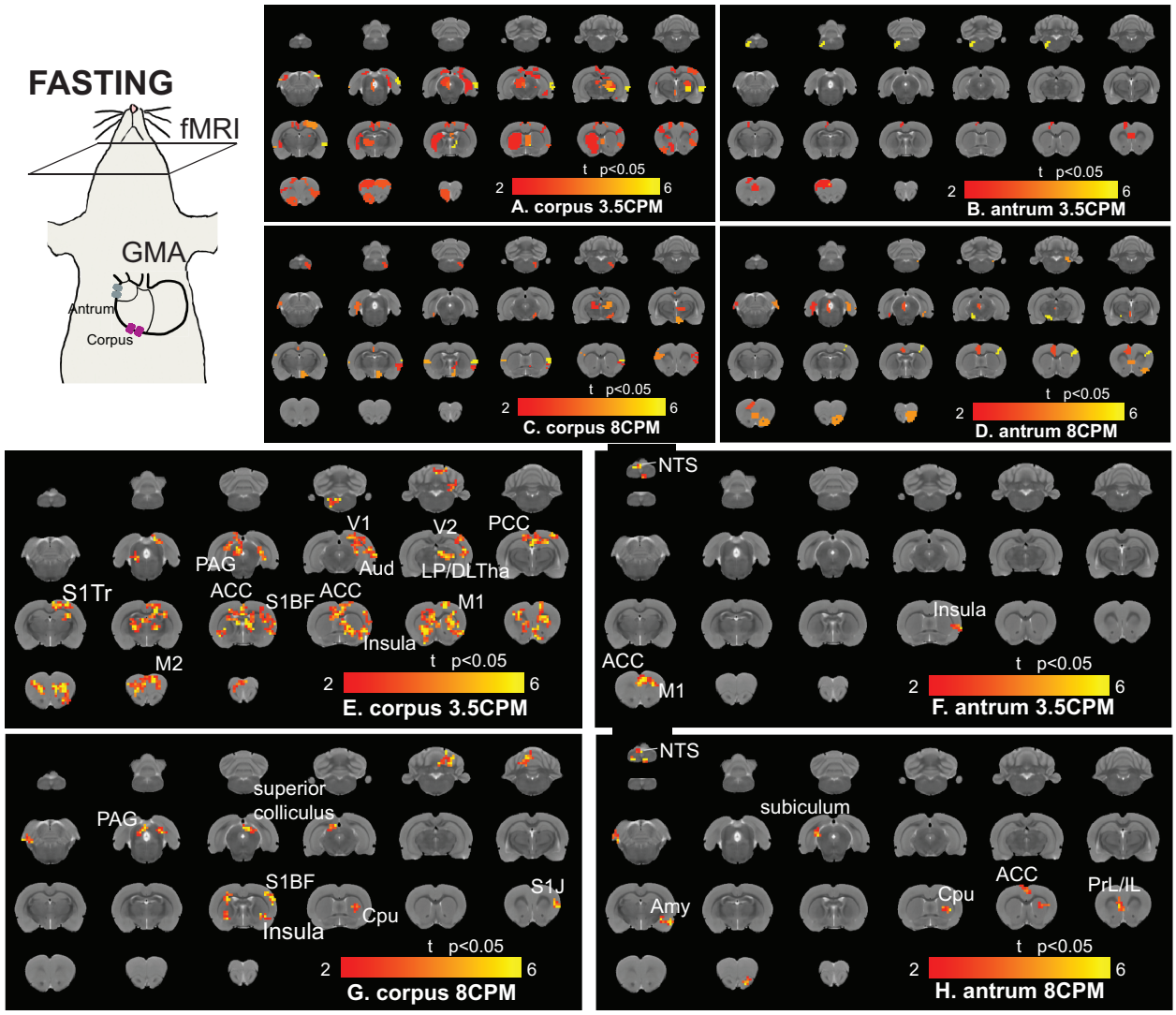

Figure 6-6 Fasting-state gastric power networks for dysrhythmic gastric activity. *ABCD highlight brain regions having significant correlation between GMA power and fMRI signals at the fasting state with GMA from the corpus and antrum and with frequency at 3.5CPM and 8CPM respectively. EFGH show the fasting-state gastric power networks with GMA from the corpus and antrum and with frequency at 3.5CPM and 8CPM respectively. The color encodes t statistic with $p<0.05$.*

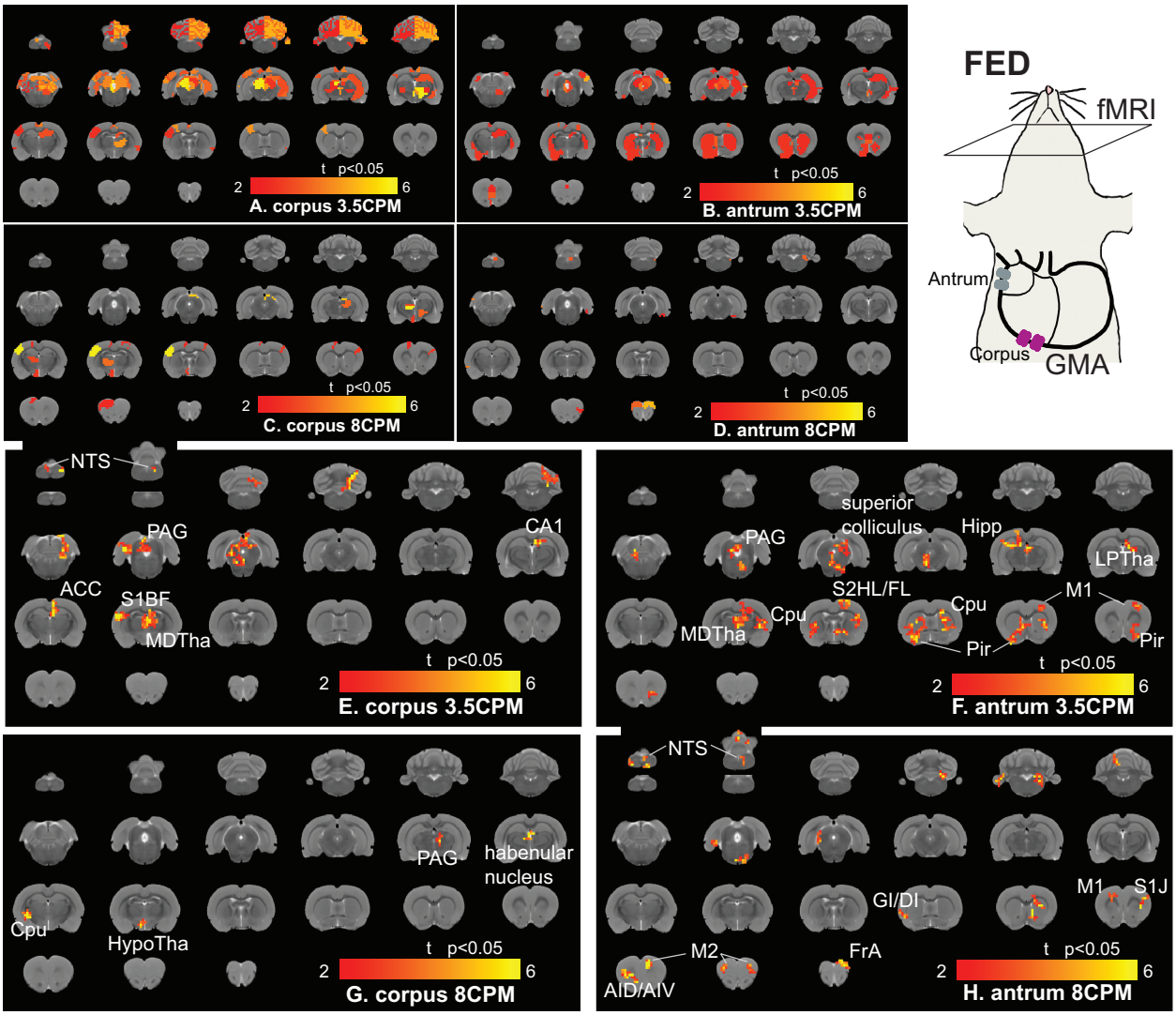

Figure 6-7 Fed-state gastric power networks for dysrhythmic gastric activity. *ABCD highlight brain regions having significant correlation between GMA power and fMRI signals at the postprandial (fed) state with GMA from the corpus and antrum and with frequency at 3.5CPM and 8CPM respectively. EFGH show the fed-state gastric power networks with GMA from the corpus and antrum and with frequency at 3.5CPM and 8CPM respectively. The color encodes t statistic with p<0.05.*

Discussion

This section focused on assessing the synchronization between brain fMRI activity and gastric myoelectrical activity (GMA) from different stomach segments. We reported that gastric pace-making activity in both the corpus and antrum was phase-coupled with BOLD activity in the brain but with stronger phase-coupling for the corpus. The phase-coupling showed lateralization

in the brain, with the right hemisphere more phase-coupled to the corpus and the left hemisphere more phase-coupled to the antrum. The phase-coupling was also gastric-state-dependent. At the fed state, the phase-coupling was stronger with the antrum and weaker with the corpus. Beyond the phase-coupling, BOLD activity in the brain was also correlated with the power fluctuations of GMA. Compared to the antrum, power fluctuations in the corpus more significantly impacted BOLD activity at 5CPM (phase-making frequency) and 3.5CPM (low frequency). The power correlation also showed gastric-state-dependency, with the antrum having a more extensive influence on the brain at the fed state.

Biological meaning of gastric myoelectrical activity

GMA is a mixture of gastric slow waves and myoelectrical activity from gastric smooth muscles. Gastric slow waves are initiated by ICC cells as a highly sinusoidal signal (Hansen, 2003; Sanders et al., 2006). They can set the basic rhythm for gastric contractions, with the onset corresponding to the starting point of a smooth muscle contraction. Gastric myoelectrical activity sits on top of gastric slow waves and make occurrences of smooth muscle contraction visible in GMA. When a strong contraction occurs, the power of GMA becomes larger. In contrast, if there is no contraction, the power of GMA is smaller. Beside the normal condition, the frequency of GMA can also be lower or higher, named bradygastria and tachygastria. The dysrhythmic activity is associated with abnormal gastric condition, such as nausea and vomiting (Chen et al., 1995). Therefore, results shown in this study can be interpreted given the physiological meaning of GMA. The phase-coupling between GMA and BOLD activity suggest that the gastric activity and neural activity in the brain are synchronized with each other, likely in the case that the brain follows the gastric rhythm. Besides, the correlation between GMA power and BOLD activity indicates that the brain keeps track of the contractional power of the stomach. Last, the correspondence between

GMA power at abnormal frequency support that the brain monitors gastric dysrhythmic activity constantly.

Difference between the antrum and corpus

Our results suggest different behavior of the antrum and corpus when interacting with the brain. The corpus is the main body of the stomach, with the primary function of grinding and mixing food (Boeckxstaens et al., 2016). The corpus also initiates gastric slow waves, which propagate to the antrum and drives gastric contractions. The antrum receives gastric slow waves and incorporates with its own rhythm to generate contractions. The contractions in the antrum are much stronger than corpus and help to mix food and empty the stomach. The corpus and antrum are also different anatomically (Boeckxstaens et al., 2016). The corpus has more IGLEs, which are vagal afferent terminals on the stomach and have close contacts with the enteric neurons (Powley et al., 2019). The antrum has more intramuscular arrays (IMAs), which are also vagal afferent terminals but presumably to be stretch receptors (Powley et al., 2019). Our result reveals that antrum and corpus are phase-coupled with different brain regions, suggesting a functional difference in cooperating with the brain. of the phase-coupling. The stronger phase-coupling with the corpus suggests that the brain care more about the initiation of gastric slow waves and may regulate gastric slows in corpus. Based on the anatomical evidence that more IGLEs presents in corpus, suggesting that the phase-coupling is likely relayed by IGLEs.

Compared with the corpus, contraction in antrum is an important feature for the stomach. The strong contractions in antrum can better grinding the food and empty the stomach. However, our result suggest that the brain is less correlated with GMA power in the antrum. The lack of correlation is likely due to the less variation of GMA power. Based on the result, power fluctuations in the corpus are more dynamic and vary a lot in time. Monitoring the power

fluctuations in corpus is more meaningful. Besides, stronger contractions are often initiated in the corpus and propagate to the antrum. To follow the strong contractions, it is efficient to have a single point monitor, and the monitored point is better to be corpus.

Lateralization in the gastric network

This study reports lateralization of the phase-coupling between BOLD activity and gastric activity from the antrum and corpus. The antrum tends to have stronger phase-coupling with BOLD activity in the left hemisphere, while the corpus has stronger phase-coupling with the right hemisphere. The lateralization is a common phenomenon in the CNS organization, such as the visual system, sensorimotor system, with one hemisphere being more engaged in a functional role (Kapreli et al., 2016; Tomasi & Volkow, 2012; Tucker, 1981). In the stomach-brain neuroaxis, the lateralization is clear between the stomach and dorsal vagal complex. The left vagus nerve innervates the ventral stomach and the right vagus nerve innervates the dorsal vagus nerve. However, the knowledge of the lateralization becomes less clear going beyond the dorsal vagal complex. Presumably, the right insula is more relevant to energy expenditure and arousal, and the left insula is more engaged in energy nourishment and appetite behavior (Craig, 2009, 2014). Speculatively, the lateralization observed in this study is based on the function of antrum and corpus. the corpus initiates gastric slow waves and interact more with the right hemisphere. The antrum is more semi-automatic and interacts more with the left hemisphere.

Limitation and the future direction

This study reports the stomach-brain synchronization from the aspect of phase-coupling and amplitude correlation, which represent a few aspects of the gastric activity. Other features are also important in terms of the stomach-brain interactions, such as the effects of different nutrients. It is necessary to investigated whether different nutrients have significant impacts on the brain at

the intrinsic manner. Besides, gastric activity induces a broad effect on brain activity. It is of great interest to predict the neural activity in the brain with gastric activity and see how much the gastric activity can explain the neural activity in the brain.

Chapter 7 Conclusion

Summary of this dissertation

This dissertation focuses on the functional activities along the stomach-brain neuroaxis during electric modulations and intrinsic gastric conditions.

Firstly, the study in Chapter 2 proposes a new parameter, the orientation of current flow, for gastric electrical stimulation (GES) and confirms that neural responses in the brainstem are selective to stimulation orientation. With a carefully designed stimulation protocol, GES can also evoke the central gastric network beyond the brainstem. This stimulation drives the fast blood-oxygen-level-dependent (BOLD) activity in the brain, primarily covering the somatosensory cortex, motor cortex, insular cortex, cingulate cortex, and thalamus (as described in Chapter 3). These regions match well with the central gastric network identified with histological mapping, suggesting the efficient modulatory effect of GES on the stomach-brain interaction.

Then, the study in Chapter 4 targets the stimulation on the vagus nerve (VNS), which is the primary neural pathway connecting the stomach and the brain. As illustrated in the result, VNS triggers widespread BOLD responses in the brain and regulates the functional connectivity across various brain regions, within and beyond the central gastric network. This result suggests that VNS has the potential to regulate the stomach-brain interaction but yield nonspecific stimulating effects.

The following two chapters further discuss the functional role of the stomach-brain interaction during intrinsic gastric conditions. The stomach-brain interaction is assessed with the simultaneous recording of gastric slow waves and fMRI signals. Within the gastric network, BOLD activity is phase-coupled with gastric rhythms and follows the power of gastric contractions.

This relationship depends on gastric conditions, with different BOLD activity at the postprandial and fasting states. Besides, the functional activity within the gastric network is primarily mediated by the vagus nerve and largely attributed to the gastric activity in the corpus. This result indicates that the brain interacts with the stomach continuously and monitors gastric activity from various aspects.

These findings provide a systematic assessment of the central gastric network and build a foundation for functional mapping of the central gastric network, thus allowing more systematic investigations of the stomach-brain neuroaxis in the future.

Future directions

Moving forward, more studies can be down to further delineate the stomach-brain interaction.

This study primarily focuses on the mechanical activity of the stomach within the stomach-brain interaction. The hormonal signaling is another important feature associated with the digestive process and plays an essential role in the communication between the stomach and the brain (Psichas et al., 2015). For example, the lateral hypothalamus and area postrema (Browning & Travagli, 2011), as part of the gastric network, consistently monitor hormones in the blood stream and respond directly to alter neural activity in the central gastric network. Therefore, it is necessary to incorporate the hormonal signaling when delineate neural activity at various gastric conditions.

Sexual difference is another critical point given the concept of the stomach-brain interaction. Based on previous studies, 70-80% of patients with functional dyspepsia and gastroparesis are females (Ford et al., 2020; Lacy et al., 2009; Stanghellini, 2016; Talley & Ford, 2015). This sexual bias suggests the fundamental differences between male and female subjects. For example, the hormonal changes in females may disrupt the stomach-brain interaction and alter

normal gastric function. Therefore, it is important to investigate the stomach-brain interaction in female subjects and to identify the sexual differences. A clear understanding of the sexual differences may facilitate to discover a better understanding of disease conditions and potential therapeutical strategies to repair the stomach-brain interaction.

Last but not least, it is of great interest to fully delineate the gastric component of the resting-state neural activity in the brain. There is increasing discussion that the interoceptive signal shapes the brain and determines how we think and feel (Craig, 2008; Underwood, 2021). The stomach, as one of the internal organs, can make a great contribution to the interceptive feeling. If we can acquire the gastric activity, it might be possible to predict a significant part of the resting state neural activity. This prediction requires a clear understanding of gastric activity and how the gastric activity being represented as neural activity in the brain. The successful prediction will not only help the understanding of normal and abnormal stomach-brain interaction, but also open a new revenue in studying the cognition and emotion.

Conclusion

In conclusion, studies in this dissertation reveal a widespread coverage of the central gastric network during GES, VNS, and intrinsic gastric conditions. Specifically, mediated by an orientation-specific GES, gastric neurons in the brainstem are selective to the orientation of muscle activity relayed through intramuscular arrays. The orientation-specific GES can modulate BOLD activity beyond the brainstem and drive a fast BOLD activity in the central gastric network. The GES-evoked functional network is partially overlapped with the VNS-evoked network and can be explained by the intrinsic stomach-brain synchronization, supported by the phase-coupling and power correlation between gastric slow waves and BOLD activity in the brain. These findings provide a systematic assessment of the central gastric network, laying the foundation of mapping

and characterizing the central and peripheral mechanisms of gastric interoception and shedding new light on where and how to stimulate the peripheral nerves to modulate stomach-brain interactions.

Bibliography

Abell, T. L., & Malagelada, J. R. (1988). Electrogastrography. Digestive diseases and sciences, 33(8), 982-992.

Abell, T., McCallum, R., Hocking, M., Koch, K., Abrahamsson, H., LeBlanc, I., Lindberg, G., Konturek, J., Nowak, T., Quigley, E.M. and Tougas, G., & Starkebaum, W. (2003). Gastric electrical stimulation for medically refractory gastroparesis. Gastroenterology, 125(2), 421-428.

Al Omran, Y., & Aziz, Q. (2014). Functional brain imaging in gastroenterology: to new beginnings. Nature Reviews Gastroenterology & Hepatology, 11(9), 565.

Anastassiou, C. A., & Shai, A. S. (2016). Psyche, signals and systems. Micro-, Meso-and Macro-Dynamics of the Brain, 107-156.

Aro, P., Talley, N. J., Ronkainen, J., Storskrubb, T., Vieth, M., Johansson, S. E., Bolling–Sternevald, E., & Agréus, L. (2009). Anxiety is associated with uninvestigated and functional dyspepsia (Rome III criteria) in a Swedish population-based study. Gastroenterology, 137(1), 94-100.

Aziz, Q., Thompson, D. G., Ng, V. W. K., Hamdy, S., Sarkar, S., Brammer, M. J., Bullmore, E. T., Hobson, A., Tracey, I., Gregory, L. and Simmons, A., & Williams, S. C. R. (2000). Cortical processing of human somatic and visceral sensation. Journal of Neuroscience, 20(7), 2657-2663.

Balleine, B. W., Delgado, M. R., & Hikosaka, O. (2007). The role of the dorsal striatum in reward and decision-making. Journal of Neuroscience, 27(31), 8161-8165.

Bandettini, P. A., Wong, E. C., Hinks, R. S., Tikofsky, R. S., & Hyde, J. S. (1992). Time course EPI of human brain function during task activation. Magnetic resonance in medicine, 25(2), 390-397.

Bartolomei, F., Bonini, F., Vidal, E., Trébuchon, A., Lagarde, S., Lambert, I., McGonigal, A., Scavarda, D., Carron, R., & Benar, C. G. (2016). How does vagal nerve stimulation (VNS) change EEG brain functional connectivity?. Epilepsy research, 126, 141-146.

Bean, B. P. (2007). The action potential in mammalian central neurons. Nature Reviews Neuroscience, 8(6), 451-465.

Beaumont, E., Campbell, R. P., Andresen, M. C., Scofield, S., Singh, K., Libbus, I., KenKnight, B. H., Snyder, L., & Cantrell, N. (2017). Cervical vagus nerve stimulation augments spontaneous discharge in second-and higher-order sensory neurons in the rat nucleus of the solitary tract. American journal of physiology-heart and circulatory physiology, 313(2), H354-H367.

Beckmann, C. F., & Smith, S. M. (2004). Probabilistic independent component analysis for functional magnetic resonance imaging. IEEE transactions on medical imaging, 23(2), 137-152.

Ben-Menachem, E. (2002). Vagus-nerve stimulation for the treatment of epilepsy. The Lancet Neurology, 1(8), 477-482.

Berthoud, H. R., Jedrzejewska, A., & Powley, T. L. (1990). Simultaneous labeling of vagal innervation of the gut and afferent projections from the visceral forebrain with dil injected into the dorsal vagal complex in the rat. Journal of comparative neurology, 301(1), 65-79.

Birn, R. M., Diamond, J. B., Smith, M. A., & Bandettini, P. A. (2006). Separating respiratory-variation-related fluctuations from neuronal-activity-related fluctuations in fMRI. Neuroimage, 31(4), 1536-1548.

Biswal, B., Zerrin Yetkin, F., Haughton, V. M., & Hyde, J. S. (1995). Functional connectivity in the motor cortex of resting human brain using echo-planar MRI. Magnetic resonance in medicine, 34(4), 537-541.

Bodenlos, J. S., Kose, S., Borckardt, J. J., Nahas, Z., Shaw, D., O'Neil, P. M., & George, M. S. (2007). Vagus nerve stimulation acutely alters food craving in adults with depression. Appetite, 48(2), 145-153.

Boeckxstaens, G., Camilleri, M., Sifrim, D., Houghton, L. A., Elsenbruch, S., Lindberg, G., Azpiroz, F., & Parkman, H. P. (2016). Fundamentals of neurogastroenterology: physiology/motility–sensation. Gastroenterology, 150(6), 1292-1304.

Bohning, D. E., Lomarev, M. P., Denslow, S., Nahas, Z., Shastri, A., & George, M. S. (2001). Feasibility of vagus nerve stimulation–synchronized blood oxygenation level–dependent functional MRI. Investigative Radiology, 36(8), 470-479.

Bor, C., Bordin, D., Demirag, K., & Uyar, M. (2016). The effect of brain death and coma on gastric myoelectrical activity. Turk J Gastroenterol, 27(3), 216-220.

Boynton, G. M., Engel, S. A., Glover, G. H., & Heeger, D. J. (1996). Linear systems analysis of functional magnetic resonance imaging in human V1. Journal of Neuroscience, 16(13), 4207-4221.

Brookes, S. J., Spencer, N. J., Costa, M., & Zagorodnyuk, V. P. (2013). Extrinsic primary afferent signalling in the gut. Nature reviews Gastroenterology & hepatology, 10(5), 286-296.

Browning, K. N., & Travagli, R. A. (2011). Central nervous system control of gastrointestinal motility and secretion and modulation of gastrointestinal functions. Comprehensive physiology, 4(4), 1339-1368.

Brüggemann, J., Shi, T., & Apkarian, A. V. (1997). Viscero-somatic neurons in the primary somatosensory cortex (SI) of the squirrel monkey. Brain research, 756(1-2), 297-300.

Bush, G., Luu, P., & Posner, M. I. (2000). Cognitive and emotional influences in anterior cingulate cortex. Trends in cognitive sciences, 4(6), 215-222.

Buxton, R. B., Uludağ, K., Dubowitz, D. J., & Liu, T. T. (2004). Modeling the hemodynamic response to brain activation. Neuroimage, 23, S220-S233.

Buzsáki, G. (2004). Large-scale recording of neuronal ensembles. Nature neuroscience, 7(5), 446-451.

Camilleri, M., Chedid, V., Ford, A. C., Haruma, K., Horowitz, M., Jones, K. L., Low, P.A., Park, S. Y., Parkman, H. P., & Stanghellini, V. (2018). Gastroparesis. Nature reviews Disease primers, 4(1), 1-19.

Camilleri, M., Malagelada, J. R., Brown, M. L., Becker, G., & Zinsmeister, A. R. (1985). Relation between antral motility and gastric emptying of solids and liquids in humans. American Journal of Physiology-Gastrointestinal and Liver Physiology, 249(5), G580-G585.

Cao, J., Lu, K. H., Oleson, S. T., Phillips, R. J., Jaffey, D., Hendren, C. L., Powley, T. L., & Liu, Z. (2019). Gastric stimulation drives fast BOLD responses of neural origin. Neuroimage, 197, 200-211.

Cao, J., Lu, K. H., Powley, T. L., & Liu, Z. (2017). Vagal nerve stimulation triggers widespread responses and alters large-scale functional connectivity in the rat brain. PloS one, 12(12), e0189518.

Cao, J., Mandal R., Lu, K.H., Hendren C.L., Phillips R., Powley, T.L. and Liu, Z., (2019). The brain responds to gastric electric stimulation with orientation selectivity. International society for autonomic neuroscience.

Cao, J., Wang, X., Powley, TL., and Liu, Z., (in submission). Neurons in the Nucleus Tractus Solitarius are Selective to the Orientation of Gastric Electrical Stimulation. Journal of Neuroscience.

Cao, J., Wang, X., Scheven, U., and Liu, Z., (in preparation). Gastric Myoelectrical Activity is Synchronized with BOLD Activity in the Brain at Intrinsic States.

Cao, J., Wang, X., Scheven, U., and Liu, Z., (in preparation). The Stomach and the Brain are Intrinsically Phase-Coupled in Rats.

Carabotti, M., Scirocco, A., Maselli, M. A., & Severi, C. (2015). The gut-brain axis: interactions between enteric microbiota, central and enteric nervous systems. Annals of gastroenterology: quarterly publication of the Hellenic Society of Gastroenterology, 28(2), 203.

Carmagnola, S., Cantù, P., & Penagini, R. (2005). Mechanoreceptors of the proximal stomach and perception of gastric distension. American Journal of Gastroenterology, 100(8), 1704-1710.

Chae, J. H., Nahas, Z., Lomarev, M., Denslow, S., Lorberbaum, J. P., Bohning, D. E., & George, M. S. (2003). A review of functional neuroimaging studies of vagus nerve stimulation (VNS). Journal of psychiatric research, 37(6), 443-455.

Chase, M. H., Nakamura, Y., Clemente, C. D., & Sterman, M. B. (1967). Afferent vagal stimulation: neurographic correlates of induced EEG synchronization and desynchronization. Brain research, 5(2), 236-249.

Chen, J. D. Z., Pan, J., & McCallum, R. W. (1995). Clinical significance of gastric myoelectrical dysrhythmias. Digestive Diseases, 13(5), 275-290.

Chen, J. E., Jahanian, H., & Glover, G. H. (2017). Nuisance regression of high-frequency functional magnetic resonance imaging data: denoising can be noisy. Brain connectivity, 7(1), 13-24.

Cheung, B., & Vaitkus, P. (1998). Perspectives of electrogastrography and motion sickness. Brain research bulletin, 47(5), 421-431.

Cheyuo, C., Jacob, A., Wu, R., Zhou, M., Coppa, G. F., & Wang, P. (2011). The parasympathetic nervous system in the quest for stroke therapeutics. Journal of cerebral blood flow & metabolism, 31(5), 1187-1195.

Choe, A. S., Tang, B., Smith, K. R., Honari, H., Lindquist, M. A., Caffo, B. S., & Pekar, J. J. (2021). Phase-locking of resting-state brain networks with the gastric basal electrical rhythm. Plos one, 16(1), e0244756.

Cigaina, V. (2002). Gastric pacing as therapy for morbid obesity: preliminary results. Obesity surgery, 12(1), S12-S16.

Code, C. F., & Marlett, J. A. (1975). The interdigestive myo-electric complex of the stomach and small bowel of dogs. The Journal of Physiology, 246(2), 289-309.

Cox, R. W. (1996). AFNI: software for analysis and visualization of functional magnetic resonance neuroimages. Computers and Biomedical research, 29(3), 162-173.

Cox, R. W., Chen, G., Glen, D. R., Reynolds, R. C., & Taylor, P. A. (2017). FMRI clustering in AFNI: false-positive rates redux. Brain connectivity, 7(3), 152-171.

Craig, A. D. (2002). How do you feel? Interoception: the sense of the physiological condition of the body. Nature reviews neuroscience, 3(8), 655-666.

Craig, A. D. (2008). Interoception and emotion: a neuroanatomical perspective. Handbook of emotions, 3(602), 272-88.

Craig, A. D. (2009). How do you feel--now? The anterior insula and human awareness. Nature reviews neuroscience, 10(1).

Craig, A. D. (2014). How do you feel?: an interoceptive moment with your neurobiological self. Princeton University Press.

Davis, C. J., Harding, R. K., Leslie, R. A., & Andrews, P. L. R. (1986). The organisation of vomiting as a protective reflex. In Nausea and vomiting: Mechanisms and treatment (pp. 65-75). Springer, Berlin, Heidelberg.

De Ponti, F., Azpiroz, F., & Malagelada, J. R. (1987). Reflex gastric relaxation in response to distention of the duodenum. American Journal of Physiology-Gastrointestinal and Liver Physiology, 252(5), G595-G601.

De Ridder, D., Vanneste, S., Engineer, N. D., & Kilgard, M. P. (2014). Safety and efficacy of vagus nerve stimulation paired with tones for the treatment of tinnitus: a case series. Neuromodulation: Technology at the Neural Interface, 17(2), 170-179.

de Zwart, J. A., Silva, A. C., van Gelderen, P., Kellman, P., Fukunaga, M., Chu, R., Koretsky, A. P., Frank, J. A., & Duyn, J. H. (2005). Temporal dynamics of the BOLD fMRI impulse response. Neuroimage, 24(3), 667-677.

Devous, M. D., Husain, M., Harris, T. S., & Rush, A. J. (2002). Effects of VNS on regional cerebral blood flow in depressed subjects. European Psychiatry, 17(S1), 113s-114s.

Dorr, A. E., & Debonnel, G. (2006). Effect of vagus nerve stimulation on serotonergic and noradrenergic transmission. Journal of Pharmacology and Experimental Therapeutics, 318(2), 890-898.

Drossman, D. A. (2016). Functional gastrointestinal disorders: history, pathophysiology, clinical features, and Rome IV. Gastroenterology, 150(6), 1262-1279.

Drossman, D. A., Creed, F. H., Olden, K. W., Svedlund, J., Toner, B. B., & Whitehead, W. E. (1999). Psychosocial aspects of the functional gastrointestinal disorders. Gut, 45(suppl 2), II25-II30.

Du, P., Li, S., O'Grady, G., Cheng, L. K., Pullan, A. J., & Chen, J. D. (2009). Effects of electrical stimulation on isolated rodent gastric smooth muscle cells evaluated via a joint computational simulation and experimental approach. American Journal of Physiology-Gastrointestinal and Liver Physiology, 297(4), G672-G680.

Du, P., O'Grady, G., Cheng, L. K., & Pullan, A. J. (2010). A multiscale model of the electrophysiological basis of the human electrogastrogram. Biophysical journal, 99(9), 2784-2792.

Ehrlein, H. J., & Schemann, M. (2005). Gastrointestinal motility. Technische Universität München, Munich.

Enck, P., Azpiroz, F., Boeckxstaens, G., Elsenbruch, S., Feinle-Bisset, C., Holtmann, G., Lackner, J. M., Ronkainen, J., Schemann, M., Stengel, A. and Tack, J. Stephan, Z., & Talley, N. J. (2017). Functional dyspepsia. Nature Reviews Disease Primers, 3(1), 1-20.

Fang, J., Rong, P., Hong, Y., Fan, Y., Liu, J., Wang, H., Zhang, G., Chen, X., Shi, S., Wang, L. and Liu, R., Hwang, J., Li, Z., Tao, J., Wang, Y., Zhu, B., & Kong, J. (2016). Transcutaneous vagus nerve stimulation modulates default mode network in major depressive disorder. Biological psychiatry, 79(4), 266-273.

Farmer, A. D. (2020). Non-inasive vagus nerve stimulation—Hope or hype?. Neurogastroenterology & Motility, 32(4), e13822.

Farmer, A. D., Ruffle, J. K., & Aziz, Q. (2018). Brain Processing of Gastrointestinal Sensory Signaling. In Physiology of the Gastrointestinal Tract (pp. 373-385). Academic Press.

Farr, O. M., Chiang-shan, R. L., & Mantzoros, C. S. (2016). Central nervous system regulation of eating: Insights from human brain imaging. Metabolism, 65(5), 699-713.

Ford, A. C., Mahadeva, S., Carbone, M. F., Lacy, B. E., & Talley, N. J. (2020). Functional dyspepsia. The Lancet.

Fox, M. D., & Raichle, M. E. (2007). Spontaneous fluctuations in brain activity observed with functional magnetic resonance imaging. Nature reviews neuroscience, 8(9), 700-711.

Frangos, E., & Komisaruk, B. R. (2017). Access to vagal projections via cutaneous electrical stimulation of the neck: fMRI evidence in healthy humans. Brain stimulation, 10(1), 19-27.

Friston, K. J., Fletcher, P., Josephs, O., Holmes, A. N. D. R. E. W., Rugg, M. D., & Turner, R. (1998). Event-related fMRI: characterizing differential responses. Neuroimage, 7(1), 30-40.

Furness, J. B., & Stebbing, M. J. (2018). The first brain: Species comparisons and evolutionary implications for the enteric and central nervous systems. Neurogastroenterology & motility, 30(2), e13234.

Furness, J. B., Callaghan, B. P., Rivera, L. R., & Cho, H. J. (2014). The enteric nervous system and gastrointestinal innervation: integrated local and central control. Microbial endocrinology: The microbiota-gut-brain axis in health and disease, 39-71.

Furness, J. B., Di Natale, M., Hunne, B., Oparija-Rogenmozere, L., Ward, S. M., Sasse, K. C., Powley, T. L., Stebbing, M. J., Jaffey, D., & Fothergill, L. J. (2020). The identification of neuronal control pathways supplying effector tissues in the stomach. Cell and Tissue Research, 1-13.

Furness, J. B., Rivera, L. R., Cho, H. J., Bravo, D. M., & Callaghan, B. (2013). The gut as a sensory organ. Nature reviews Gastroenterology & hepatology, 10(12), 729.

Gao, Y. R., Ma, Y., Zhang, Q., Winder, A. T., Liang, Z., Antinori, L., Drew, P. J., & Zhang, N. (2017). Time to wake up: Studying neurovascular coupling and brain-wide circuit function in the un-anesthetized animal. Neuroimage, 153, 382-398.

Garnett, E. S., Nahmias, C., Scheffel, A., Firnau, G., & Upton, A. R. M. (1992). Regional cerebral blood flow in man manipulated by direct vagal stimulation. Pacing and Clinical Electrophysiology, 15(10), 1579-1580.

Gaskell, W. H. (1886). The electrical changes in the quiescent cardiac muscle which accompany stimulation of the vagus nerve. The Journal of physiology, 7(5-6), 451.

Gastroparesisclinic.org. (2014). What is gastroparesis? Retrieved June 29, 2021, from https://www.gastroparesisclinic.org/index.php?pageId=1149&moduleId=195

George, M. S., Sackeim, H. A., Rush, A. J., Marangell, L. B., Nahas, Z., Husain, M. M., Lisanby, S., Burt, T., Goldman, J., & Ballenger, J. C. (2000). Vagus nerve stimulation: a new tool for brain research and therapy∗. Biological psychiatry, 47(4), 287-295.

Gharibans, A. A., Kim, S., Kunkel, D. C., & Coleman, T. P. (2016). High-resolution electrogastrogram: a novel, noninvasive method for determining gastric slow-wave direction and speed. IEEE Transactions on Biomedical Engineering, 64(4), 807-815.

Glover, G. H., Li, T. Q., & Ress, D. (2000). Image-based method for retrospective correction of physiological motion effects in fMRI: RETROICOR. Magnetic Resonance in Medicine: An Official Journal of the International Society for Magnetic Resonance in Medicine, 44(1), 162-167.

Gold, C., Henze, D. A., Koch, C., & Buzsaki, G. (2006). On the origin of the extracellular action potential waveform: a modeling study. Journal of neurophysiology, 95(5), 3113-3128.

Gonzalez-Castillo, J., Saad, Z. S., Handwerker, D. A., Inati, S. J., Brenowitz, N., & Bandettini, P. A. (2012). Whole-brain, time-locked activation with simple tasks revealed using massive averaging and model-free analysis. Proceedings of the National Academy of Sciences, 109(14), 5487-5492.

Gonzalez, H. C., & Velanovich, V. (2010). Enterra® Therapy: gastric neurostimulator for gastroparesis. Expert review of medical devices, 7(3), 319-332.

Gottfried-Blackmore, A., Adler, E. P., Fernandez-Becker, N., Clarke, J., Habtezion, A., & Nguyen, L. (2020). Open-label pilot study: Non-invasive vagal nerve stimulation improves symptoms and gastric emptying in patients with idiopathic gastroparesis. Neurogastroenterology & Motility, 32(4), e13769.

Goyal, R. K., Guo, Y., & Mashimo, H. (2019). Advances in the physiology of gastric emptying. Neurogastroenterology & Motility, 31(4), e13546.

Griffin, M. J., & Newman, M. M. (2004). Visual field effects on motion sickness in cars. Aviation, space, and environmental medicine, 75(9), 739-748.

Groves, D. A., Bowman, E. M., & Brown, V. J. (2005). Recordings from the rat locus coeruleus during acute vagal nerve stimulation in the anaesthetised rat. Neuroscience letters, 379(3), 174-179.

Hachem, L. D., Wong, S. M., & Ibrahim, G. M. (2018). The vagus afferent network: emerging role in translational connectomics. Neurosurgical focus, 45(3), E2.

Han, W., Tellez, L. A., Perkins, M. H., Perez, I. O., Qu, T., Ferreira, J., Ferreira, T. L., Quinn, D., Liu, Z. W., Gao, X. B. and Kaelberer, M. M., Bohórquez, D. V., Shammah-Lagnado, S. J., Lartigue, G., & de Araujo, I. E. (2018). A neural circuit for gut-induced reward. Cell, 175(3), 665-678.

Hansen, M. B. (2003). The enteric nervous system I: organisation and classification. Pharmacology & toxicology, 92(3), 105-113.

Harper, A. A., Kidd, C., & Scratcherd, T. (1959). Vago-vagal reflex effects on gastric and pancreatic secretion and gastro-intestinal motility. The Journal of physiology, 148(2), 417.

Hartono, J. L., Mahadeva, S., & GOH, K. L. (2012). Anxiety and depression in various functional gastrointestinal disorders: do differences exist?. Journal of digestive diseases, 13(5), 252-257.

Hasler, W. L. (2009). Methods of gastric electrical stimulation and pacing: a review of their benefits and mechanisms of action in gastroparesis and obesity. Neurogastroenterology & Motility, 21(3), 229-243.

Hathout, G. M., Gopi, R. K., Bandettini, P., & Gambhir, S. S. (1999). The lag of cerebral hemodynamics with rapidly alternating periodic stimulation: modeling for functional MRI. Magnetic resonance imaging, 17(1), 9-20.

Haug, T. T., Mykletun, A., & Dahl, A. A. (2002). Are anxiety and depression related to gastrointestinal symptoms in the general population?. Scandinavian Journal of Gastroenterology, 37(3), 294-298.

Henry, T. R. (2002). Therapeutic mechanisms of vagus nerve stimulation. Neurology, 59(6 suppl 4), S3-S14.

Henry, T. R., Votaw, J. R., Pennell, P. B., Epstein, C. M., Bakay, R. A. E., Faber, T. L., Grafton, S. T., & Hoffman, J. M. (1999). Acute blood flow changes and efficacy of vagus nerve stimulation in partial epilepsy. Neurology, 52(6), 1166-1166.

Hillman, E. M. (2014). Coupling mechanism and significance of the BOLD signal: a status report. Annual review of neuroscience, 37, 161-181.

Holtmann, G., & Talley, N. J. (2014). The stomach–brain axis. Best Practice & Research Clinical Gastroenterology, 28(6), 967-979.

Horowitz, M., Dent, J., Fraser, R., Sun, W., & Hebbard, G. (1994). Role and integration of mechanisms controlling gastric emptying. Digestive diseases and sciences, 39(12), 7S-13S.

Hulsey, D. R., Riley, J. R., Loerwald, K. W., Rennaker II, R. L., Kilgard, M. P., & Hays, S. A. (2017). Parametric characterization of neural activity in the locus coeruleus in response to vagus nerve stimulation. Experimental neurology, 289, 21-30.

Irimia, A., Chambers, M. C., Torgerson, C. M., & Van Horn, J. D. (2012). Circular representation of human cortical networks for subject and population-level connectomic visualization. Neuroimage, 60(2), 1340-1351.

Jänig, W. (2008). Integrative action of the autonomic nervous system: Neurobiology of homeostasis. Cambridge University Press.

Janz, C., Heinrich, S. P., Kornmayer, J., Bach, M., & Hennig, J. (2001). Coupling of neural activity and BOLD fMRI response: new insights by combination of fMRI and VEP experiments in transition from single events to continuous stimulation. Magnetic Resonance in Medicine: An Official Journal of the International Society for Magnetic Resonance in Medicine, 46(3), 482-486.

Jenkinson, M., Beckmann, C. F., Behrens, T. E., & Woolrich, M. W. (2012). Smith SM. FSL neuroimage, 62, 782-90.

Johnson, A. C., Myers, B., Lazovic, J., Towner, R., & Greenwood-Van Meerveld, B. (2010). Brain activation in response to visceral stimulation in rats with amygdala implants of corticosterone: an FMRI study. PloS one, 5(1), e8573.

Jung, H. K., Locke III, G. R., Schleck, C. D., Zinsmeister, A. R., Szarka, L. A., Mullan, B., & Talley, N. J. (2009). The incidence, prevalence, and outcomes of patients with gastroparesis in Olmsted County, Minnesota, from 1996 to 2006. Gastroenterology, 136(4), 1225-1233.

Kani, H. T., Dural, U., Sakalli Kani, A., Yanartas, O., Kiziltas, S., Yilmaz Enc, F., Atug, O., Deyneli, O., Kuscu, K., & Imeryuz, N. (2019). Evaluation of depression, anxiety, alexithymia, attachment, social support and somatization in functional dyspepsia. Psychiatry and Clinical Psychopharmacology, 29(1), 45-51.

Kapreli, E., Athanasopoulos, S., Papathanasiou, M., Van Hecke, P., Strimpakos, N., Gouliamos, A., Peeters, R., & Sunaert, S. (2006). Lateralization of brain activity during lower limb joints movement. An fMRI study. Neuroimage, 32(4), 1709-1721.

Kelly, K. A., & La Force, R. C. (1972). Pacing the canine stomach with electric stimulation. American Journal of Physiology-Legacy Content, 222(3), 588-594.

Kennedy, R. S., Drexler, J., & Kennedy, R. C. (2010). Research in visually induced motion sickness. Applied ergonomics, 41(4), 494-503.

Klarer, M., Arnold, M., Günther, L., Winter, C., Langhans, W., & Meyer, U. (2014). Gut vagal afferents differentially modulate innate anxiety and learned fear. Journal of Neuroscience, 34(21), 7067-7076.

Klarer, M., Krieger, J. P., Richetto, J., Weber-Stadlbauer, U., Günther, L., Winter, C., Arnold, M., Langhans, W., & Meyer, U. (2018). Abdominal vagal afferents modulate the brain transcriptome and behaviors relevant to schizophrenia. Journal of Neuroscience, 38(7), 1634-1647.

Ko, D., Heck, C., Grafton, S., Apuzzo, M. L., Couldwell, W. T., Chen, T., Day, J. D., Zelman, V., Smith, T., & DeGiorgio, C. M. (1996). Vagus nerve stimulation activates central nervous system structures in epileptic patients during PET H215O blood flow imaging. Neurosurgery, 39(2), 426-431.

Koch, K. L. (2014). Gastric dysrhythmias: a potential objective measure of nausea. Experimental brain research, 232(8), 2553-2561.

Krahl, S. E., Clark, K. B., Smith, D. C., & Browning, R. A. (1998). Locus coeruleus lesions suppress the seizure-attenuating effects of vagus nerve stimulation. Epilepsia, 39(7), 709-714.

Kraus, T., Hösl, K., Kiess, O., Schanze, A., Kornhuber, J., & Forster, C. B. O. L. D. (2007). BOLD fMRI deactivation of limbic and temporal brain structures and mood enhancing effect by transcutaneous vagus nerve stimulation. Journal of neural transmission, 114(11), 1485-1493.

Kraus, T., Kiess, O., Hösl, K., Terekhin, P., Kornhuber, J., & Forster, C. (2013). CNS BOLD fMRI effects of sham-controlled transcutaneous electrical nerve stimulation in the left outer auditory canal–a pilot study. Brain stimulation, 6(5), 798-804.

Krygowska-Wajs, A., Furgala, A., Gorecka-Mazur, A., Pietraszko, W., Thor, P., Potasz-Kulikowska, K., & Moskala, M. (2016). The effect of subthalamic deep brain stimulation on gastric motility in Parkinson's disease. Parkinsonism & related disorders, 26, 35-40.

Krygowska-Wajs, A., Lorens, K., Thor, P., Szczudlik, A., & Konturek, S. (2000). Gastric electromechanical dysfunction in Parkinson's disease. Functional neurology, 15(1), 41-46.

Kundu, P., Brenowitz, N. D., Voon, V., Worbe, Y., Vértes, P. E., Inati, S. J., Saad, Z. S., Bandettini, P. A., & Bullmore, E. T. (2013). Integrated strategy for improving functional connectivity mapping using multiecho fMRI. Proceedings of the National Academy of Sciences, 110(40), 16187-16192.

Kundu, P., Inati, S. J., Evans, J. W., Luh, W. M., & Bandettini, P. A. (2012). Differentiating BOLD and non-BOLD signals in fMRI time series using multi-echo EPI. Neuroimage, 60(3), 1759-1770.

Kundu, P., Santin, M. D., Bandettini, P. A., Bullmore, E. T., & Petiet, A. (2014). Differentiating BOLD and non-BOLD signals in fMRI time series from anesthetized rats using multi-echo EPI at 11.7 T. Neuroimage, 102, 861-874.

Kwiatek, M. A., Steingoetter, A., Pal, A., Menne, D., Brasseur, J. G., Hebbard, G. S., Boesiger, P., Thumshirn, M., Fried, M., & Schwizer, W. (2006). Quantification of distal antral contractile motility in healthy human stomach with magnetic resonance imaging. Journal of Magnetic

Resonance Imaging: An Official Journal of the International Society for Magnetic Resonance in Medicine, 24(5), 1101-1109.

Kwong, K. K., Belliveau, J. W., Chesler, D. A., Goldberg, I. E., Weisskoff, R. M., Poncelet, B. P., Kennedy, D. N., Hoppel, B. E., Cohen, M. S., & Turner, R. (1992). Dynamic magnetic resonance imaging of human brain activity during primary sensory stimulation. Proceedings of the National Academy of Sciences, 89(12), 5675-5679.

Lacy, B. E., & Weiser, K. (2005). Gastric motility, gastroparesis, and gastric stimulation. The Surgical clinics of North America, 85(5), 967-87.

Lacy, B. E., Weiser, K. T., Kennedy, A. T., Crowell, M. D., & Talley, N. J. (2013). Functional dyspepsia: the economic impact to patients. Alimentary pharmacology & therapeutics, 38(2), 170-177.

Ladabaum, U. R. I., Minoshima, S., Hasler, W. L., Cross, D., Chey, W. D., & Owyang, C. (2001). Gastric distention correlates with activation of multiple cortical and subcortical regions. Gastroenterology, 120(2), 369-376.

Lal, N., Livemore, S., Dunne, D., & Khan, I. (2015). Gastric electrical stimulation with the enterra system: a systematic review. Gastroenterology research and practice, 2015.

Larsen, L. E., Wadman, W. J., Marinazzo, D., van Mierlo, P., Delbeke, J., Daelemans, S., Sprengers, M., Thyrion, L., Van Lysebettens, W., Carrette, E., & Raedt, R. (2016). Vagus nerve stimulation applied with a rapid cycle has more profound influence on hippocampal electrophysiology than a standard cycle. Neurotherapeutics, 13(3), 592-602.

Lee, H. L., Zahneisen, B., Hugger, T., LeVan, P., & Hennig, J. (2013). Tracking dynamic resting-state networks at higher frequencies using MR-encephalography. Neuroimage, 65, 216-222.

Lee, I. S., Wang, H., Chae, Y., Preissl, H., & Enck, P. (2016). Functional neuroimaging studies in functional dyspepsia patients: a systematic review. Neurogastroenterology & Motility, 28(6), 793-805.

Lee, J. H., Durand, R., Gradinaru, V., Zhang, F., Goshen, I., Kim, D. S., Fenno, L.E., Ramakrishnan, C., & Deisseroth, K. (2010). Global and local fMRI signals driven by neurons defined optogenetically by type and wiring. Nature, 465(7299), 788-792.

LeVan, P., Akin, B., & Hennig, J. (2018). Fast imaging for mapping dynamic networks. NeuroImage, 180, 547-558.

Levinthal, D. J., & Bielefeldt, K. (2017). Systematic review and meta-analysis: Gastric electrical stimulation for gastroparesis. Autonomic Neuroscience, 202, 45-55.

Levinthal, D. J., & Strick, P. L. (2020). Multiple areas of the cerebral cortex influence the stomach. Proceedings of the National Academy of Sciences, 117(23), 13078-13083.

Levy, R. L., Olden, K. W., Naliboff, B. D., Bradley, L. A., Francisconi, C., Drossman, D. A., & Creed, F. (2006). Psychosocial aspects of the functional gastrointestinal disorders. Gastroenterology, 130(5), 1447-1458.

Lewicki, M. S. (1998). A review of methods for spike sorting: the detection and classification of neural action potentials. Network: Computation in Neural Systems, 9(4), R53-R78.

Lewis, L. D., Setsompop, K., Rosen, B. R., & Polimeni, J. R. (2016). Fast fMRI can detect oscillatory neural activity in humans. Proceedings of the national academy of sciences, 113(43), E6679-E6685.

Lewis, L. D., Setsompop, K., Rosen, B. R., & Polimeni, J. R. (2018). Stimulus-dependent hemodynamic response timing across the human subcortical-cortical visual pathway identified through high spatiotemporal resolution 7T fMRI. Neuroimage, 181, 279-291.

Li, B., & Freeman, R. D. (2010). Neurometabolic coupling in the lateral geniculate nucleus changes with extended age. Journal of neurophysiology, 104(1), 414-425.

Li, S., & Chen, J. D. (2010). Cellular effects of gastric electrical stimulation on antral smooth muscle cells in rats. American Journal of Physiology-Regulatory, Integrative and Comparative Physiology, 298(6), R1580-R1587.

Liang, Z., Liu, X., & Zhang, N. (2015). Dynamic resting state functional connectivity in awake and anesthetized rodents. Neuroimage, 104, 89-99.

Lin, Z., Sarosiek, I., Forster, J., & McCallum, R. W. (2006). Symptom responses, long-term outcomes and adverse events beyond 3 years of high-frequency gastric electrical stimulation for gastroparesis. Neurogastroenterology & Motility, 18(1), 18-27.

Liu, J., Qiao, X., & Chen, J. Z. (2004). Vagal afferent is involved in short-pulse gastric electrical stimulation in rats. Digestive diseases and sciences, 49(5), 729-737.

Liu, W. C., Mosier, K., Kalnin, A., & Marks, D. (2001). Vagus Nerve Stimulation in patients: a BOLD fMRI study. NeuroImage, 6(13), 810.

Liu, Z., Rios, C., Zhang, N., Yang, L., Chen, W., & He, B. (2010). Linear and nonlinear relationships between visual stimuli, EEG and BOLD fMRI signals. Neuroimage, 50(3), 1054-1066.

Logothetis, N. K., & Wandell, B. A. (2004). Interpreting the BOLD signal. Annu. Rev. Physiol., 66, 735-769.

Lomarev, M., Denslow, S., Nahas, Z., Chae, J. H., George, M. S., & Bohning, D. E. (2002). Vagus nerve stimulation (VNS) synchronized BOLD fMRI suggests that VNS in depressed adults has frequency/dose dependent effects. Journal of psychiatric research, 36(4), 219-227.

Lu, K. H., Cao, J., Oleson, S. T., Powley, T. L., & Liu, Z. (2017). Contrast-enhanced magnetic resonance imaging of gastric emptying and motility in rats. IEEE Transactions on Biomedical Engineering, 64(11), 2546-2554.

Ma, Y., Shaik, M. A., Kozberg, M. G., Kim, S. H., Portes, J. P., Timerman, D., & Hillman, E. M. (2016). Resting-state hemodynamics are spatiotemporally coupled to synchronized and symmetric neural activity in excitatory neurons. Proceedings of the National Academy of Sciences, 113(52), E8463-E8471.

Ma, Z., Perez, P., Ma, Z., Liu, Y., Hamilton, C., Liang, Z., & Zhang, N. (2018). Functional atlas of the awake rat brain: A neuroimaging study of rat brain specialization and integration. Neuroimage, 170, 95-112.

Magnuson, M. E., Thompson, G. J., Pan, W. J., & Keilholz, S. D. (2014). Time-dependent effects of isoflurane and dexmedetomidine on functional connectivity, spectral characteristics, and spatial distribution of spontaneous BOLD fluctuations. NMR in biomedicine, 27(3), 291-303.

Malone, J. C., & Thavamani, A. (2020). Physiology, Gastrocolic Reflex. StatPearls [Internet].

Malow, B. A., Edwards, J., Marzec, M., Sagher, O., & Fromes, G. (2000). Effects of vagus nerve stimulation on respiration during sleep: a pilot study. Neurology, 55(10), 1450-1454.

Manta, S., Dong, J., Debonnel, G., & Blier, P. (2009). Enhancement of the function of rat serotonin and norepinephrine neurons by sustained vagus nerve stimulation. Journal of psychiatry & neuroscience: JPN, 34(4), 272.

Martindale, J., Mayhew, J., Berwick, J., Jones, M., Martin, C., Johnston, D., Redgrave, P., & Zheng, Y. (2003). The hemodynamic impulse response to a single neural event. Journal of Cerebral Blood Flow & Metabolism, 23(5), 546-555.

Mayer, E. A. (2000). The neurobiology of stress and gastrointestinal disease. Gut, 47(6), 861-869.

Mayer, E. A. (2011). Gut feelings: the emerging biology of gut–brain communication. Nature Reviews Neuroscience, 12(8), 453-466.

Mayer, E. A., Aziz, Q., Coen, S., Kern, M., Labus, J. S., Lane, R., Kuo, B., Naliboff, B., & Tracey, I. (2009). Brain imaging approaches to the study of functional GI disorders: a Rome working team report. Neurogastroenterology & Motility, 21(6), 579-596.

Mayer, E. A., Craske, M., & Naliboff, B. D. (2001). Depression, anxiety, and the gastrointestinal system. Journal of Clinical Psychiatry, 62, 28-37.

Mayer, E. A., Labus, J., Aziz, Q., Tracey, I., Kilpatrick, L., Elsenbruch, S., Schweinhardt, P., Van Oudenhove, L., & Borsook, D. (2019). Role of brain imaging in disorders of brain–gut interaction: a Rome Working Team Report. Gut, 68(9), 1701-1715.

Mayer, E. A., Tillisch, K., & Bradesi, S. (2006). modulation of the brain–gut axis as a therapeutic approach in gastrointestinal disease. Alimentary pharmacology & therapeutics, 24(6), 919-933.

McCallum, R. W., Sarosiek, I., Parkman, H. P., Snape, W., Brody, F., Wo, J., & Nowak, T. (2013). Gastric electrical stimulation with Enterra therapy improves symptoms of idiopathic gastroparesis. Neurogastroenterology & Motility, 25(10), 815-e636.

McCallum, R. W., Snape, W., Brody, F., Wo, J., Parkman, H. P., & Nowak, T. (2010). Gastric electrical stimulation with Enterra therapy improves symptoms from diabetic gastroparesis in a prospective study. Clinical Gastroenterology and Hepatology, 8(11), 947-954.

Mesulam, M. M., Mufson, E. J., Wainer, B. H., & Levey, A. I. (1983). Central cholinergic pathways in the rat: an overview based on an alternative nomenclature (Ch1–Ch6). Neuroscience, 10(4), 1185-1201.

Min, D. K., Tuor, U. I., & Chelikani, P. K. (2011). Gastric distention induced functional magnetic resonance signal changes in the rodent brain. Neuroscience, 179, 151-158.

Min, D. K., Tuor, U. I., Koopmans, H. S., & Chelikani, P. K. (2011). Changes in differential functional magnetic resonance signals in the rodent brain elicited by mixed-nutrient or protein-enriched meals. Gastroenterology, 141(5), 1832-1841.

Murray, B. J., Matheson, J. K., & Scammell, T. E. (2001). Effects of vagus nerve stimulation on respiration during sleep. Neurology, 57(8), 1523-1524.

Naftali, T., Gadoth, N., Huberman, M., & Novis, B. (2005). Electrogastrography in patients with Parkinson's disease. Canadian journal of neurological sciences, 32(1), 82-86.

Nahas, Z., Teneback, C., Chae, J. H., Mu, Q., Molnar, C., Kozel, F. A., Walker, J., Anderson, B., Koola, J., Kose, S., & George, M. S. (2007). Serial vagus nerve stimulation functional MRI in treatment-resistant depression. Neuropsychopharmacology, 32(8), 1649-1660.

Naliboff, B. D., Berman, S., Suyenobu, B., Labus, J. S., Chang, L., Stains, J., Mandelkern, M. A., & Mayer, E. A. (2006). Longitudinal change in perceptual and brain activation response to visceral stimuli in irritable bowel syndrome patients. Gastroenterology, 131(2), 352-365.

Nemeroff, C. B., Mayberg, H. S., Krahl, S. E., McNamara, J., Frazer, A., Henry, T. R., George, M. S., Charney, D. S., & Brannan, S. K. (2006). VNS therapy in treatment-resistant depression: clinical evidence and putative neurobiological mechanisms. Neuropsychopharmacology, 31(7), 1345-1355.

Nichols, J. A., Nichols, A. R., Smirnakis, S. M., Engineer, N. D., Kilgard, M. P., & Atzori, M. (2011). Vagus nerve stimulation modulates cortical synchrony and excitability through the activation of muscarinic receptors. Neuroscience, 189, 207-214.

Nieh, E. H., Matthews, G. A., Allsop, S. A., Presbrey, K. N., Leppla, C. A., Wichmann, R., Neve, R., Wildes, C. P., & Tye, K. M. (2015). Decoding neural circuits that control compulsive sucrose seeking. Cell, 160(3), 528-541.

O'Grady, G., Du, P., Cheng, L. K., Egbuji, J. U., Lammers, W. J., Windsor, J. A., & Pullan, A. J. (2010). Origin and propagation of human gastric slow-wave activity defined by high-resolution mapping. American Journal of Physiology-Gastrointestinal and Liver Physiology, 299(3), G585-G592.

Obata, T., Liu, T. T., Miller, K. L., Luh, W. M., Wong, E. C., Frank, L. R., & Buxton, R. B. (2004). Discrepancies between BOLD and flow dynamics in primary and supplementary motor areas: application of the balloon model to the interpretation of BOLD transients. NeuroImage, 21(1), 144-153.

Ogawa, S., Lee, T. M., Kay, A. R., & Tank, D. W. (1990a). Brain magnetic resonance imaging with contrast dependent on blood oxygenation. proceedings of the National Academy of Sciences, 87(24), 9868-9872.

Ogawa, S., Lee, T. M., Nayak, A. S., & Glynn, P. (1990b). Oxygenation-sensitive contrast in magnetic resonance image of rodent brain at high magnetic fields. Magnetic resonance in medicine, 14(1), 68-78.

Ogawa, S., Menon, R. S., Kim, S. G., & Ugurbil, K. (1998). On the characteristics of functional magnetic resonance imaging of the brain. Annual review of biophysics and biomolecular structure, 27(1), 447-474.

Ogawa, S., Tank, D. W., Menon, R., Ellermann, J. M., Kim, S. G., Merkle, H., & Ugurbil, K. (1992). Intrinsic signal changes accompanying sensory stimulation: functional brain mapping with magnetic resonance imaging. Proceedings of the National Academy of Sciences, 89(13), 5951-5955.

Papp, E. A., Leergaard, T. B., Calabrese, E., Johnson, G. A., & Bjaalie, J. G. (2014). Waxholm Space atlas of the Sprague Dawley rat brain. Neuroimage, 97, 374-386.

Pardo, J. V., Sheikh, S. A., Kuskowski, M. A., Surerus-Johnson, C., Hagen, M. C., Lee, J. T., Rittberg, B. R., & Adson, D. E. (2007). Weight loss during chronic, cervical vagus nerve stimulation in depressed patients with obesity: an observation. International journal of obesity, 31(11), 1756-1759.

Parkinson, J. A., Willoughby, P. J., Robbins, T. W., & Everitt, B. J. (2000). Disconnection of the anterior cingulate cortex and nucleus accumbens core impairs Pavlovian approach behavior: Further evidence for limbic cortical–ventral striatopallidal systems. Behavioral neuroscience, 114(1), 42.

Parkman, H. P., Hasler, W. L., Barnett, J. L., & Eaker, E. Y. (2003). Electrogastrography: a document prepared by the gastric section of the American Motility Society Clinical GI Motility Testing Task Force. Neurogastroenterology & Motility, 15(2), 89-102.

Patterson, L. M., Zheng, H., & Berthoud, H. R. (2002). Vagal afferents innervating the gastrointestinal tract and CCKA-receptor immunoreactivity. The Anatomical Record: An Official Publication of the American Association of Anatomists, 266(1), 10-20.

Paulon, E., Nastou, D., Jaboli, F., Marin, J., Liebler, E., & Epstein, O. (2017). Proof of concept: short-term non-invasive cervical vagus nerve stimulation in patients with drug-refractory gastroparesis. Frontline gastroenterology, 8(4), 325-330.

Pawela, C. P., Biswal, B. B., Hudetz, A. G., Schulte, M. L., Li, R., Jones, S. R., Cho, Y. R., Matloub, H. S., & Hyde, J. S. (2009). A protocol for use of medetomidine anesthesia in rats for extended studies using task-induced BOLD contrast and resting-state functional connectivity. Neuroimage, 46(4), 1137-1147.

Paxinos, G. (Ed.). (2014). The rat nervous system. Academic press.

Paxinos, G., & Watson, C. (2006). The rat brain in stereotaxic coordinates: hard cover edition. Elsevier.

Payne, S. C., Furness, J. B., & Stebbing, M. J. (2019). Bioelectric neuromodulation for gastrointestinal disorders: effectiveness and mechanisms. Nature reviews Gastroenterology & hepatology, 16(2), 89-105.

Peltier, S. J., & Noll, D. C. (2002). T2* dependence of low frequency functional connectivity. Neuroimage, 16(4), 985-992.

Peña, D. F., Engineer, N. D., & McIntyre, C. K. (2013). Rapid remission of conditioned fear expression with extinction training paired with vagus nerve stimulation. Biological psychiatry, 73(11), 1071-1077.

Pfeuffer, J., McCullough, J. C., Van de Moortele, P. F., Ugurbil, K., & Hu, X. (2003). Spatial dependence of the nonlinear BOLD response at short stimulus duration. Neuroimage, 18(4), 990-1000.

Piessevaux, H., Tack, J., Wilmer, A., Coulie, B., Geubel, A., & Janssens, J. (2001). Perception of changes in wall tension of the proximal stomach in humans. Gut, 49(2), 203-208.

Powley, T. L. (2013). Central control of autonomic functions: organization of the autonomic nervous system. In Fundamental neuroscience (pp. 729-747). Academic Press.

Powley, T. L., & Phillips, R. J. (2002). I. Morphology and topography of vagal afferents innervating the GI tract. American Journal of Physiology-Gastrointestinal and Liver Physiology, 283(6), G1217-G1225.

Powley, T. L., & Phillips, R. J. (2011). Vagal intramuscular array afferents form complexes with interstitial cells of Cajal in gastrointestinal smooth muscle: analogues of muscle spindle organs?. Neuroscience, 186, 188-200.

Powley, T. L., Hudson, C. N., McAdams, J. L., Baronowsky, E. A., & Phillips, R. J. (2016). Vagal intramuscular arrays: the specialized mechanoreceptor arbors that innervate the smooth muscle layers of the stomach examined in the rat. Journal of Comparative Neurology, 524(4), 713-737.

Powley, T. L., Hudson, C. N., McAdams, J. L., Baronowsky, E. A., Martin, F. N., Mason, J. K., & Phillips, R. J. (2014). Organization of vagal afferents in pylorus: mechanoreceptors arrayed for high sensitivity and fine spatial resolution?. Autonomic Neuroscience, 183, 36-48.

Powley, T. L., Jaffey, D. M., McAdams, J., Baronowsky, E. A., Black, D., Chesney, L., ... & Phillips, R. J. (2019). Vagal innervation of the stomach reassessed: brain− gut connectome uses smart terminals. Annals of the New York Academy of Sciences, 1454(1), 14.

Powley, T. L., Spaulding, R. A., & Haglof, S. A. (2011). Vagal afferent innervation of the proximal gastrointestinal tract mucosa: chemoreceptor and mechanoreceptor architecture. Journal of Comparative Neurology, 519(4), 644-660.

Psichas, A., Reimann, F., & Gribble, F. M. (2015). Gut chemosensing mechanisms. The Journal of clinical investigation, 125(3), 908-917.

Qin, C., Chen, J. D., Zhang, J., & Foreman, R. D. (2007). Modulatory effects and afferent pathways of gastric electrical stimulation on rat thoracic spinal neurons receiving input from the stomach. Neuroscience research, 57(1), 29-39.

Qin, C., Sun, Y., Chen, J. D. Z., & Foreman, R. D. (2005). Gastric electrical stimulation modulates neuronal activity in nucleus tractus solitarii in rats. Autonomic Neuroscience, 119(1), 1-8.

Rebollo, I., Devauchelle, A. D., Béranger, B., & Tallon-Baudry, C. (2018). Stomach-brain synchrony reveals a novel, delayed-connectivity resting-state network in humans. Elife, 7, e33321.

Renvall, V., & Hari, R. (2009). Transients may occur in functional magnetic resonance imaging without physiological basis. Proceedings of the National Academy of Sciences, 106(48), 20510-20514.

Ressler, K. J., & Mayberg, H. S. (2007). Targeting abnormal neural circuits in mood and anxiety disorders: from the laboratory to the clinic. Nature neuroscience, 10(9), 1116-1124.

Reyt, S., Picq, C., Sinniger, V., Clarençon, D., Bonaz, B., & David, O. (2010). Dynamic Causal Modelling and physiological confounds: a functional MRI study of vagus nerve stimulation. Neuroimage, 52(4), 1456-1464.

Richter, C. G., Babo-Rebelo, M., Schwartz, D., & Tallon-Baudry, C. (2017). Phase-amplitude coupling at the organism level: The amplitude of spontaneous alpha rhythm fluctuations varies with the phase of the infra-slow gastric basal rhythm. NeuroImage, 146, 951-958.

Robinson, C., & Draper, G. (1912). STUDIES WITH THE ELECTROCARDIOGRAPH ON THE ACTION OF THE VAGUS NERVE ON THE HUMAN HEART: II. The Effects of Vagus Stimulation on the Hearts of Children with Chronic Valvular Disease. The Journal of experimental medicine, 15(1), 14-48.

Rogers, R. C., Hermann, G. E., & Travagli, R. A. (1999). Brainstem pathways responsible for oesophageal control of gastric motility and tone in the rat. The Journal of Physiology, 514(2), 369-383.

Rogers, R. C., McTIGUE, D. M., & Hermann, G. E. (1995). Vagovagal reflex control of digestion: afferent modulation by neural and" endoneurocrine" factors. American Journal of Physiology-Gastrointestinal and Liver Physiology, 268(1), G1-G10.

Ruffoli, R., Giorgi, F. S., Pizzanelli, C., Murri, L., Paparelli, A., & Fornai, F. (2011). The chemical neuroanatomy of vagus nerve stimulation. Journal of chemical neuroanatomy, 42(4), 288-296.

Sackeim, H. A., Rush, A. J., George, M. S., Marangell, L. B., Husain, M. M., Nahas, Z., Johnson, C.R., Seidman, S., Giller, C., Haines, S., & Goodman, R. R. (2001). Vagus nerve stimulation (VNS™) for treatment-resistant depression: efficacy, side effects, and predictors of outcome. Neuropsychopharmacology, 25(5), 713-728.

Sanders, K. M., Koh, S. D., & Ward, S. M. (2006). Interstitial cells of Cajal as pacemakers in the gastrointestinal tract. Annu. Rev. Physiol., 68, 307-343.

Schapiro, H., & Woodward, E. R. (1959). Pathway of enterogastric reflex. Proceedings of the Society for Experimental Biology and Medicine, 101(3), 407-409.

Schemann, M., & Grundy, D. (1992). Electrophysiological identification of vagally innervated enteric neurons in guinea pig stomach. American Journal of Physiology-Gastrointestinal and Liver Physiology, 263(5), G709-G718.

Schulze-Delrieu, K. (1983). Volume accommodation by distension of gastric fundus (rabbit) and gastric corpus (cat). Digestive diseases and sciences, 28(7), 625-632.

Schwarz, L. A., & Luo, L. (2015). Organization of the locus coeruleus-norepinephrine system. Current Biology, 25(21), R1051-R1056.

Sierakowiak, A., Monnot, C., Aski, S. N., Uppman, M., Li, T. Q., Damberg, P., & Brené, S. (2015). Default mode network, motor network, dorsal and ventral basal ganglia networks in the rat brain: comparison to human networks using resting state-fMRI. PloS one, 10(3), e0120345.

Smout, A. J. P. M., Van der Schee, E. J., & Grashuis, J. L. (1980). What is measured in electrogastrography?. Digestive diseases and sciences, 25(3), 179-187.

Spencer, N. J., Kyloh, M., Beckett, E. A., Brookes, S., & Hibberd, T. (2016). Different types of spinal afferent nerve endings in stomach and esophagus identified by anterograde tracing from dorsal root ganglia. Journal of Comparative Neurology, 524(15), 3064-3083.

Sperber, A. D., Bangdiwala, S. I., Drossman, D. A., Ghoshal, U. C., Simren, M., Tack, J., ... & Palsson, O. S. (2021). Worldwide prevalence and burden of functional gastrointestinal disorders, results of Rome Foundation global study. Gastroenterology, 160(1), 99-114.

Stanghellini, V., Chan, F. K., Hasler, W. L., Malagelada, J. R., Suzuki, H., Tack, J., & Talley, N. J. (2016). Gastroduodenal disorders. Gastroenterology, 150(6), 1380-1392.

Strigo, I. A., Duncan, G. H., Boivin, M., & Bushnell, M. C. (2003). Differentiation of visceral and cutaneous pain in the human brain. Journal of neurophysiology, 89(6), 3294-3303.

Suarez, A. N., Hsu, T. M., Liu, C. M., Noble, E. E., Cortella, A. M., Nakamoto, E. M., Hahn, J. D., de Lartigue, G., & Kanoski, S. E. (2018). Gut vagal sensory signaling regulates hippocampus function through multi-order pathways. Nature communications, 9(1), 1-15.

Sucholeiki, R., Alsaadi, T. M., Morris Iii, G. L., Ulmer, J. L., Biswal, B., & Mueller, W. M. (2002). fMRI in patients implanted with a vagal nerve stimulator. Seizure, 11(3), 157-162.

Tack, J., Bisschops, R. A. F., & Sarnelli, G. (2004). Pathophysiology and treatment of functional dyspepsia. Gastroenterology, 127(4), 1239-1255.

Tack, J., Demedts, I., Meulemans, A., Schuurkes, J., & Janssens, J. (2002). Role of nitric oxide in the gastric accommodation reflex and in meal induced satiety in humans. Gut, 51(2), 219-224.

Tack, J., Piessevaux, H., Coulie, B., Caenepeel, P., & Janssens, J. (1998). Role of impaired gastric accommodation to a meal in functional dyspepsia. Gastroenterology, 115(6), 1346-1352.

Takahashi, T., & Owyang, C. (1997). Characterization of vagal pathways mediating gastric accommodation reflex in rats. The Journal of physiology, 504(2), 479-488.

Talley, N. J., & Ford, A. C. (2015). Functional dyspepsia. New England Journal of Medicine, 373(19), 1853-1863.

Tang, M., Zhang, J., & Chen, J. D. Z. (2006). Central mechanisms of gastric electrical stimulation involving neurons in the paraventricular nucleus of the hypothalamus in rats. Obesity surgery, 16(3), 344-352.

Thor, P. J., Gościński, I., Kolasińska-Kloch, W., Mądroszkiewicz, D., Mądroszkiewicz, E., & Furgała, A. (2003). Gastric myoelectric activity in patients with closed head brain injury. Medical Science Monitor, 9(9), CR392-CR395.

Tian, P., Teng, I. C., May, L. D., Kurz, R., Lu, K., Scadeng, M., Hillman, E. M. C., De Crespigny, A J., D'Arceuil, H. E., Mandeville, J. B., Marota, J. J. A., Rosen, B. R., Liu, T. T., Boas, D. A., Buxton, R. B., Dale, A. M., & Devor, A. (2010). Cortical depth-specific microvascular dilation underlies laminar differences in blood oxygenation level-dependent functional MRI signal. Proceedings of the National Academy of Sciences, 107(34), 15246-15251.

Tillisch, K., Labus, J. S., & Naliboff, B. D. (2018). Neuroimaging of brain-gut interactions in functional gastrointestinal disorders. In Physiology of the Gastrointestinal Tract (pp. 419-428). Academic Press.

Tomasi, D., & Volkow, N. D. (2012). Laterality patterns of brain functional connectivity: gender effects. Cerebral Cortex, 22(6), 1455-1462.

Tomita, T. (1966). Electrical responses of smooth muscle to external stimulation in hypertonic solution. The Journal of physiology, 183(2), 450-468.

Travagli, R. A., & Anselmi, L. (2016). Vagal neurocircuitry and its influence on gastric motility. Nature Reviews Gastroenterology & Hepatology, 13(7), 389.

Travagli, R. A., Hermann, G. E., Browning, K. N., & Rogers, R. C. (2003). Musings on the Wanderer: What's New in our Understanding of Vago-Vagal Reflexes?: III. Activity-dependent plasticity in vago-vagal reflexes controlling the stomach. American journal of physiology. Gastrointestinal and liver physiology, 284(2), G180.

Travagli, R. A., Hermann, G. E., Browning, K. N., & Rogers, R. C. (2006). Brainstem circuits regulating gastric function. Annu. Rev. Physiol., 68, 279-305.

Tucker, D. M. (1981). Lateral brain function, emotion, and conceptualization. Psychological bulletin, 89(1), 19.

U.S. Food and Drug Administration, Center for Devices and Radiological Health. Gastric Electrical Stimulation (GES) System H990014 approval letter, March 31, 2000. Retrieved March 29, 2021, from https://www.accessdata.fda.gov/cdrh_docs/pdf/H990014A.pdf.

Underwood, E. (2021). A sense of self.

Valdes Hernandez, P. A., Sumiyoshi, A., Nonaka, H., Haga, R., Aubert Vasquez, E., Ogawa, T., Iturria-Medina, Y., Riera, J. J., & Kawashima, R. (2011). An in vivo MRI template set for morphometry, tissue segmentation, and fMRI localization in rats. Frontiers in neuroinformatics, 5, 26.

Van Bockstaele, E. J., Peoples, J., & Valentino, R. J. (1999). Anatomic basis for differential regulation of the rostrolateral peri–locus coeruleus region by limbic afferents. Biological psychiatry, 46(10), 1352-1363.

Van Den Heuvel, M. P., & Pol, H. E. H. (2010). Exploring the brain network: a review on resting-state fMRI functional connectivity. European neuropsychopharmacology, 20(8), 519-534.

Van Oudenhove, L., Demyttenaere, K., Tack, J., & Aziz, Q. (2004). Central nervous system involvement in functional gastrointestinal disorders. Best Practice & Research Clinical Gastroenterology, 18(4), 663-680.

Viswanathan, A., & Freeman, R. D. (2007). Neurometabolic coupling in cerebral cortex reflects synaptic more than spiking activity. Nature neuroscience, 10(10), 1308-1312.

Vogt, B. A., Finch, D. M., & Olson, C. R. (1992). Functional heterogeneity in cingulate cortex: the anterior executive and posterior evaluative regions. Cerebral cortex, 2(6), 435-443.

Wang, G. J., Tomasi, D., Backus, W., Wang, R., Telang, F., Geliebter, A., Korner, J., Baumanac, A., Fowler, J. S., Panayotis, K. T., & Volkow, N. D. (2008). Gastric distention activates satiety circuitry in the human brain. Neuroimage, 39(4), 1824-1831.

Wang, Z., Bradesi, S., Maarek, J. M. I., Lee, K., Winchester, W. J., Mayer, E. A., & Holschneider, D. P. (2008). Regional brain activation in conscious, nonrestrained rats in response to noxious visceral stimulation. Pain, 138(1), 233-243.

Weber, B., Burger, C., Wyss, M. T., Von Schulthess, G. K., Scheffold, F., & Buck, A. (2004). Optical imaging of the spatiotemporal dynamics of cerebral blood flow and oxidative metabolism in the rat barrel cortex. European Journal of Neuroscience, 20(10), 2664-2670.

Weinkauf, J. G., Yiannopoulos, A., & Faul, J. L. (2005). Transcutaneous electrical nerve stimulation for severe gastroparesis after lung transplantation. The Journal of Heart and Lung Transplantation, 24(9), 1444-e1.

Williams, K. A., Magnuson, M., Majeed, W., LaConte, S. M., Peltier, S. J., Hu, X., & Keilholz, S. D. (2010). Comparison of α-chloralose, medetomidine and isoflurane anesthesia for functional connectivity mapping in the rat. Magnetic resonance imaging, 28(7), 995-1003.

Wolpert, N., Rebollo, I., & Tallon-Baudry, C. (2020). Electrogastrography for psychophysiological research: Practical considerations, analysis pipeline, and normative data in a large sample. Psychophysiology, 57(9), e13599.

Woodhouse, S., Hebbard, G., & Knowles, S. R. (2017). Psychological controversies in gastroparesis: A systematic review. World journal of gastroenterology, 23(7), 1298.

Yeşilyurt, B., Uğurbil, K., & Uludağ, K. (2008). Dynamics and nonlinearities of the BOLD response at very short stimulus durations. Magnetic resonance imaging, 26(7), 853-862.

Yin, J., & Chen, J. D. (2008). Implantable gastric electrical stimulation: ready for prime time?. Gastroenterology, 134(3), 665-667.

Yin, J., & Chen, J. D. (2013). Electrogastrography: methodology, validation and applications. Journal of neurogastroenterology and motility, 19(1), 5.

Yu, X., Glen, D., Wang, S., Dodd, S., Hirano, Y., Saad, Z., Reynolds, R., Silva, A. C., & Koretsky, A. P. (2012). Direct imaging of macrovascular and microvascular contributions to BOLD fMRI in layers IV–V of the rat whisker–barrel cortex. Neuroimage, 59(2), 1451-1460.

Zaaimi B, Grebe R, & Wallois F. Animal model of the short-term cardiorespiratory effects of intermittent vagus nerve stimulation. Auton Neurosci. 2008;143(1-2):20-6.

Zabara J. Inhibition of experimental seizures in canines by repetitive vagal stimulation. Epilepsia. 1992;33(6):1005-12.

Zhang, N., Zhu, X. H., & Chen, W. (2008). Investigating the source of BOLD nonlinearity in human visual cortex in response to paired visual stimuli. Neuroimage, 43(2), 204-212.

Zobel A, Joe A, Freymann N, Clusmann H, Schramm J, Reinhardt M, Biersack, H., Maiera, W., & Broicha, K. Changes in regional cerebral blood flow by therapeutic vagus nerve stimulation in depression: an exploratory approach. Psychiatry Res. 2005;139(3):165-79.